

**INTRAMOLECULARLY SENSITIZED PRECIPITONS: APPLICATION TO
METAL SEQUESTRATION**

by

Mark R. Ams

B.A., Albion College, 2002

Submitted to the Graduate Faculty of
University of Pittsburgh in partial fulfillment
of the requirements for the degree of
Doctor of Philosophy

University of Pittsburgh

2005

UNIVERSITY OF PITTSBURGH
FACULTY OF ARTS AND SCIENCES

This thesis was presented

by

Mark R. Ams

It was defended on

11-30-04

and approved by

Craig Wilcox

Dennis Curran

Stephane Petoud

Craig Wilcox
Thesis Director

INTRAMOLECULARLY SENSITIZED PRECIPITONS: APPLICATION TO METAL SEQUESTRATION

Mark R. Ams

University of Pittsburgh, 2005

It has been demonstrated previously that precipitons can be successfully utilized in the area of chemical synthesis. Herein, we describe the properties of precipitons attached to metal complexes. Our preliminary studies show that the rate of an intermolecularly sensitized precipiton obeys first-order kinetics. A microcrystal suspension forms during the reaction, and we are interested in learning more about this process. To demonstrate intramolecular energy transfer, two new precipitons were designed, synthesized, and characterized. They represented two types of triplet energy transfer: Förster and Dexter. The Förster precipiton (10 μM solution) reached a photostationary state within 2 minutes when irradiated with visible light. In contrast, intermolecular sensitization (10 μM precipiton + 10 μM $\text{Ru}(\text{bpy})_3\text{Cl}_2$) proceeded approximately 10 times more slowly. What we have learned will be useful for metal sequestration applications.

TABLE OF CONTENTS

1.	Introduction.....	1
1.1.	Introduction to Precipitons.....	1
1.2.	<i>Z-E</i> Isomerization.....	4
1.3.	Mechanism of Triplet Energy Transfer.....	7
1.4.	Applications of Precipitons.....	9
2.	INTRAMOLECULARLY SENSITIZED PRECIPITONS: APPLICATIONS TO METAL SEQUESTRATION.....	16
2.1.	Metal Scavenging Methods.....	16
2.2.	Precipitons: Application to Light-Driven Metal Sequestration.....	21
2.3.	Inter- and Intra- Molecular Isomerization by Inorganic/Organometallic Sensitizers.....	24
3.	RESULTS AND DISCUSSION.....	31
3.1.	Intermolecular Sensitization of Precipitons.....	31
3.2.	Intramolecular Sensitization of Precipitons.....	44
3.3.	Förster Class Precipiton.....	48
3.3.1.	Synthesis.....	48
3.3.2.	Absorption and Emission Spectroscopy.....	53
3.3.3.	Photoisomerization Reactivity.....	61
3.3.3.1.	Key Reaction Rate Comparisons.....	61
3.3.3.2.	¹ NMR Monitored Isomerization Studies.....	63
3.3.3.3.	Electronic Absorption Monitored Isomerization Studies.....	65
3.4.	Investigation of Tetraethyldiethylenetriamine (TEDETA) Functionalized Precipitons.....	68
3.5.	Dexter Class Precipiton.....	73
4.	SUMMARY.....	78
5.	FUTURE DIRECTIONS.....	79
6.	EXPERIMENTAL.....	81
6.1.	General.....	81
6.2.	Experimental Procedures.....	83
6.2.1.	Synthesis and Characterization.....	83
6.2.2.	Photoisomerization Studies.....	94
APPENDIX A.....		96
6.3.	Dexter Class Precipiton.....	97
6.3.1.	Synthesis.....	97
6.3.2.	Photochemical Challenges of Sequestration.....	99
6.4.	¹ H- ¹ H COSY SPECTRA.....	102

LIST OF TABLES

Table 1	Solubilities and melting points of <i>Z</i> and <i>E</i> 1,2-bis(biphenyl)ethene alcohol.....	4
Table 2	Summary of $3Z \rightarrow 3E$ isomerization rates after 4 min ($[3Z] = 20$ mM, $[\text{Ru}(\text{bpy})_3^{2+}] = 50$ μM , $[3E] = \text{saturated}$, solvent = 1/1 $\text{CD}_3\text{CN}/\text{CD}_2\text{Cl}_2$).....	44
Table 3	Summary of the absorption spectroscopic data.	55
Table 4	Summary of the emission spectroscopic data. a $\lambda_{\text{exc}} = 450$ nm. b $\lambda_{\text{exc}} = 285$ nm.	55
Table 5	Key experiments for comparison of relative photoisomerization rates.	62
Table 6	Outcome of photochemical isomerization studies of 13Z.	70
Table 7	Summary of isomerization rates after 30 min of irradiation.....	75

LIST OF FIGURES

Figure 1	The precipiton approach for achieving product isolation.....	2
Figure 2	Structure of stilbenes.....	3
Figure 3	Triplet energy transfer to stilbene.....	6
Figure 4	Energy diagram showing the photoisomerization of stilbene.....	7
Figure 5	Energy transfer from an excited donor to a ground state acceptor.....	7
Figure 6	Electron energy transfer through a Dexter mechanism.....	8
Figure 7	Electron energy transfer through a Forster mechanism.....	8
Figure 8	Illustration of the precipiton process for isoxazoline isolation.....	9
Figure 9	The precipiton approach for reagent scavenging.....	10
Figure 10	Illustration of the precipiton process for amine scavenging.....	11
Figure 11	Copper removal from polymethyl methacrylate using a TEDETA-functionalized precipiton.....	13
Figure 12	Polyethylene supported pyridylmethanimine ligand and TEDETA functionalized JandaJel resin for copper removal.....	15
Figure 13	Negishi coupling to produce PDE472.....	17
Figure 14	Polymer-bound ethylenediamine derivatives.....	18
Figure 15	Synthesis of E2040 via the Suzuki-Miyaura cross coupling.....	18
Figure 16	Silica bound scavengers developed by SiliCycle Inc.....	19
Figure 17	2,4,6-Trimercaptotriazine (TMT).....	19
Figure 18	Palladium-catalyzed indolization and treatment with TMT to produce an antimigraine agent.....	20
Figure 19	Proposed organopalladium complex.....	21
Figure 20	An intramolecularly "triggered" precipitation process to remove metal impurities.....	23
Figure 21	Energy level diagram illustrating MLTC for $\text{Ru}(\text{bpy})_3^{2+}$	25
Figure 22	Intermolecular sensitization of trans-stilbene by $\text{Ru}(\text{bpy})_3^{2+}$	26
Figure 23	Intermolecular sensitization of trans-stilbene by $\text{fac-ClRe}(\text{CO})_3(\text{phpyr})_2^{2+}$	27
Figure 24	A rhenium(I) complex with a stilbene-containing ligand.....	28
Figure 25	A trinuclear rhenium(I) complex linked by an isomerizable stilbene-like ligands.....	29
Figure 26	$\text{Ru}(2,2'\text{-bpy})_2(\text{cis-4-stilbazole})_2^{2+}$	30
Figure 27	Intermolecular sensitization of precipiton 3Z by $\text{Ru}(\text{bpy})_3^{2+}$	32
Figure 28	Method A for kinetic data collection.....	33
Figure 29	Method B for kinetic data collection.....	34
Figure 30	Reaction progress of $3Z \rightarrow 3E$ isomerization with/out 3E ($[3Z] = 20 \text{ mM}$, $[3E] = \text{saturated}$; $[\text{Ru}(\text{bpy})_3^{2+}] = 50 \text{ }\mu\text{M}$, solvent = 1/1 $\text{CD}_3\text{CN}/\text{CD}_2\text{Cl}_2$).....	36
Figure 31	Reaction 1 plotted according to an irreversible first-order rate law ($k_{\text{obs}} = 0.028 \text{ s}^{-1}$) and a reversible first-order rate law ($k_{\text{obs}} = 0.035 \text{ s}^{-1}$).....	38
Figure 32	Reaction progress of $3Z \rightarrow 3E$ isomerization with/out 3E and $\text{Ru}(\text{bpy})_3^{2+}$ ($[3Z] = 20 \text{ mM}$, $[3E] = \text{saturated}$; solvent = 99/1 $\text{CD}_3\text{CN}/\text{D}_2\text{O}$).....	40
Figure 33	Reaction progress of $3Z \rightarrow 3E$ isomerization using Method A and Method B ($[3Z] = 20 \text{ mM}$, $[\text{Ru}(\text{bpy})_3^{2+}] = 50 \text{ }\mu\text{M}$, solvent = 1/1 $\text{CD}_3\text{CN}/\text{CD}_2\text{Cl}_2$).....	41

Figure 34	A Ru-pyr complex exhibiting Förster-type intramolecular energy transfer...	45
Figure 35	A precipiton linked to a sensitizer.....	46
Figure 36	A Ru-Os complex exhibiting Dexter-type intramolecular energy transfer.	47
Figure 37	A precipiton linked to a sensitizer.....	48
Figure 38	Synthesis of 1,2-bis(biphenyl)ethene alcohol precipiton 3Z.....	49
Figure 39	Synthesis of 5-bromomethyl-2,2'-bipyridine 6.....	50
Figure 40	Alkylation of 7 with 3Z to generate Förster precipiton 8Z.....	50
Figure 41	Synthesis of Ru-bound Förster precipiton 9Z.....	52
Figure 42	Synthesis of Ru-bound Förster precipiton 9E.....	53
Figure 43	Absorption spectra of complex 9Z and related components (10 μ M, air equilibrated CH ₃ CN, T = 298 K).....	54
Figure 44	Excitation spectra (λ_{em} = 610 nm) and emission spectra (λ_{exc} = 450 nm) of... 57	
Figure 45	Emission spectra (λ_{exc} = 450 nm) of complexes 9Z, 9E, and Ru(bpy) ₃ ²⁺	58
Figure 46	Energy level diagram describing the photophysical processes of 9Z.....	60
Figure 47	Receiver-antenna relationship of complex 9Z.....	60
Figure 48	¹ H NMR spectroscopic changes of 9Z and 9E in CD ₃ CN at 298 K during irradiation at λ_{exc} = 400nm.....	64
Figure 49	Plot of the percentage decrease of 9Z against time of irradiation at \geq 400 nm (1mM, degassed CD ₃ CN, T = 298 K).....	65
Figure 50	Photoisomerization of 9Z upon irradiation at \geq 400 nm (10 μ M, degassed CH ₃ CN, T = 298 K).....	66
Figure 51	Photoisomerization of 9E upon irradiation at \geq 400 nm (10 μ M, degassed CH ₃ CN, T = 298 K).....	67
Figure 52	Synthesis of TEDETA functionalized precipiton 13Z.....	69
Figure 53	Cycloaddition products possible from 350 nm irradiation of 13Z.....	72
Figure 54	. Dexter-type precipiton 22Z.....	73
Figure 55	Plot of photoisomerization reactions 1-7 ([3Z], [22Z] = 1mM; [Ru(bpy) ₃ ²⁺],[Ru(bpy) ₂ ²⁺] = 50 μ M, solvent = 1/1 CD ₂ Cl ₂ /CD ₃ CN).....	74
Figure 56	Plot of photoisomerization reactions 8-11. Reactions 8 and 9 are performed in one NMR tube and reactions 10 and 11 are performed in one NMR tube.....	76
Figure 57	Synthesis of pinacolatoboronic ester 17Z.....	97
Figure 58	Synthesis of 4-(4-bromo-phenyl)-[2,2']bipyridine 21.....	98
Figure 59	Synthesis of Dexter class precipiton 22Z.....	98
Figure 60	Absorbance spectra of the dilution of a 1/1 mixture of 2,2'-bipyridine and Ru(bpy) ₂ ²⁺ (1/1 CH ₂ Cl ₂ /CH ₃ CN, λ_{abs} = 376 nm, R ² = 0.999).....	99
Figure 61	Room-temperature absorption spectra of 3Z and 16Z (10 μ M, air-equilibrated.....	100
Figure 62	Modes of ring opening that can result in the formation of photosubstitution	101
Figure 63	¹ H- ¹ H COSY of compound 7.....	102
Figure 64	¹ H- ¹ H COSY of compound 8Z.....	103
Figure 65	¹ H- ¹ H COSY of compound 9Z.....	104
Figure 66	¹ H- ¹ H COSY of compound 9E.....	105
Figure 67	¹ H- ¹ H COSY of compound 21.....	106
Figure 68	¹ H- ¹ H COSY of compound 22Z.....	107

1. Introduction

1.1. Introduction to Precipitons

The Wilcox group has demonstrated the use of “precipitons” as a new type of phase tag for the separation of desired molecules from a chemical mixture. A “precipiton” is defined as a group of atoms (molecular fragment) that is purposefully attached to a reactant molecule to facilitate precipitation or phase transfer of the attached group at a selected time.¹ Rather than changing the solvent or environment of the desired group to initiate a separation process, it was envisioned that the solubility of the precipiton itself could be changed to cause precipitation. This change in the solubility of the precipiton can be accomplished if the precipiton exists in two isomeric forms: one freely soluble in a given solvent and the other form insoluble in the same solvent. The desired molecule, which is attached to the precipiton could be isolated directly from a reaction mixture by inducing isomerization of the precipiton phase tag.

One type of precipiton that has been well established in the Wilcox group is based on the structure of stilbene. Stilbene is an alkene that exists in two interconvertible isomeric *cis* and *trans* forms. Because the *cis* isomer is often more soluble than the *trans* isomer, stilbene was utilized as a molecular building block in the chemical structure of

¹ Bosanac, T.; Yang, J.; Wilcox, C. S. *Angew. Chem. Int. Ed.* **2001**, *40*, 1875.

precipitons.² The precipiton approach for achieving product isolation is illustrated in Figure 1 where stilbene is used as a model precipiton.³

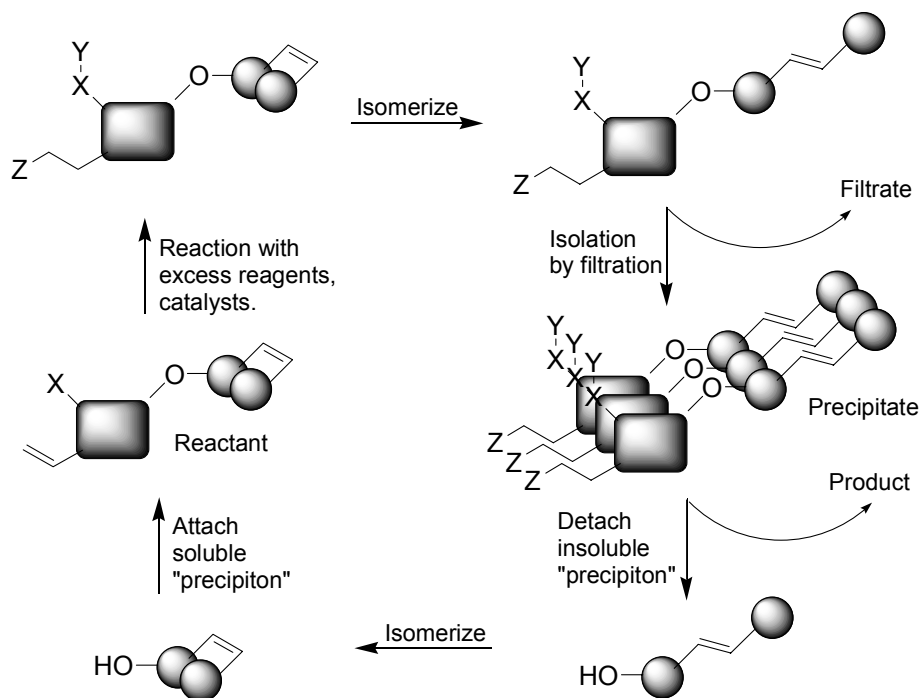


Figure 1 The precipiton approach for achieving product isolation.

The precipiton in its soluble *cis* form is first attached to a reactant. The reactant is then converted to product through a chemical reaction. Finally, the *cis* precipiton is isomerized to its insoluble *trans* form to allow for isolation of the attached product by filtration. The phase tag can be cleaved to yield the desired free product.

The *Z* and *E* stilbene isomers each have their own unique structural, physical, and photochemical properties (Figure 2). *Z*-stilbene is non-planar, due to

² (a) Crombie, L.; Shah, J. D. *J. Chem. Soc.* **1955**, 4244. (b) Crombie, L.; Tayler, J. L. *J. Chem. Soc.* **1957**, 2760.

³ Bosanac, T. Ph. D. Dissertation, University of Pittsburgh, **2003**.

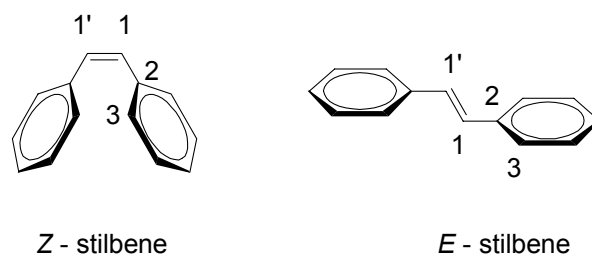


Figure 2 Structure of stilbenes.

positional twisting of the phenyl rings in response to mutual van der Waals repulsion. The angle between the planes of the central double bond and a phenyl ring (dihedral angle) (C1'-C1-C2-C3) of *Z*-stilbene is 43.2°, determined by gas phase electron diffraction.⁴ In contrast, *E*-stilbene is nearly planar in structure, determined by X-ray analysis. An X-ray crystal structure of *E*-stilbene revealed two forms, α and β , and the dihedral angles (C1'-C1-C2-C3) were 1° and 5° respectively.⁵

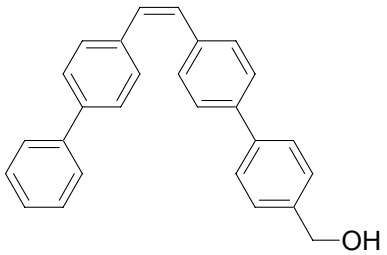
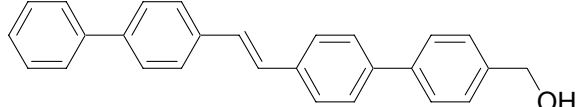
The significant differences in solubility and melting points between *Z* and *E*-stilbene may be explained by their molecular shapes. One likely reason *E*-stilbene has a high melting point (125 °C)⁶ and low solubility is due to its nearly planar structure, capable of strong pi-stacking interactions. *Z*-stilbene (m.p. = 5 °C), having a cup-shaped structure, would have poor pi-stacking interactions. Additional phenyl units on stilbene, shown in Table 1 for 1,2-bis(biphenyl)ethene alcohol, lead to molecules with drastically decreased

⁴ Tratterberg, M.; Franstein, E. B. *J. Mol. Struct.* **1975**, 26, 69.

⁵ (a) Finder, C. J.; Newton, M. G.; Allinger, N. L. *Acta. Cryst.* **1974**, B30, 411. (b) Harada, J.; Ogawa, K. *J. Am. Chem. Soc.* **2001**, 123, 10884.

⁶ Caia, V.; Cum, G.; Gallo, R.; Mancini, V.; Pitoni, E. *Tetrahedron Lett.* **1983**, 24, 3903.

Table 1 Solubilities and melting points of *Z* and *E* 1,2-bis(biphenyl)ethene alcohol.

Compound	Solubility (mM, THF-d ₈)	mp (°C)
	> 20 ^a	142 - 143 °C
	2.2 ^b	> 300 °C

^a 20 mM is not the maximum solubility of isomer *Z*. It was the starting concentration before isomerization to the *E* isomer. ^b Obtained by triplet sensitized isomerization of 20 mM *Z* isomer and analyzing remaining *E* isomer by ¹H NMR spectroscopy.

solubility in THF and increased melting point. The addition of phenyl units has been a useful strategy for tuning the solubility of precipitons. For example, if the functional group or substrate attached to a precipiton increases its solubility, which often occurs, precipitation from solution may be less successful. Additional phenyl units help prevent this effect.

1.2. *Z-E* Isomerization

The geometrical interconversion of stilbene isomers includes both $Z \rightarrow E$ and $E \rightarrow Z$ isomerization. *Z*-Stilbene is less stable than *E*-stilbene by 4.59 kcal/mol due to the

eclipsing phenyl-phenyl interaction in *Z*-stilbene.⁷ However, the *Z*- and *E*- isomers are still interchangeable by thermal,⁸ chemical,⁹ and photochemical methods.¹⁰

Photochemical *Z-E* isomerization can be achieved by either direct irradiation¹⁰ or by photosensitizer-assisted irradiation (triplet-sensitized).¹¹ In a direct irradiation process, absorption of a photon excites stilbene to the singlet state which eliminates π -bonding in the alkene. Since the barrier to rotation about the former double bond is removed, rotation toward a 90° orientation of the two p orbitals occurs to reduce the energy of the excited state.¹² At this point, the twisted excited singlet will relax to either *cis* or *trans* ground states by radiationless decay, producing an approximately equal mixture of *cis* and *trans* isomers. However, a mixture enriched in one isomer can be prepared by selecting a wavelength of light in which one isomer absorbs more strongly than the other.

The excited triplet state of stilbene can be reached directly using an excited state sensitizer (Figure 3). A sensitizer **S** acts by absorbing light, then undergoing intersystem crossing to its triplet state ³**S**, then taking part in an energy transfer process with stilbene (*E* or *Z*) through an electron exchange mechanism. Triplet energy transfer to ground state stilbene results in triplet excited stilbene. Regardless of which isomer is

⁷ Saltiel, J. S.; Ganapathy, S.; Werking, C. *J. Phys. Chem.* **1987**, *91*, 2755.

⁸ Coyle, J. D. *Introduction to Organic Photochemistry*; John Wiley & Sons Press: Great Britain, 1998.

⁹ (a) Sonnet, P. E. *Tetrahedron* **1980**, *36*, 557. (b) Vedejs, E.; Fuchs, P. L. *J. Am. Chem. Soc.* **1971**, *93*, 4070.

¹⁰ Waldeck, P. H. *Chem. Rev.* **1991**, *91*, 415.

¹¹ Hammond, G. S.; Saltiel, J.; Lamola, A. A.; Turro, N. J.; Bradshaw, J. S.; Cowan, D. D.; Counsell, R. C.; Vogt, V.; Dalton, C. J. *J. Am. Chem. Soc.* **1964**, *86*, 3197.

¹² Carroll, F. *Perspectives in Structure and Mechanism in Organic Chemistry*; Brooks/Cole Press: Pacific Grove, U.S., 1998.

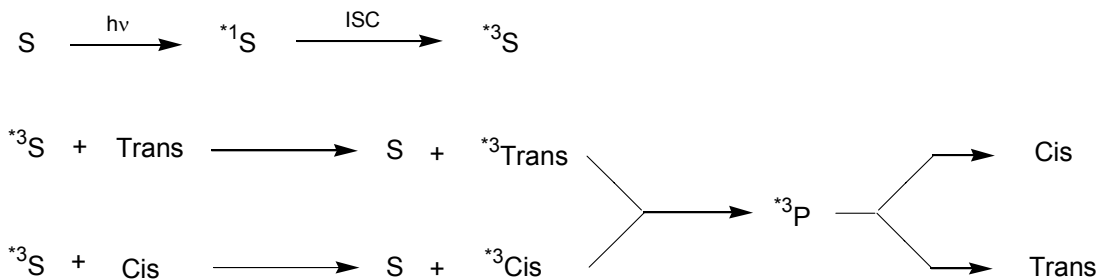


Figure 3 Triplet energy transfer to stilbene.

sensitized, the excited state triplet relaxes to a common 90° twisted excited state called the phantom triplet state ${}^3\text{P}$. From here, the phantom triplet decays to either *cis* or *trans* isomer (Figure 4).¹³ A photostationary state (PSS) occurs when further irradiation of the reaction yields no change in the product ratio of *cis* and *trans* isomers. This equilibrium is due to the rate of formation of each isomer equaling the rate of its removal by sensitization. Depending on the energy of the sensitizer, a photostationary state enriched in one isomer can be produced.

¹³ (a) Herkstroeter, W. G.; Hammond, G. S. *J. Am. Chem. Soc.* **1966**, *88*, 4769. (b) Hammond, G. S.; Saltiel, J. *J. Am. Chem. Soc.* **1963**, *85*, 2516. (c) Saltiel, J.; Charlton, J. L.; Mueller, W.B. *J. Am. Chem. Soc.* **1979**, *101*, 1347.

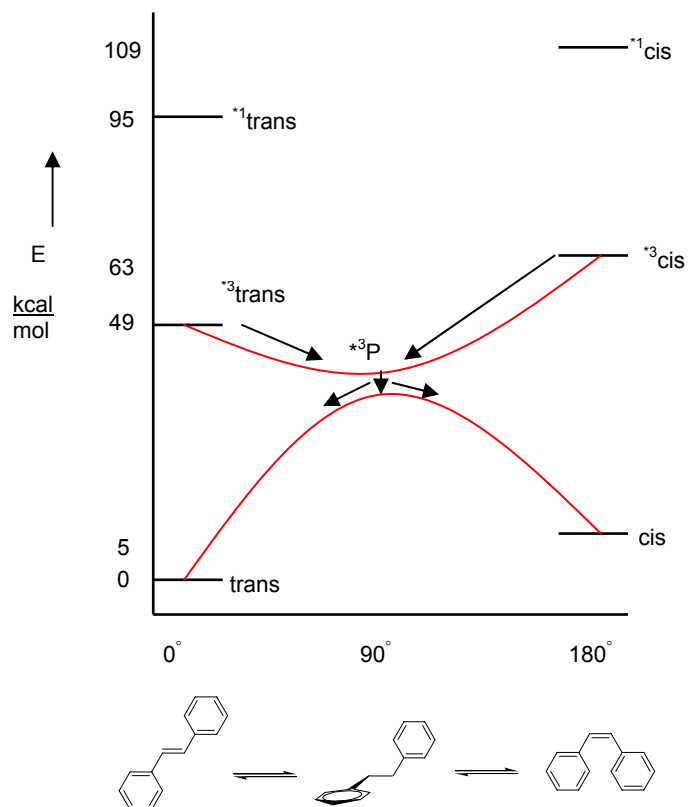


Figure 4 Energy diagram showing the photoisomerization of stilbene.

1.3. Mechanism of Triplet Energy Transfer

Electronic energy transfer from an excited state donor to a ground state acceptor (Figure 5) can occur by two different mechanisms: a Dexter-type¹⁴ mechanism and a Förster-type¹⁵ mechanism.

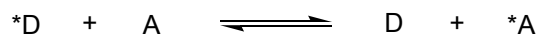


Figure 5 Energy transfer from an excited donor to a ground state acceptor.

¹⁴ Dexter, D. L. *J. Chem. Phys.* **1953**, *21*, 836.

¹⁵ Förster, Th. H. *Discuss. Faraday Soc.* **1959**, *27*, 7.

Dexter energy transfer requires physical collision between the donor and acceptor. If the collision allows for favorable orbital overlap between partners, an exchange of electrons may take place (Figure 6).¹⁶

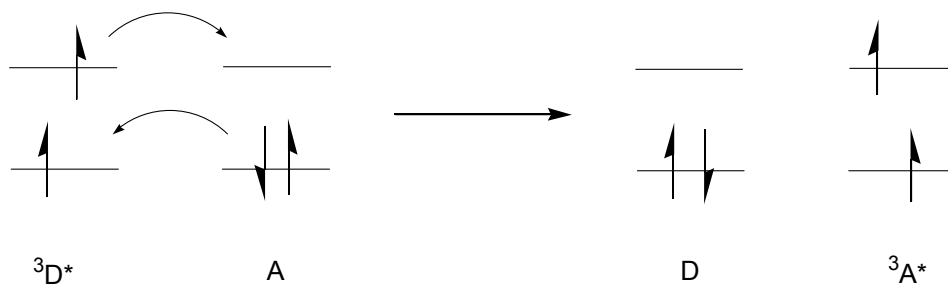


Figure 6 Electron energy transfer through a Dexter mechanism.

In contrast, Förster energy transfer does not require physical contact between interacting partners or strong orbital overlap. Energy is transferred through a dipole-dipole electromagnetic interaction that can occur over long distances (as large as 100 Å) (Figure 7). In a Förster energy transfer, the rate of transfer decreases in proportion to the sixth power of the distance between the donor and acceptor.

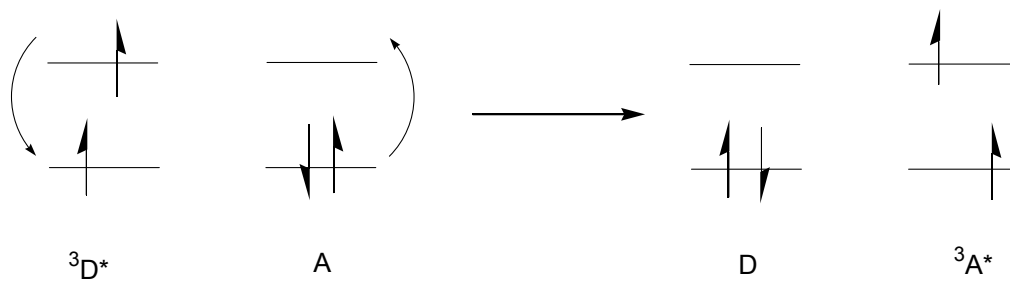


Figure 7 Electron energy transfer through a Förster mechanism.

¹⁶ Kalyanasundaram, K. *Photochemistry of Polypyridine and Porphyrin Complexes*; Academic Press: London, U.K., 1992.

1.4. Applications of Precipitons

The stilbene precipiton approach has been successfully applied to product isolation, reagent scavenging, metal scavenging, and by-product removal. Product isolation was first demonstrated by the synthesis and isolation of pure isoxazoline products, as shown in Figure 8. Isoxazolines were synthesized on 1,2-biphenylphenylethene precipitons in

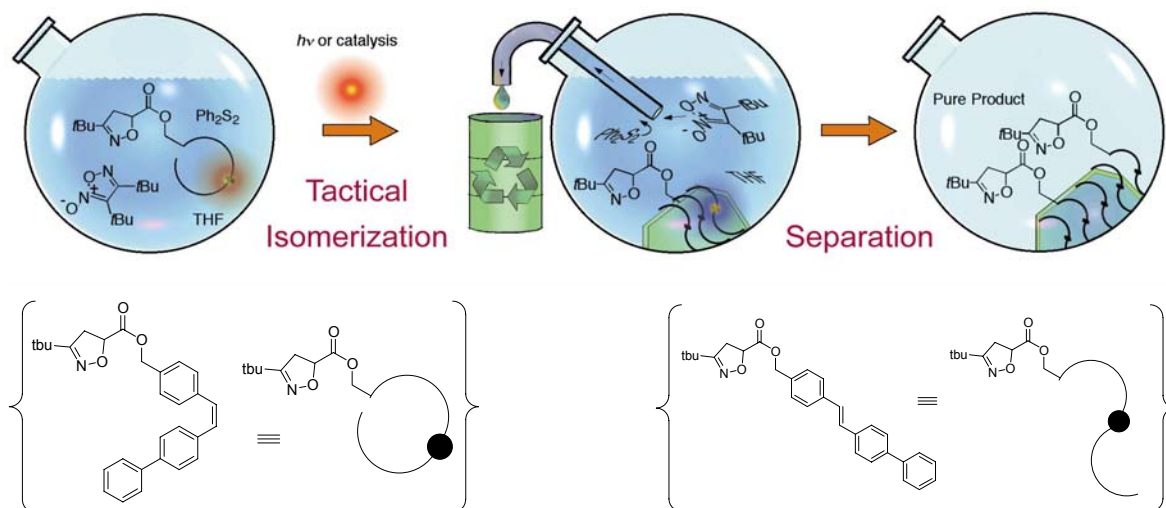


Figure 8 Illustration of the precipiton process for isoxazoline isolation.

ether. When the reaction was complete, the ether was removed and the crude residue was diluted with THF. The precipiton phase tag was then isomerized to its *trans* isomer using diphenyl disulfide. After isomerization the THF was removed and the solid was washed remove any byproducts. Finally, the *trans*-precipiton bound isoxazoline products were cleaved from the precipiton tag in THF using methanol and triethylamine.

Precipitons can also be used to precipitate excess reagents as a method for purifying desired products. This approach is shown in Figure 9. Compound **A** and excess compound **B** are reacted together to form product **C** in a reaction mixture with left over compound **B**. A precipiton in the soluble *cis* form can be added to the reaction mixture to scavenge **B**, and can then be isomerized to its insoluble *trans* form. The precipiton-tagged excess **B** precipitates from solution, leaving only product **C** in solution.

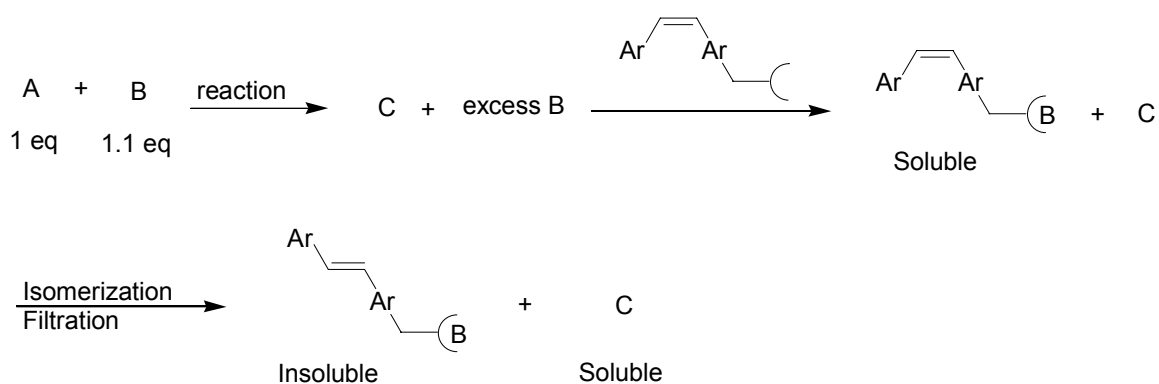


Figure 9 The precipiton approach for reagent scavenging.

This method has been demonstrated in the scavenging of amines using an isocyanate functionalized precipiton.¹⁷ Ureas and thioureas were synthesized by reaction of excess amine and phenyl isocyanate. The excess amine was then covalently scavenged by the isocyanate functionalized *cis*-precipiton, isomerized to the insoluble *trans* form, and filtered to give pure product in high yield. Figure 10 illustrates a model study to test amine scavenging, where an isocyanate functionalized precipiton was added to a mixture

¹⁷ Bosanac, T.; Wilcox, C. S. *J. Am. Chem. Soc.* **2002**, *124*, 4194.

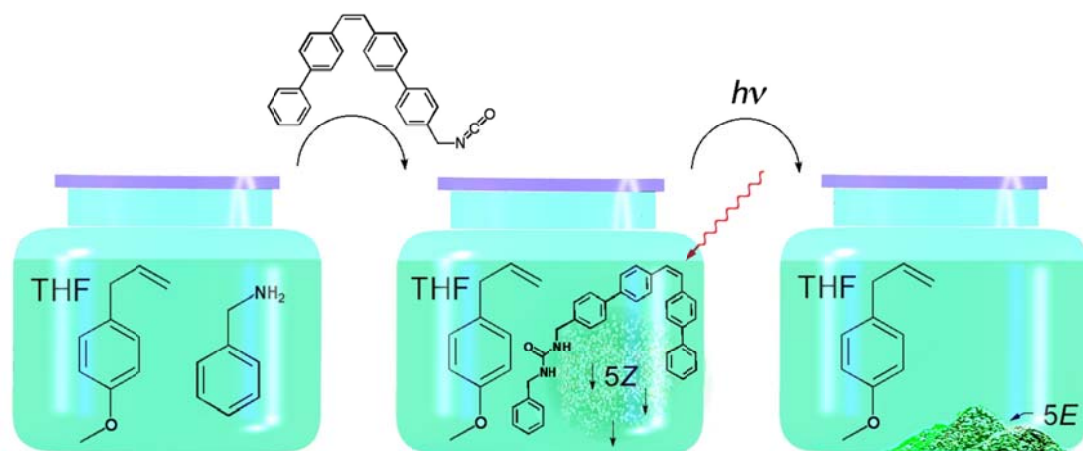


Figure 10 Illustration of the precipiton process for amine scavenging.

of benzylamine and 4-allylanisole. Only 1.1 equiv of isocyanate was needed to completely consume benzylamine in less than 10 min.

In addition to reagent scavenging, precipitons have also been applied to inorganic catalyst removal. Brittain and coworkers at the University of Akron demonstrated that precipitons containing a tetraethyldiethylenetriamine (TEDETA) ligand were able to successfully scavenge copper catalyst after an atom transfer radical polymerization (ATRP) reaction of methyl methacrylate (Figure 11).¹⁸ The TEDETA functionalized 1,2-bis(biphenyl)ethene precipiton shown above was combined with methyl methacrylate, CuBr, and ethyl 2-bromoisobutyrate in toluene. After heating for 12 h, the product mixture was irradiated with a xenon arc lamp for 2 h. The polymer solution was decanted from the precipitated precipiton/CuBr complex. ICP analysis of the copper

¹⁸ Honigfort, M.; Brittain, W. J.; Bosanac, T.; Wilcox, C. S. *Macromolecules* **2002**, *35*, 4849.

content in the polymer, without further purification, determined that less than 1% of the original amount of copper remained in the polymethyl methacrylate product.

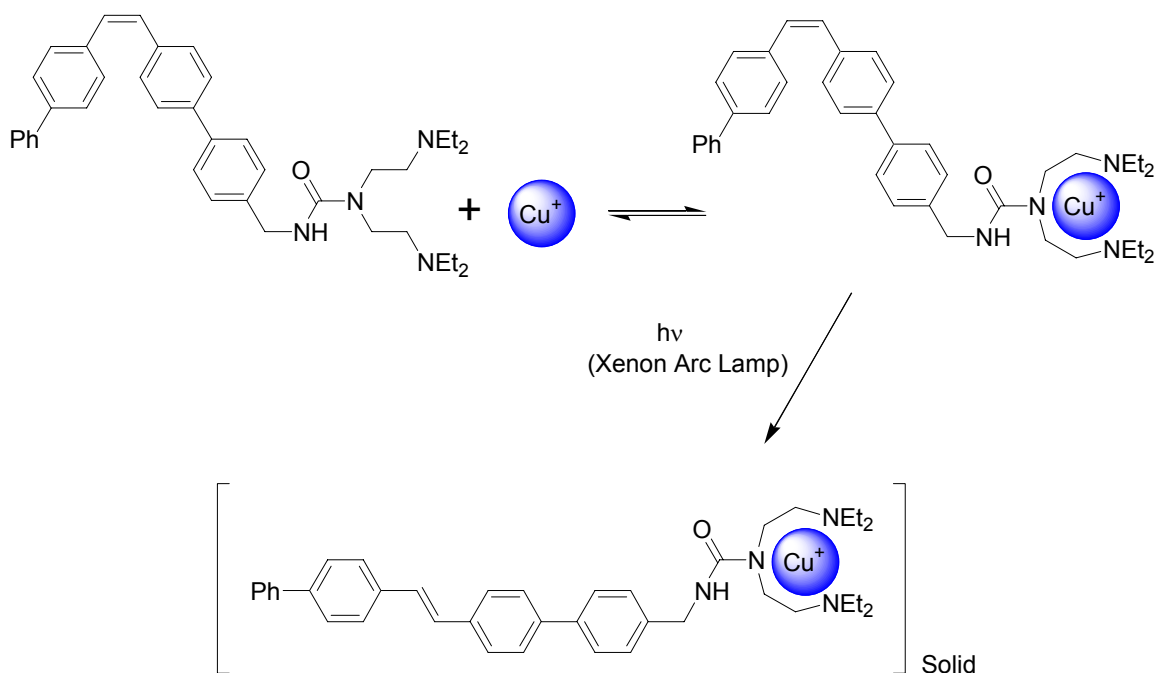
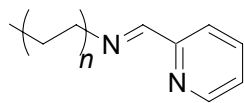


Figure 11 Copper removal from polymethyl methacrylate using a TEDETA-functionalized precipiton.

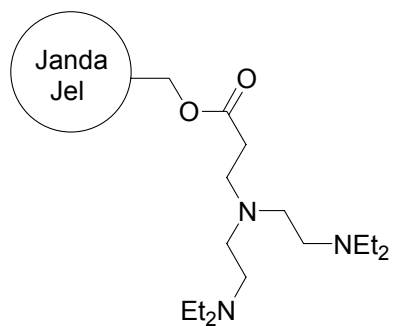
In a case study by Brittain, the precipiton approach to copper removal from ATRP reactions was compared with several other copper removal techniques.¹⁹ These methods included a homogeneous polyethylene (PE) supported pyridylmethanimine ligand and polystyrene JandaJel™ resins functionalized with TEDETA or imine ligands (Figure 12). The PE-imine ligand was shown to effectively remove copper catalyst from a methyl methacrylate polymerization. Just 1% of the original copper had remained in the final product. However, reaction times were over twice as long (18-26 h) compared to a conventional ATRP reaction. A steric effect caused by the long PE chains was proposed to be responsible for retarding Cu complexation to the PE-ligand. In the JandaJel study,

¹⁹ Honigfort, M.; Shingtza, L.; Rademacher, J.; Malaba, D.; Bosanac, T.; Wilcox, C. S.; Brittain, W. J. *ACS Symposium Series* **2003**, 854, 250.

ATRP reactions were much faster (6-8 h) compared to the PE-ligand/CuBr catalyst system. However, the JandaJels were less effective at removing copper (4-5% Cu remaining). The TEDETA functionalized precipitons were effective at both removing copper (<1% original amount of copper remaining in the unpurified polymer) and maintaining reasonable reaction times (12 h).



PE supported pyridylmethanimine ligand



JandaJel TEDETA ligand

Figure 12 Polyethylene supported pyridylmethanimine ligand and TEDETA functionalized JandaJel resin for copper removal.

2. INTRAMOLECULARLY SENSITIZED PRECIPITONS: APPLICATIONS TO METAL SEQUESTRATION

2.1. Metal Scavenging Methods

The area of chemical synthesis has evolved tremendously over the last several decades. New strategies, reactions, and techniques are now available to make even the most sophisticated organic molecules. Despite these improvements, purification is one crucial aspect of synthesis that has not been improved significantly over the years.²⁰ In the area of medicinal chemistry, for example, adequate purification is a challenge in the production of new drugs. In the pharmaceutical industry, removing toxic impurities such as palladium from active pharmaceutical ingredients (API's) can be a major purity concern.²¹ Pharmaceutical manufacturers strive to produce API's containing no more than 5 ppm palladium. Reducing contaminants to this level is difficult because the API can often be a good ligand for complexation to the metal impurity. For example, chemists at Novartis Pharma AG synthesize 5-[2-methoxy-5-(4-pyridinyl)phenyl]-2,1,3-benzoxadiazole (PDE472) on a multikilogram scale for the treatment of asthma.²² The final step of the synthetic sequence is a Negishi aryl-aryl coupling (Figure 13). Even after chromatography and crystallization, the final product is still contaminated with high amounts of palladium (300 – 800 ppm). The authors suggested that this may be due to

²⁰ Curran, D. P. *Angew. Chem. Int. Ed.* **1998**, 37, 1174.

²¹ Urawa, Y.; Miyazawa, M.; Ozeki, N.; Ogura, K. *Org. Process Res. Dev.* **2003**, 7, 191.

²² Manley, P.; Acemoglu M.; Marterer, W.; Pachinger, W. *Org. Process Res. Dev.* **2003**, 7, 436.

strong complexation of PDE472 with Pd(0). The 4-(4-methoxyphenyl)-pyridine substructure is a good candidate ligand for Pd(0); 4-methoxypyridines are well-known to ligate palladium. Novartis Pharma AG chemists solve this purity problem by treating PDE472 with maleic acid to produce the hemi-maleate salt. However, the salt must be converted back to the free base, treated with active charcoal, and recrystallized again.

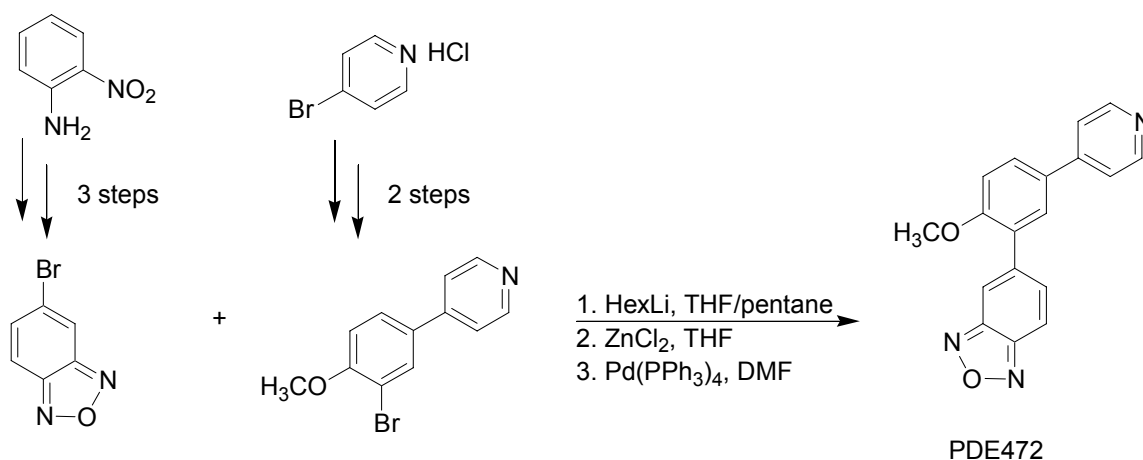


Figure 13 Negishi coupling to produce PDE472.

An alternative method for catalyst removal from reaction mixtures involves solid supported scavengers. These scavengers, now commercially available, are added directly to the reaction mixture or used in a column to selectively remove the metal. Two common types of solid supported scavengers are silica and polymer-bound scavengers. It was reported by Ogura and coworkers that polymer-supported derivatives of ethylenediamine (Figure 14) can be employed for the efficient removal of residual palladium from drug candidate E2040 (Figure 15). A key synthetic step is the Suzuki-Miyaura coupling of 1-{3-bromo-4-chloro-5-[1-(R)-fluoropropyl]}-phenylpiperazine with 2-(1,3,2-dioxaborinan-2-yl)benzotrile. The crude 2'-cyanobiphenyl product was

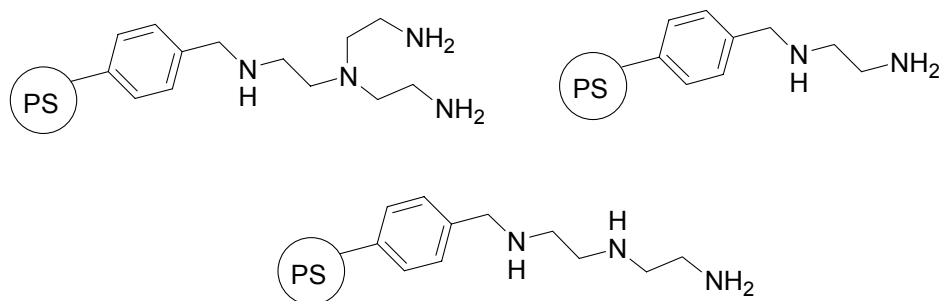


Figure 14 Polymer-bound ethylenediamine derivatives.

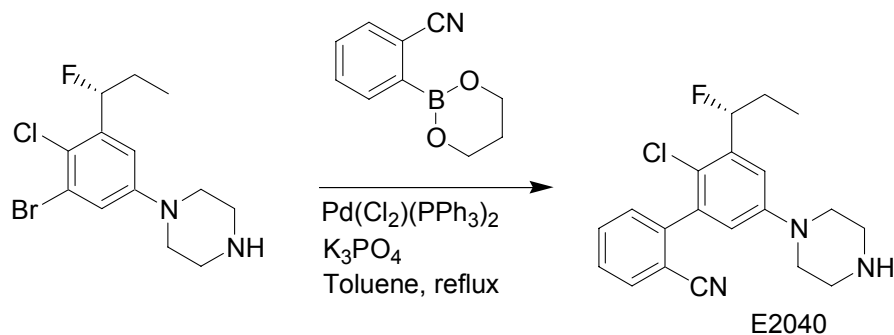


Figure 15 Synthesis of E2040 via the Suzuki-Miyaura cross coupling.

treated with the polymer-bound ethylene-diamine to reduce the palladium content of the crude product from 2000 – 3000 ppm to 100 – 200 ppm. However, subsequent purification by salt formation was necessary to attain a palladium content less than 10 ppm. Silica bound scavengers can also be effective in the removal of palladium. Thiol, thiourea, and triamine silica bound scavengers are commercially available (Figure 16).²³

²³ SiliCycle® Inc., 1200 Ave St-Jean-Baptiste, Suite 114, Quebec City, Quebec G2E 5E8, Canada. Phone:

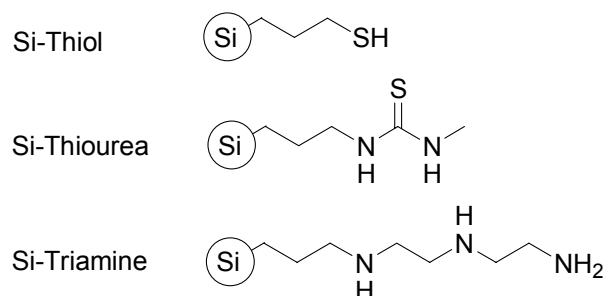


Figure 16 Silica bound scavengers developed by SiliCycle Inc.

In addition to solid support scavengers, 2,4,6-trimercaptotriazine (TMT) (Figure 17) has also been used effectively to bind and precipitate palladium and other heavy metals from solution. TMT has been used to precipitate heavy metals from wastewaters, flue

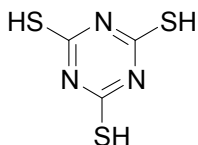


Figure 17 2,4,6-Trimercaptotriazine (TMT)

gases, and soils, and has exhibited high affinity for cupric ion.²⁴ Studies have also shown that TMT has low toxicity toward humans and animals. One limitation of TMT is that TMT-palladium complexes tend to be soluble in polar organic solvents. To solve this, a

(418)874-0054, Fax: (418)874-0355.

²⁴ Rosso, V. W.; Lust, D. A.; Bernot, P. J.; Grosso, J. A.; Modi, S. P.; Rusowicz, A.; Sedergran, T. C.; Simpson, J. H.; Srivastava, S.K.; Humora, M. J.; Anderson, N. G. *Org. Process Res & Dev.* **1997**, *1*, 311.

polymer-bound version of TMT was prepared by covalently attaching TMT to an insoluble gel-type polystyrene support.²⁵ This resin was shown to effectively reduce palladium(II) acetate concentration in THF by a factor of 1,000. However, 2-5 equivalents of resin relative to palladium and long reaction times (16-24 h) are necessary.

A comparison of TMT with other methods demonstrated that TMT was most effective at removing palladium from the antimigraine candidate 4-(5-methoxy-4-pyrimidinyl)-1-[3-[5-[[[(methyl-amino)sulfonyl]methyl]-1H-indol-3-yl]propyl]piperazine. The final step in the piperazine synthesis is a palladium-catalyzed indolization (Figure 18). The level of palladium in the final product after synthesis was usually 600-650 ppm, and multiple recrystallizations reduced the levels to 25-30 ppm. Filtration of solutions of the

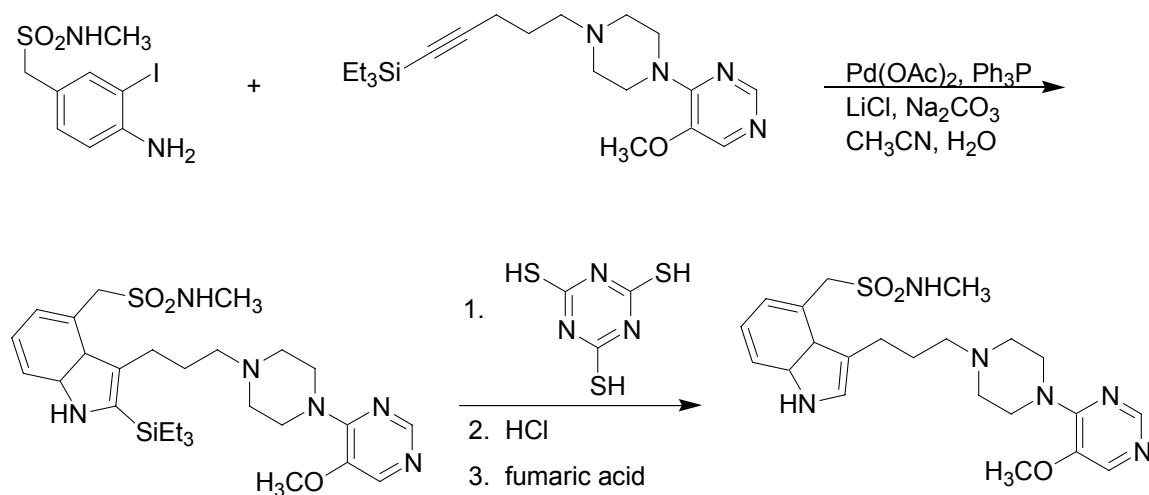


Figure 18 Palladium-catalyzed indolization and treatment with TMT to produce an antimigraine agent.

²⁵ Ishihara, K.; Nakayama, M.; Kurihara, H.; Itoh, A.; Haraguchi, H. *ChemLett.* **2000**, 1218.

drug through 0.22 μm filters, treatment with diatomaceous earth or charcoal, and reductive plating Pd(0) onto carbon electrodes were not successful at reducing the level of Pd to 5 ppm. However, addition of TMT after completion of the palladium-catalyzed indolization and subsequent salt formation of the final product reduced the palladium content to 1-4 ppm. TMT treatment was effective on a 12 kg scale, producing the piperazine drug with average palladium levels less than 1 ppm. A proposed reason for the difficulty in removing palladium catalysts is that the palladium may have been solubilized as a complex (Figure 19).

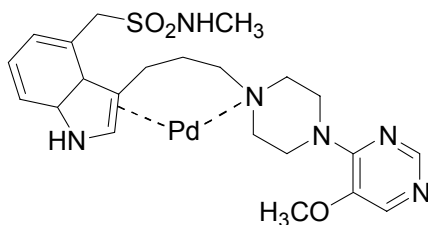


Figure 19 Proposed organopalladium complex.

2.2. Precipitons: Application to Light-Driven Metal Sequestration

Although the scavengers outlined above have shown usefulness in removing metal impurities from reaction mixtures, they have several limitations. The nature of the metal catalyst and its ligands are very important to a catalyzed chemical reaction. However, in order for a metal scavenger to be effective at removing a metal catalyst, the scavenger

ligands must have a stronger affinity for the metal than any of its competitors. For example, a scavenger must out-compete the palladium bound antimigraine drug product (Figure 19) as well as any silylated indole starting material in order to remove it. Therefore, strong competitor ligands hinder the scavenging of the metal much more than weak ones.

We hypothesized that the problem of ligand competitors could be overcome through the use of an intramolecularly sensitized precipiton, wherein the ligated metal would act to trigger precipitation. This concept is illustrated using the palladium bound antimigraine drug (Figure 20). If a small amount of *cis* scavenger precipiton is added to

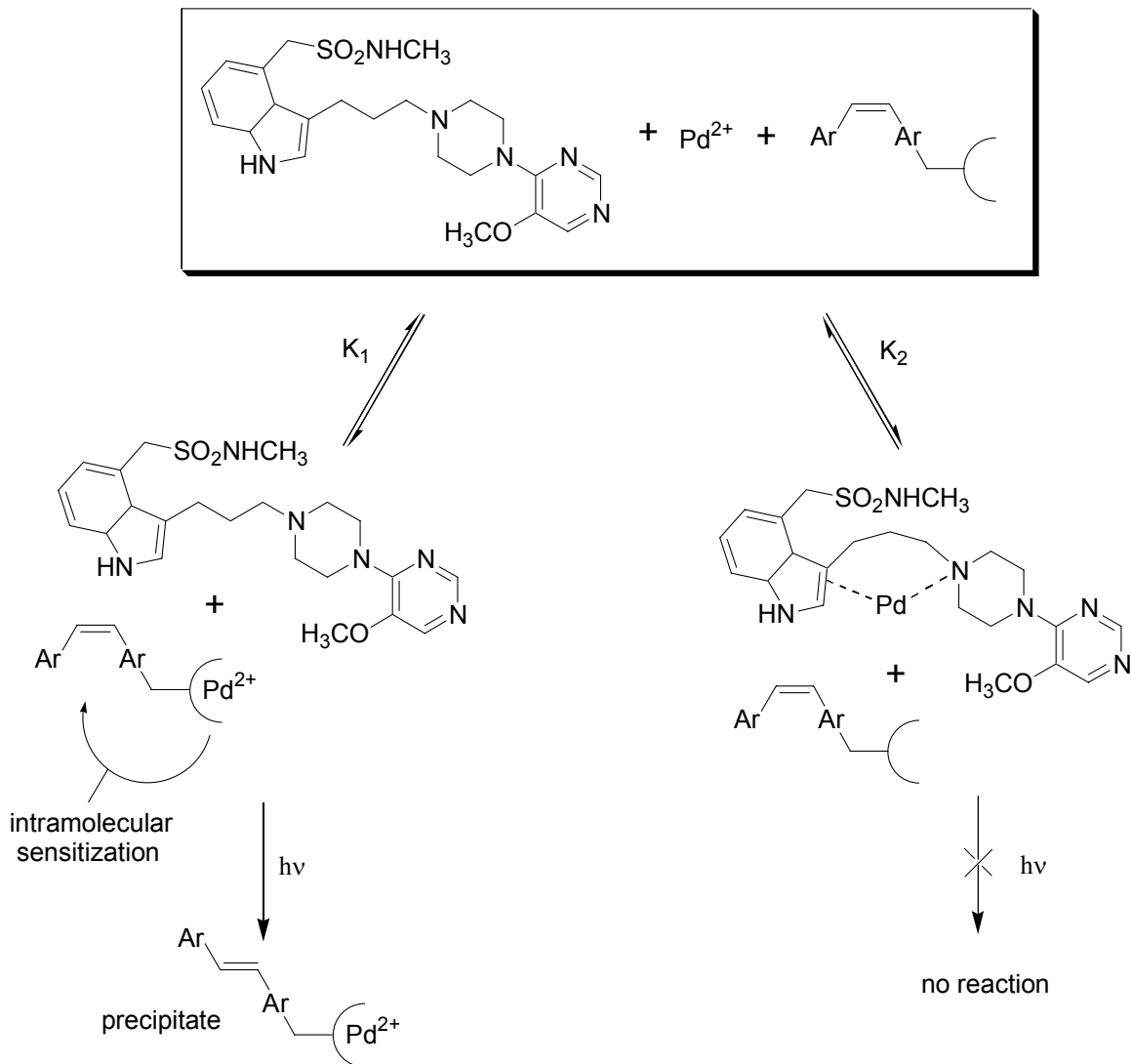


Figure 20 An intramolecularly "triggered" precipitation process to remove metal impurities.

a solution containing a very large excess of drug-contaminated palladium, the palladium will most often be bound to the drug rather than bound to the precipiton scavenger. However, in every event that palladium does bind to the precipiton, if the resulting complex can absorb light, an isomerization process is "triggered" via intramolecular sensitization to produce *trans* precipiton. *Trans* precipiton would precipitate together

with the palladium metal. The amount of palladium bound to the scavenger, originally limited by the equilibrium constants for binding to the precipiton ligand (K_1) and competing drug ligands (K_2), is increased due to precipitation. The amount of palladium in solution will be decreased by the precipitation event.

Isomerization could be “triggered” if metal ligation to the precipiton generated a chromophore capable of absorbing light and providing a triplet state from which energy could then be transferred intramolecularly to the isomerizable alkene. Only those metals that ligate to the precipiton would form triplet energy sensitizers. Due to low concentrations, only the precipiton attached to the sensitizer would isomerize. To meet this requirement, the precipiton ligand must have a unique relationship with its metal partner that does not exist without binding.

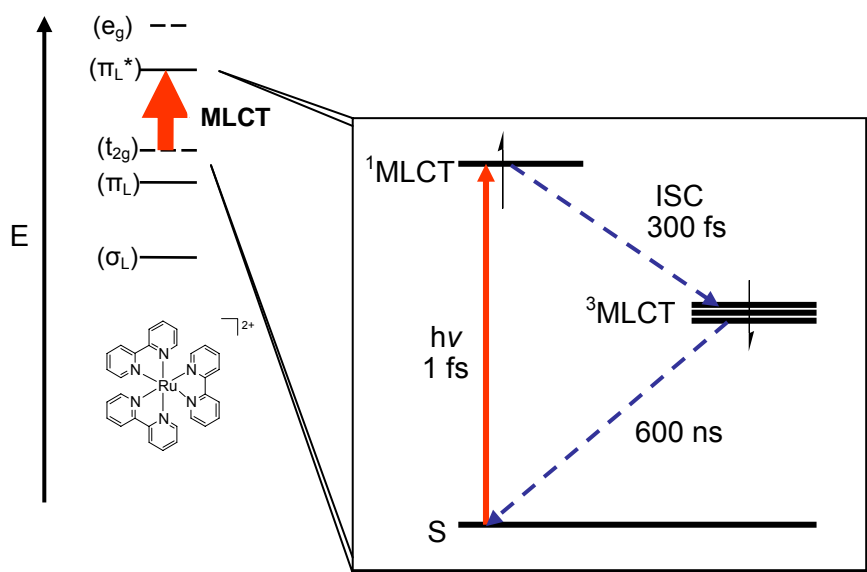
2.3. Inter- and Intra- Molecular Isomerization by Inorganic/Organometallic Sensitizers

In the literature, there are reports of photosensitive inorganic complexes that act as triplet energy sensitizers toward isomerizable azo- and ethenyl-type functionalities. These studies include both inter- and intramolecular sensitization.

Some of the most effective inorganic sensitizers are polypyridyl complexes containing low spin d^6 transition metals. This combination often allows electronic transitions to occur, such as metal-to-ligand charge transfer (MLCT).²⁶ When excited by light, an electron from the metal centered t_{2g} orbital is promoted to an empty π^* orbital of the

²⁶ Balzani, V.; Juris, A.; Venturi, M. *Chem. Rev.* **1996**, *96*, 759.

pyridyl ligand. Initially, the MLCT state is mostly singlet in character, but very rapidly intersystem crosses to the triplet state. From the $^3\text{MLCT}$ state, phosphorescence occurs in approximately 600 ns.²⁷ Polypyridyl transition metal complexes known to have triplet character include Ru(II), Re(I), Cu(I) and Os (II). Electronic states relevant to MLCT for $\text{Ru}(\text{bpy})_3^{2+}$ are shown in Figure 21.



^A Modeled on an illustration published by A. Vlcek, *Coord. Chem. Rev.* 2000, 200, 933.

Figure 21 Energy level diagram illustrating MLCT for $\text{Ru}(\text{bpy})_3^{2+}$.^A

Wrighton reported that triplet excited state $\text{Ru}(\text{bpy})_3^{2+}$ was an efficient intermolecular sensitizer for the isomerization of *trans*-stilbene (Figure 22).²⁸ At the photostationary

²⁷ Vlcek, A. *Coord. Chem. Rev.* 2000, 200-202, 933.

²⁸ Wrighton, M.; Markham, J. *J. Phys. Chem.* 1973, 77, 3042.

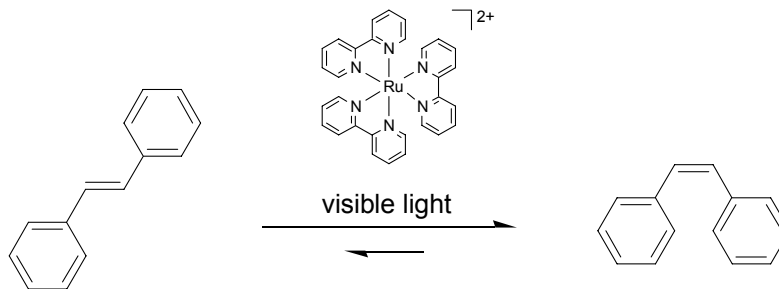


Figure 22 Intermolecular sensitization of *trans*-stilbene by $\text{Ru}(\text{bpy})_3^{2+}$.

state, 95% *cis*-stilbene had formed. This result was attributed to the nearly isoenergetic triplet energy values for $\text{Ru}(\text{bpy})_3^{2+}$ and *trans*-stilbene of 49 kcal/mol. In a similar study, photoinduced *cis* \rightarrow *trans* isomerization of stilbene was examined by using Cu(I) complexes with 2,2'-bipyridine, and 1,10-phenanthroline ligands.²⁹ These sensitizers were as efficient as $\text{Ru}(\text{bpy})_3^{2+}$ if the *cis*-stilbene/*trans*-stilbene mole ratio at the photostationary state are considered.

Fac-tricarbonylhalobis(4,4'-bipyridine)rhenium(I), one of only a few metal carbonyls known to be emissive in solution, was also demonstrated to undergo collisional triplet energy transfer with *trans*-stilbene (Figure 23).³⁰ At the photostationary state, 64 % *cis*-stilbene was formed regardless of whether starting from pure *cis* or pure *trans*. The initial *trans* \rightarrow *cis*-stilbene quantum yields are the same as those found for benzophenone sensitization, where it is assumed that every photon absorbed actually results in a *trans*-

²⁹ Sakaki, S.; Okitaka, I.; Ohkubo, K. *Inorg. Chem.* **1984**, *23*, 198.

³⁰ Wrighton, M.; Giordano, P. *J. Am. Chem. Soc.* **1979**, *101*, 2888.

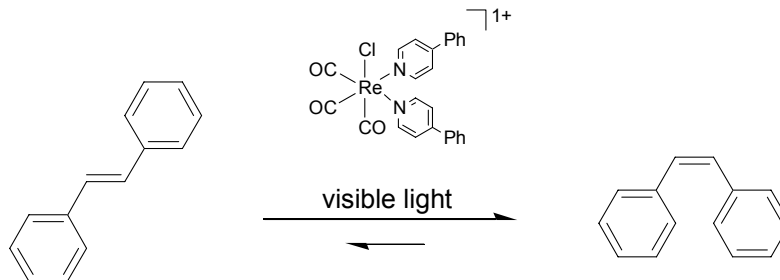


Figure 23 Intermolecular sensitization of *trans*-stilbene by $\text{fac-ClRe}(\text{CO})_3(\text{phpyr})_2^{2+}$.

stilbene triplet state.³¹ It was concluded that the excited $\text{fac-ClRe}(\text{CO})_3(4\text{-phenylpyridine})_2$ complexes also completely efficiently produce the *trans*-stilbene triplet excited state in the quenching process.

In addition to intermolecular energy transfer, intramolecular energy transfer has also been demonstrated. Earlier work by Wrighton and co-workers had shown intermolecular sensitization from the triplet excited states of Re(I) complexes to *trans*-stilbene. Subsequently, intramolecular energy transfer processes from the ³MLCT state to the azo- or stilbene-containing ligands coordinated to the Re(I) metal center were systematically studied. It was hypothesized that connecting an isomerizable unit to the Re(I) photosensitizer would shorten the energy transfer pathway.³²

Yam and coworkers synthesized a series of azo- and stilbene-containing rhenium(I) complexes. Upon irradiation, the isomerizable ligands would undergo reversible photoisomerization, which was monitored by electronic absorption and ¹H NMR spectroscopy. In the case of the stilbene-containing complex below (Figure 24),

³¹ Saltiel, J.; D'Agostino, J.; Megarity, E. D.; Metts, L.; Neuberger, K. R.; Wrighton, M. S.; Zafriou, O. C. *Org. Photochem.* **1973**, *1*, 3.

³² Yam, V. W.; Yang, Y.; Zhang, J.; Chu, W.; Zhu, N. *Organometallics* **2001**, *20*, 4918.

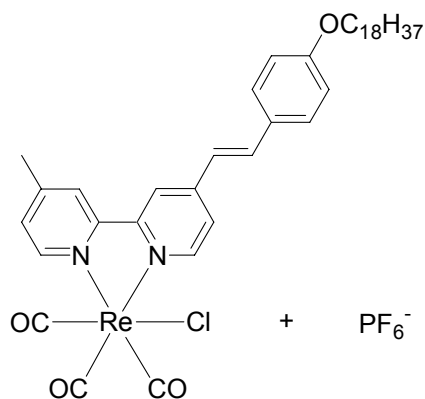


Figure 24 A rhenium(I) complex with a stilbene-containing ligand

photoisomerization occurred upon irradiation at the MLCT band at $\lambda = 480$ nm, while no photoisomerization was observed for the free ligand at the same wavelength. It was proposed that the presence of an efficient photosensitization pathway (i.e. intramolecular energy transfer from MLCT to the $^3\pi^*$) was responsible. Introduction of the Re metal center made it possible to photoisomerize stilbene-containing compounds using low energy visible light irradiation, without which higher energy irradiation would be necessary. For the above *trans*-complex, a photostationary state was not reported for irradiation at $\lambda = 480$ nm, but a photostationary state of 73% *cis*-isomer and 27% *trans*-isomer was achieved upon irradiation at $\lambda = 365$ nm.

Trinuclear *fac*-(diimine)Re(CO)₃ complexes bridged by a stilbene-like ligand have also exhibited a photoswitching property (Figure 25).^{33,34} These complexes showed only

³³ Sun, S.; Lees, A. J. *Organometallics* **2002**, *21*, 39.

³⁴ Sun, S.; Robson, E.; Dunwoody, N.; Silva, A.; Brinn, I.; Lees, A. J. *Chem. Commun.* **2000**, 201.

very weak luminescence and short excited state lifetimes, due to an efficient energy transfer process from the $^3\text{MLCT}$ excited state to the lowest $^3\pi^*$ excited state localized on the bipyridine ligand. Subsequent *trans* \rightarrow *cis* isomerization of the olefin double bond occurred. The amount of *cis,cis,cis*-bridged complex present in solution was typically in the range of 75-95% after 36 h of photolysis.

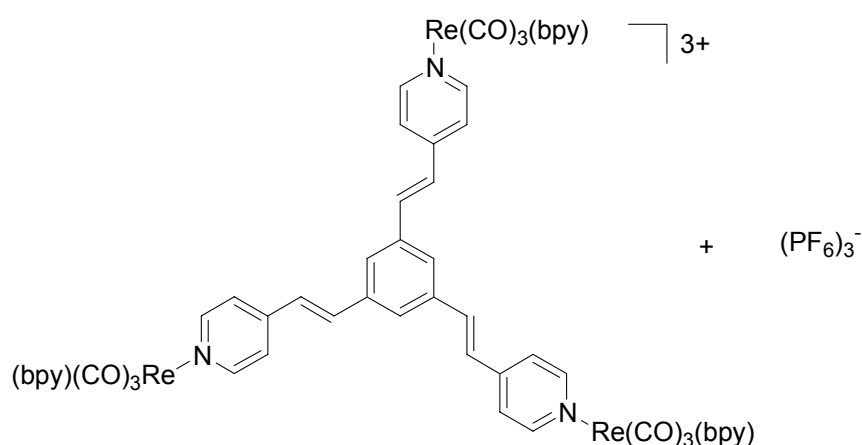


Figure 25 A trinuclear rhenium(I) complex linked by an isomerizable stilbene-like ligands.

In addition to rhenium complexes, ruthenium complexes have also been reported to undergo intramolecular isomerization processes. An investigation of the photochemistry of $\text{Ru}(2,2'\text{-bpy})_2(\text{cis-4-stilbazole})_2^{2+}$ was reported, where irradiation lead to *cis* \rightarrow *trans* isomerization of the stilbazole ligand (Figure 26).³⁵ It was determined that isomerization was wavelength dependent. Visible light irradiation produced a MLCT excited state resulting in intramolecular *cis* \rightarrow *trans* isomerization. Specifically, irradiation at $\lambda_{\text{exc}} = 436 \text{ nm}$ and $\lambda_{\text{exc}} = 570 \text{ nm}$ resulted in 85% and 87% *trans* isomer at the photostationary

³⁵ Zarnegar, P.; Bock, C. R.; Whitten, D. G. *J. Amer. Chem. Soc.* **1973**, *95*, 4367.

state, respectively. Irradiation at shorter wavelengths (313-366 nm) produced olefin-ligand excited states that are very similar in behavior to the excited states of the free ligand.

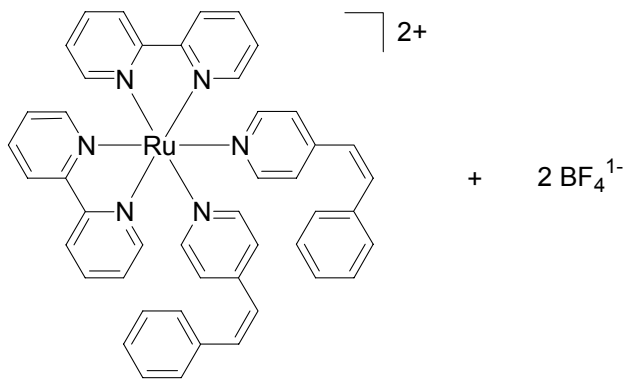


Figure 26 . $\text{Ru}(2,2'\text{-bpy})_2(\text{cis-4-stilbazole})_2^{2+}$.

3. RESULTS AND DISCUSSION

3.1. Intermolecular Sensitization of Precipitons

The literature reports described in Section 2.3 demonstrate that Ru(II) and Re(I) polypyridal complexes are capable of efficiently transferring triplet energy to stilbene compounds, causing *cis* ↔ *trans* isomerization. These energy transfer processes can occur intermolecularly between the metal complex and stilbene, or intramolecularly through a stilbene-containing pyridal ligand. It seemed reasonable that the isomerization processes in these systems could be extended to our stilbene-type precipitons. We decided the best starting point for these studies would be to investigate intermolecular sensitizer-precipiton interactions.

Our initial work focused on the intermolecular triplet sensitization of 1,2-bis-(biphenyl)ethene alcohol precipiton **3Z** using Ru(bpy)₃Cl₂ (Figure 27). Ru(bpy)₃Cl₂ was an attractive triplet sensitizer candidate due to its commercial availability and air

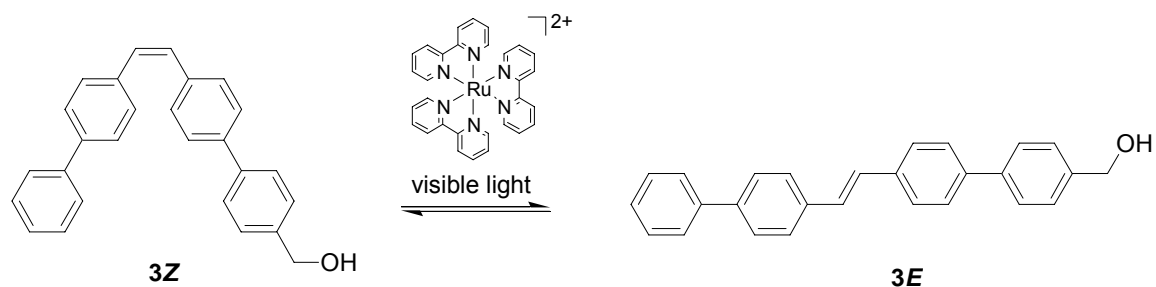


Figure 27 Intermolecular sensitization of precipiton **3Z** by $\text{Ru}(\text{bpy})_3^{2+}$.

stability. **3Z** was synthesized using previously established methods. Because bipyridyl ligands strongly coordinate to ruthenium, and $\text{Ru}(\text{bpy})_3\text{Cl}_2$ has no additional coordination sites available, we reasoned that ligand exchange with **3Z** would be unlikely.

A fundamental goal of this investigation was to acquire understanding of how effective $\text{Ru}(\text{bpy})_3^{2+}$ is at isomerizing **3Z** through intermolecular sensitization. This was possible by studying photoisomerization kinetics, which requires observing the isomerization process over time. Two basic methods were developed for observing the isomerization process, designated “A” and “B”.

In Method A, a solution of **3Z** (20 mM), $\text{Ru}(\text{bpy})_3^{2+}$ (50 μM), and an internal standard (20 mM) was added to a single NMR tube. The tube was placed in front of a light source and irradiated for a specific time interval. After that time interval, the tube was removed from the light and a ^1H NMR measurement was taken. After recording the measurement, the tube was placed in front of the light source again, and the procedure was repeated until the reaction was complete. Method A is illustrated in Figure 28.

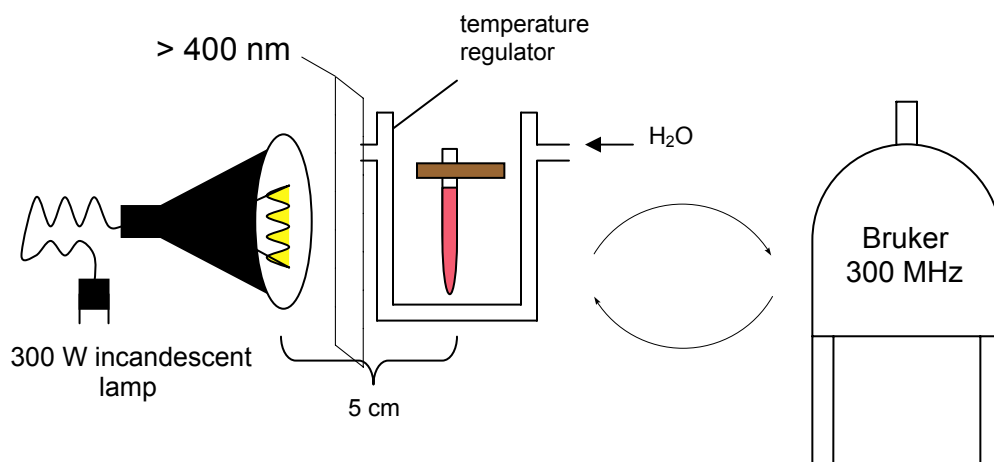


Figure 28 Method A for kinetic data collection.

In Method B, data was acquired from parallel experiments. A reaction mixture was divided among ten or more individual NMR tubes. Each tube was designated to represent a specific time period of irradiation. The tubes were gathered together and irradiated simultaneously. When an irradiation time period had expired, the designated NMR tube was removed from the light source and a 1H NMR measurement was taken. The tube was not irradiated further. This process was performed with each NMR tube until the reaction was complete. Method B is illustrated in Figure 29.

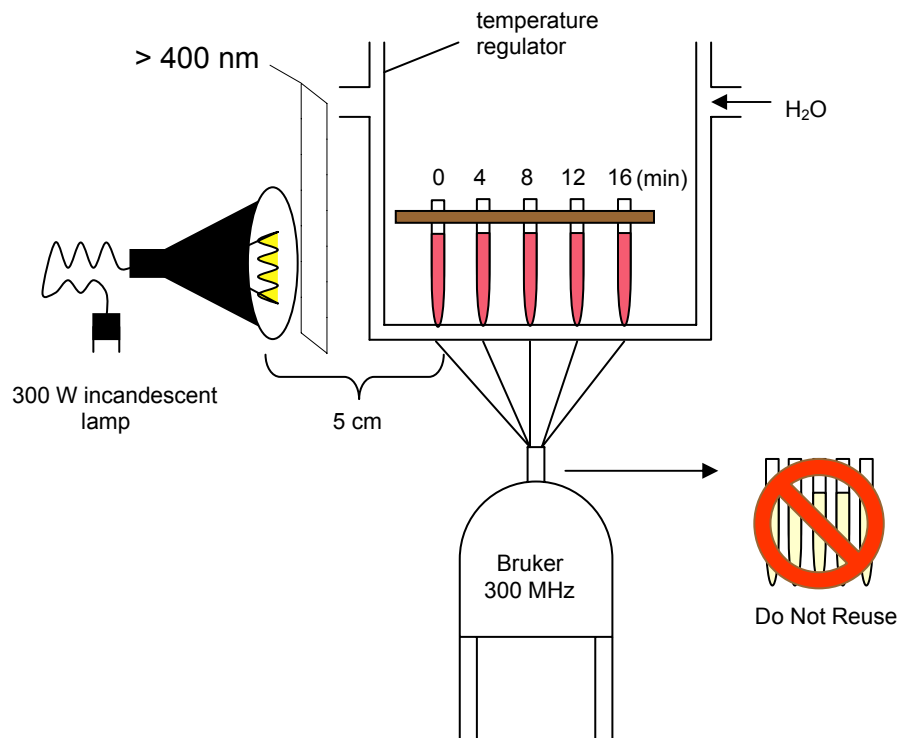


Figure 29 Method B for kinetic data collection.

It was anticipated that $\text{Ru}(\text{bpy})_3^{2+}$ sensitized isomerization of **3Z** would obey first-order kinetics, and thus a plot of the reaction progress versus time would be a simple exponential curve. To test this, a solution of 20 mM **3Z**, 50 μM $\text{Ru}(\text{bpy})_3^{2+}$, and an internal standard (20 mM) was prepared in air-equilibrated 1/1 $\text{CD}_3\text{CN}/\text{CD}_2\text{Cl}_2$ and syringed into 11 NMR tubes. The solution was irradiated at $\lambda_{\text{exc}} \geq 400$ nm and the ^1H NMR spectroscopic changes of **3Z** were observed by Method B. A plot for the reaction (Figure 30A) was not linear and had a distinct sigmoidal shape during the first 10 min. One possible explanation we considered is autocatalysis. If the *cis* \rightarrow *trans* isomerization is first-order in **3Z**, but the reaction is catalyzed by **3E**, as **3E** is formed the reaction rate will increase. The first-order plot will deviate from linearity as the plot slope increases. To test this, **3E** (~ 3 mg) was added to a solution of 20 mM **3Z**, 50 μM $\text{Ru}(\text{bpy})_3^{2+}$, and an

internal standard (20 mM) in air-equilibrated 1/1 CD₃CN/CD₂Cl₂ and syringed into 11 NMR tubes. The solution was irradiated at $\lambda_{\text{exc}} \geq 400$ nm and the ¹H NMR spectroscopic changes of **3Z** were observed by Method B. In the presence of **3E** seed crystals, the sigmoidal shape was significantly diminished (Figure 30B) and the initial reaction rate (as judged by the amount of isomerization observed by NMR after 4 min) was faster than without **3E** seed crystals.

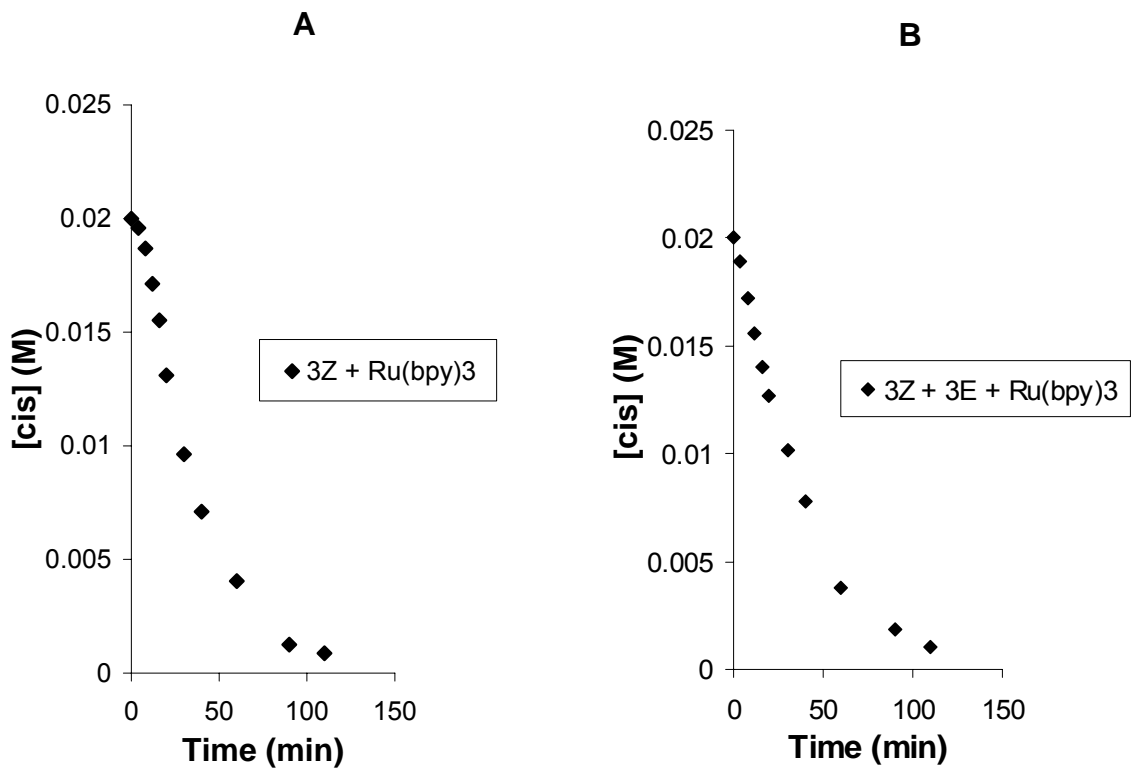


Figure 30 Reaction progress of 3Z → 3E isomerization with/out 3E ([3Z] = 20 mM, [3E] = saturated; [Ru(bpy)₃²⁺] = 50 μM, solvent = 1/1 CD₃CN/CD₂Cl₂).

Data from the reaction containing **3E** seed crystals gave a reasonable fit to first order kinetics ($R^2 = 0.997$)(Figure 31). However, there may be some small systematic deviation. A possible explanation is Ostwald ripening of the precipitate, which may interfere with the reaction kinetics. A plot of reaction 1 to reversible first-order kinetics did not fit a reversible first-order rate law as well ($R^2 = 0.986$)(Figure 31).

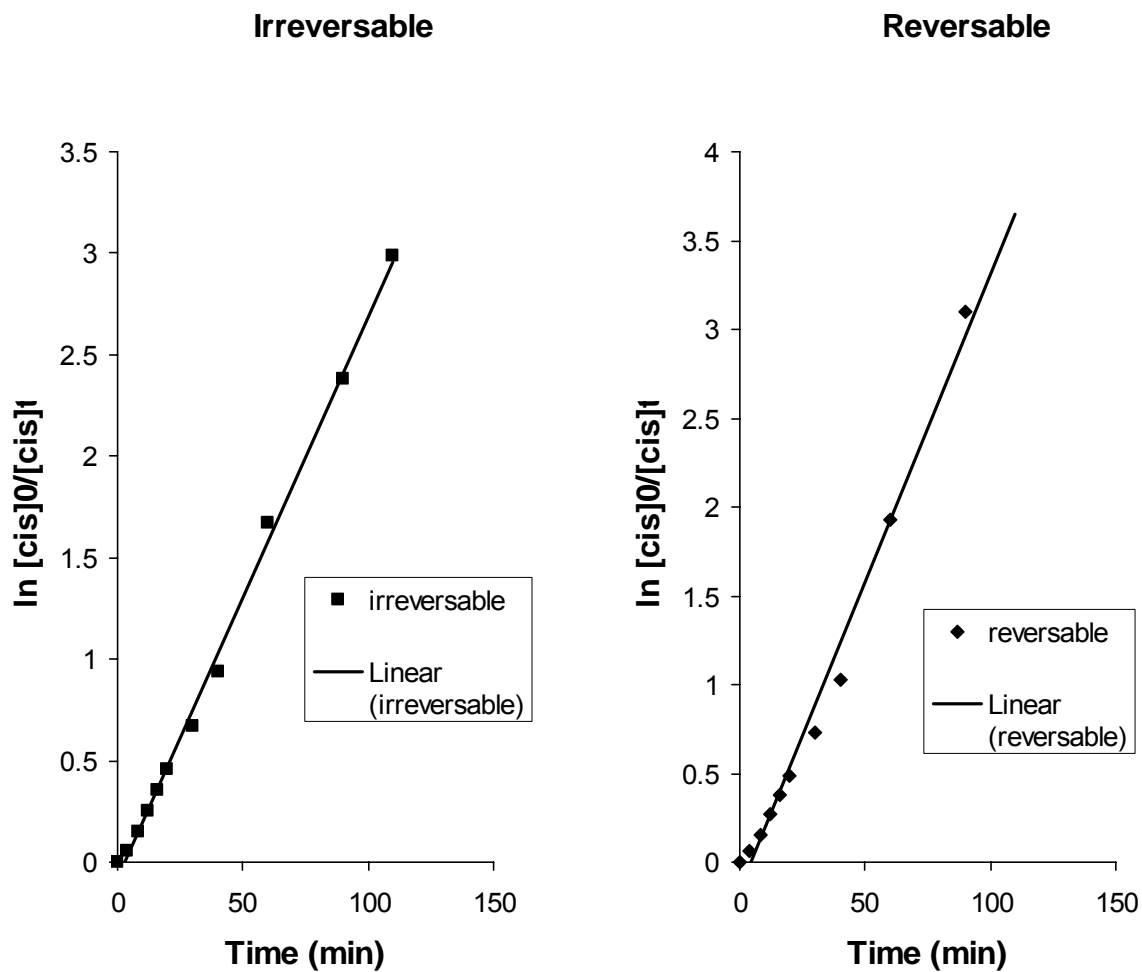


Figure 31 Reaction 1 plotted according to an irreversible first-order rate law ($k_{\text{obs}} = 0.028 \text{ s}^{-1}$) and a reversible first-order rate law ($k_{\text{obs}} = 0.035 \text{ s}^{-1}$).

If **3E** was acting as a catalyst for **3Z** isomerization, a similar rate enhancement should be observed upon irradiation without sensitizer $\text{Ru}(\text{bpy})_3^{2+}$. To test this, a 20 mM solution of **3Z**, and internal standard was prepared in air-equilibrated 99/1 $\text{CD}_3\text{CN}/\text{D}_2\text{O}$ and syringed into an NMR tube. In reaction 2 a small amount of **3E** (~ 3 mg) was then added to the tube, and the reaction mixture was sonicated for 2 min to insure saturation of **3E**. The reaction mixtures were irradiated at $\lambda_{\text{exc}} \geq 400$ nm and the ^1H NMR spectroscopic changes of **3Z** were observed by the Method B. A plot for each reaction is given in Figure 32. No rate enhancement was observed when **3E** seed crystals were initially present.

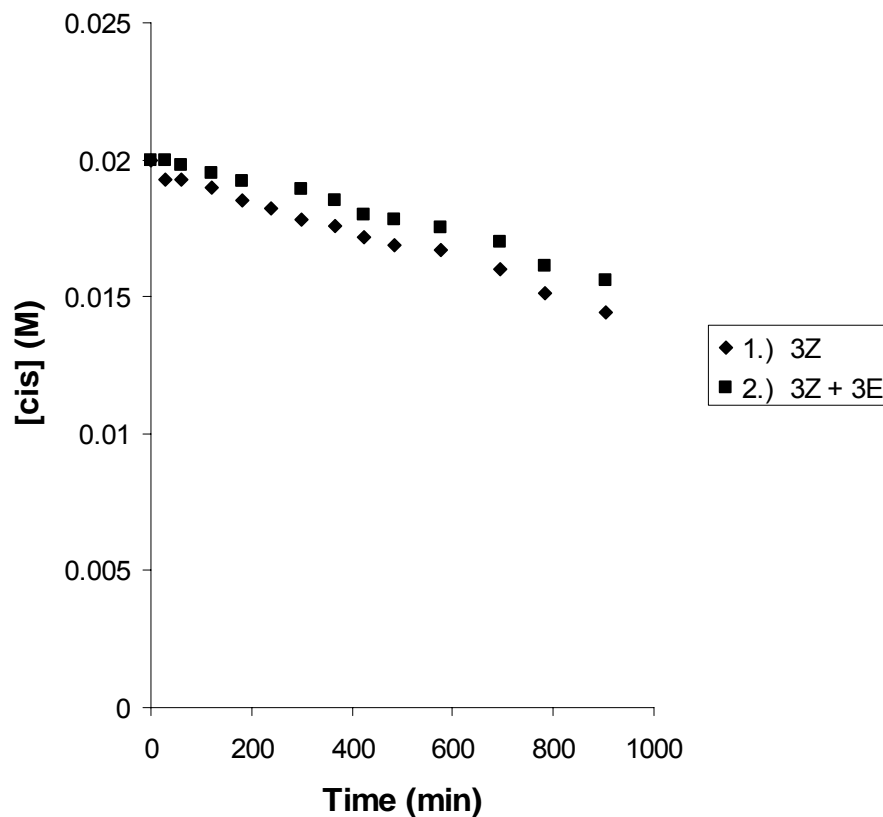


Figure 32 Reaction progress of $3Z \rightarrow 3E$ isomerization with/out $3E$ and $\text{Ru}(\text{bpy})_3^{2+}$ ($[3Z] = 20 \text{ mM}$, $[3E] = \text{saturated}$; solvent = 99/1 $\text{CD}_3\text{CN}/\text{D}_2\text{O}$).

A second explanation we considered focused on the large amount of precipitate that quickly forms early in the reaction. We hypothesized that the precipitate may impede light from penetrating the NMR tube, and thus distort the isomerization rates. To test this hypothesis, a solution of 20 mM **3Z**, 50 μM $\text{Ru}(\text{bpy})_3^{2+}$, and an internal standard was prepared in air-equilibrated 1/1 $\text{CD}_3\text{CN}/\text{CD}_2\text{Cl}_2$ and syringed into 12 NMR tubes. The reaction mixtures were irradiated at $\lambda_{\text{exc}} \geq 400 \text{ nm}$ and the ^1H NMR spectroscopic changes of **3Z** were observed. Reaction 1 was monitored by Method B and reaction 2 was monitored by Method A. A plot for each reaction is given in Figure 33.

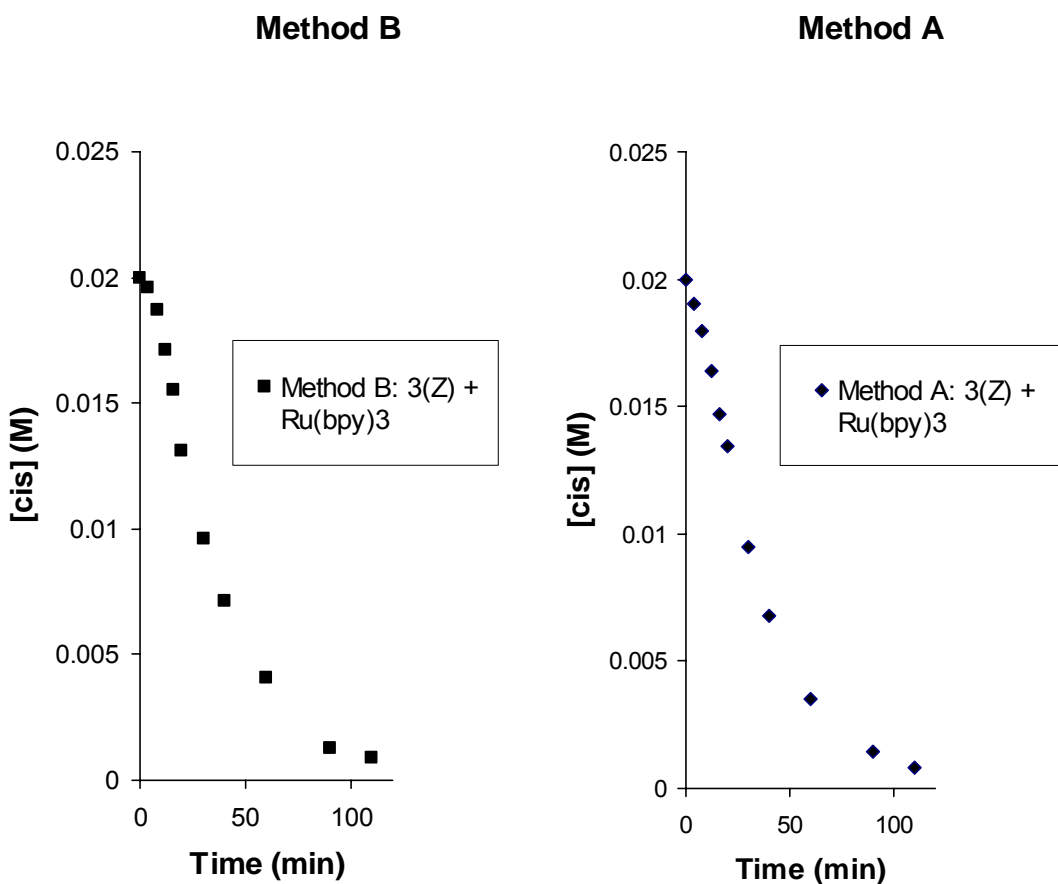


Figure 33 Reaction progress of $3Z \rightarrow 3E$ isomerization using Method A and Method B ($[3Z] = 20$ mM, $[\text{Ru}(\text{bpy})_3^{2+}] = 50$ μM , solvent = 1/1 $\text{CD}_3\text{CN}/\text{CD}_2\text{Cl}_2$).

If the precipitate was responsible for retarding the isomerization rate, then the “disturbed” method should reduce this effect by aggregating the precipitate and accelerating precipitation. Indeed, when the “disturbed” method is employed, the sigmoidal shape at the beginning of the reaction was diminished.

In the $\text{Ru}(\text{bpy})_3^{2+}$ sensitized isomerizations described above, the initially clear and homogeneous reactions mixtures were transformed into a uniform semi-opaque material within 4 min of irradiation regardless of whether Method A or B was used. We suspect

this suspension contains micro- or nanocrystals because no actual precipitation particles could be seen with the naked eye, and no precipitate settling was observed. In general, crystal development begins with molecules meeting and coalescing to form small embryos as they randomly diffuse through solution.³⁶ The embryos grow to a critical size above which they transform into crystals. Ostwald ripening can occur, where small crystals transform into large crystals.^{37,38} We have observed that if the semi-opaque material formed during isomerization is disturbed by physically handling the NMR tube, aggregation occurs and visible precipitate particles appear. In contrast, if the semi-opaque suspension is not handled (thus “undisturbed”) during isomerization or at any time before the NMR, aggregation resulting in visible precipitate particles is delayed and the optical properties of the solution are changed. This change affects the light penetration and the progress of the isomerization.

We propose that a critical distinction between Method A and Method B is the degree in which the reaction mixture is disturbed. The effect of disturbance becomes significant in kinetic studies whenever precipitation occurs. In the case of 20 mM **3Z**, **3E** product reaches saturation early in the reaction (within 2 min), which results in a large amount of precipitate. If the semi-opaque material (which is formed first) is undisturbed as in Method B, it will hinder light from penetrating the NMR tube, and thus retard the isomerization rate. If the semi-opaque material is aggregated by disturbance as in Method A, the resulting precipitate “agglomerations” permit additional light to penetrate the tube, allowing reaction kinetics to be less impeded.

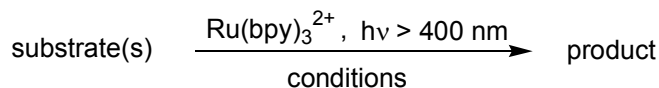
³⁶ Boistelle, R.; Astier, J.P. *J. Cryst. Growth* **1988**, *90*, 14.

³⁷ Ostwald, W. *Z. Phys. Chem.* **1897**, *22*, 289.

³⁸ Horn, D.; Rieger, J. *Angew. Chem. Int. Ed.* **2001**, *40*, 4330.

In summary, we conclude from the above experiments that the large amount of precipitate generated during the isomerization of **3Z** \rightarrow **3E** was primarily responsible for diverting the apparent reaction kinetic data from obeying irreversible first-order rate theory. Using Method A, in which the NMR tubes were not disturbed, micro- and nanocrystal formation impeded light from penetrating the reaction vessel thus decreased the reaction rate. When the solution was agitated, particles agglomerated to form precipitate aggregates, allowing more light to penetrate the reaction vessel. The precipitation process is expedited by adding **3E** to the reaction mixture before irradiation. We also observed that the lamp temperature affected isomerization rates. Beginning reaction rates were slightly faster if a pre-heated lamp is used. Table 2 summarizes the isomerization rates in each of the discussed conditions. The rates were calculated using the amount of isomerization observed by NMR after 4 min.

Table 2 Summary of 3Z → 3E isomerization rates after 4 min ([3Z] = 20 mM, [Ru(bpy)₃²⁺] = 50 μM, [3E] = saturated, solvent = 1/1 CD₃CN/CD₂Cl₂).



Substrates	Conditions	Slope (x 10 ⁻⁴)	k (min ⁻¹)	pseudo 1 st -order rxn rate (x 10 ⁻⁴)	% 3E (110 min)
3Z	hot lamp/ disturbed	2.46	0.012	2.46	96
3Z	hot lamp/ undisturbed	1.03	0.005	1.03	95
3Z + 3E	hot lamp/ disturbed	3.76	0.019	3.76	95
3Z + 3E	hot lamp/ undisturbed	2.73	0.014	2.73	95

3.2. Intramolecular Sensitization of Precipitons

The experiments described in Section 3.1 demonstrate that isomerization of **3Z** via intermolecular sensitization by Ru(bpy)₃²⁺ is a favorable process. A goal of this project is to determine if metal binding to a precipiton can facilitate intramolecular sensitization and cause isomerization. To answer this question we planned to covalently attach a metal sensitizer to a precipiton and observe if the isomerization rate increases as a result of intramolecular energy transfer. Ru(bpy)₃²⁺ is an effective intermolecular sensitizer for precipitons, so chemically attaching Ru(bpy)₃²⁺ to a precipiton may allow for intramolecular energy transfer. As previously described, triplet energy transfer from a

donor to an acceptor can occur through two basic mechanisms defined by Förster and Dexter. We designed two different types of ruthenium containing precipitons to explore triplet energy transfer through Förster- and Dexter-type mechanisms.

Ru-based polypyridine units attached to an aromatic chromophore have been studied as components for supramolecular devices.³⁹ Understanding and controlling the flow of energy from the initially excited chromophore to the site where the energy is ultimately localized is one of those goals. Recently, Barigelletti, Ward and coworkers reported the synthesis of a bichromophoric species containing a $\text{Ru}(\text{bpy})_3^{2+}$ and pyrene unit linked together by an ether spacer (Figure 34).⁴⁰ Selective excitation at $\lambda_{\text{exc}} = 532 \text{ nm}$ of the $\text{Ru}(\text{bpy})_3^{2+}$ unit lead to a Ru-based

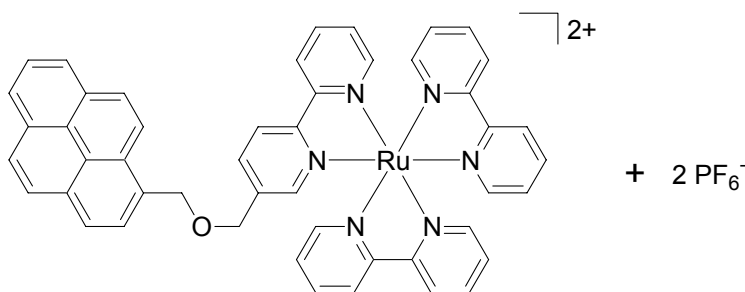


Figure 34 A Ru-pyr complex exhibiting Förster-type intramolecular energy transfer.

luminescence and a pyr-based absorption. A Förster-type energy transfer was concluded to be responsible, based on the critical transfer radius R_0 (i.e. the distance at which the

³⁹ Wilson, G.; Launikonis, A.; Sasse, W.; Mau, A. *J. Phys. Chem. A* **1997**, *101*, 4860. (b) Sohna, J.; Carrier, V.; Fages, F.; Amouyal, E. *Inorg. Chem.* **2001**, *40*, 6061. (c) Juris, A.; Prodi, L. *New J. Chem.* **2001**, *25*, 1132. (d) Tyson, D.; Bignozzi, C.; Castellano, F. *J. Am. Chem. Soc.* **2002**, *124*, 4562.

⁴⁰ Morales, A.; Accorsi, G.; Armaroli, N.; Barigelletti, F.; Pope, S.; Ward, M. D. *Inorg. Chem.* **2002**, *41*, 6711.

energy transfer efficiency is 50%) estimated to be 29 Å and the average center-to-center separation between pyr and Ru chromophores calculated to be 13.6 Å. Precipiton **9Z** was our synthetic target (Figure 35). **9Z** consists of a 1,2-bis(biphenyl)ethene precipiton connected to a Ru(bpy)₃²⁺ unit by an ether spacer. Based on the work by Barigelletti and Ward, we expected **9Z** to also undergo a Förster-type mechanism.

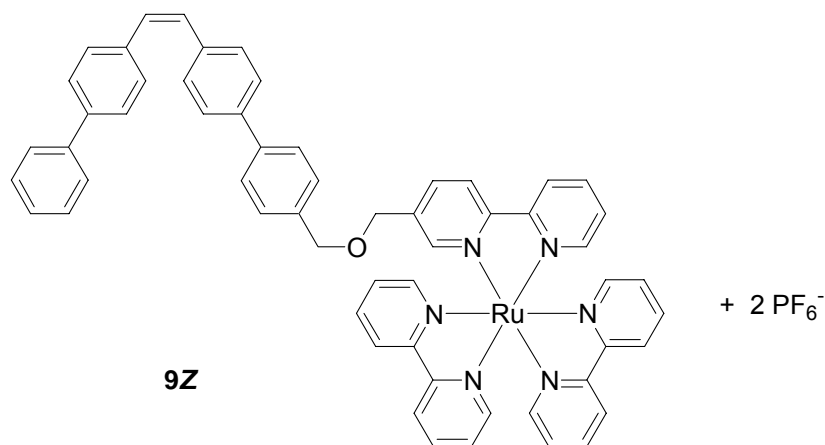


Figure 35 A precipiton linked to a sensitizer.

Balzani, Belser, and coworkers reported the synthesis and photochemistry of a heterodinuclear $[\text{Ru}(\text{bpy})_3\text{-(ph)}_3\text{-Os}(\text{bpy})_3]^{4+}$ complex (Figure 36), and concluded it underwent energy transfer through a Dexter-type mechanism.⁴¹ Upon excitation at $\lambda = 435$ nm, the phosphorescence intensity of the Ru-based unit was quenched and accompanied by a corresponding sensitization of the Os-based unit. The critical transfer radius R_0 was calculated to be 10 Å according to Förster mechanism parameters, a value

⁴¹ Schlicke, B.; Belser, P.; De Cola, L.; Sabbioni, E.; Balzani, V. *J. Am. Chem. Soc.* **1999**, *121*, 4207.

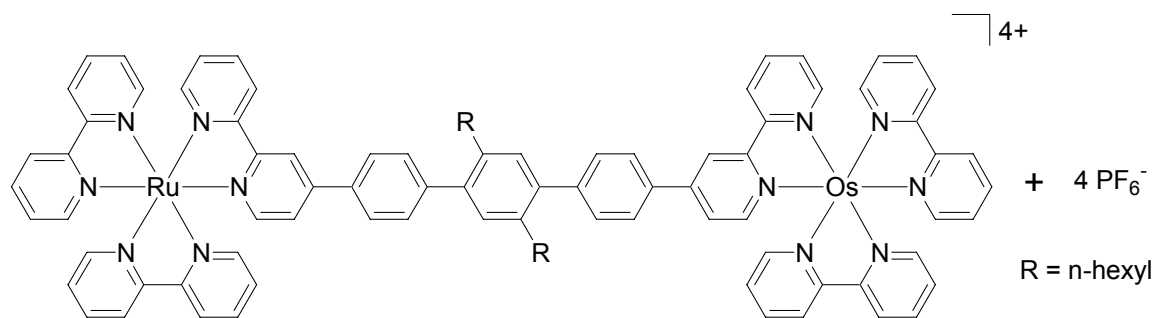


Figure 36 A Ru-Os complex exhibiting Dexter-type intramolecular energy transfer.

considerably smaller than the Ru-Os distance of 24 Å for the complex. The calculated Förster rate constant over the 24 Å distance was 2-3 times smaller than the experimental rate constant, and could not account for the fast energy transfer process experimentally observed. The experimental energy transfer rate constant was $6.7 \times 10^8 \text{ s}^{-1}$ (298 K), and it appropriately fit a Dexter-type energy transfer mechanism. We designed precipiton **14Z** as a second synthetic target (Figure 37). **14Z** consists of a 1,2-bis(biphenyl)ethene

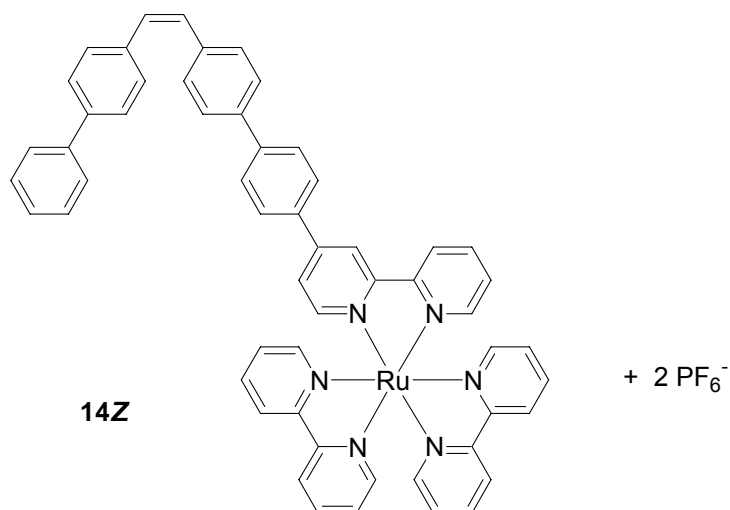


Figure 37 A precipiton linked to a sensitizer.

precipiton unit connected to a Ru(bpy)₃²⁺ unit by a phenylene spacer. Based on the work by Belser and Balzani, we expected **14Z** to also undergo a Dexter-type mechanism.

3.3. Förster Class Precipiton

3.3.1. Synthesis

The Förster precipiton **9Z** was prepared according to the synthetic sequence beginning in Figure 38. Synthesis of the monosubstituted 1,2-bis(biphenyl)ethene alcohol precipiton **3Z** commenced with a Wittig reaction between biphenylcarboxaldehyde and 4-

bromobenzyl-triphenylphosphonium bromide **1** in the presence of powdered potassium hydroxide and 18-crown-6 to generate **2Z**. This product was subject to a Suzuki reaction with 4-hydroxymethylphenylboronic acid to yield alcohol **3Z**.

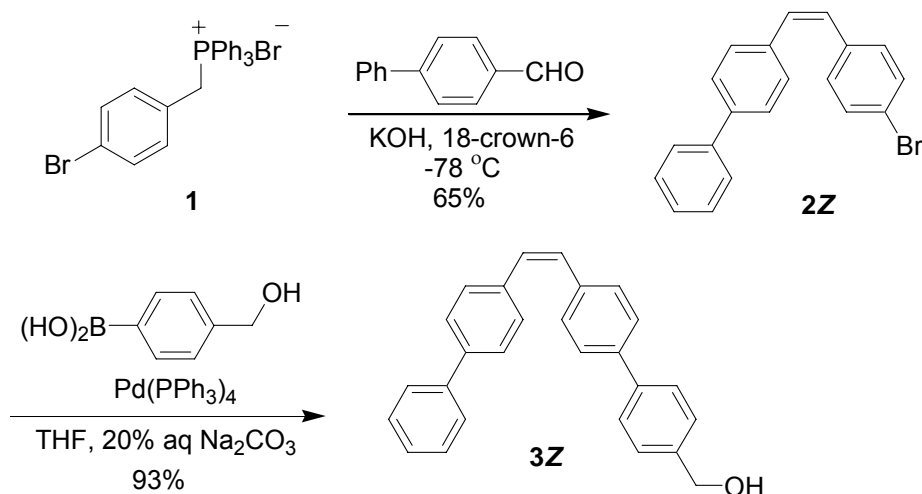


Figure 38 Synthesis of 1,2-bis(biphenyl)ethene alcohol precipiton **3Z**.

Separately, 5-methyl-2,2'-bipyridine **7** was synthesized according to protocol outlined by Ballardini, Stoddart, and coworkers (Figure 39).⁴² 2-Acetylpyridine **4** was transformed to (2-pyridacyl)pyridium iodide **5** by treatment with I₂ in pyridine. Next, **5** underwent ring annulation in the presence of methacrolein and ammonium acetate to generate **6**. Bipyridine **6** underwent AIBN-initiated bromination with NBS in CCl₄,

⁴² Ballardini, R.; Balzani, V.; Clemente-Leon, M.; Credi, A.; Gandolfi, M.; Ishow, E.; Perkins, J.; Stoddart, F.; Tseng, H.; Wenger, S. *J. Am. Chem. Soc.* **2002**, *124*, 12786.

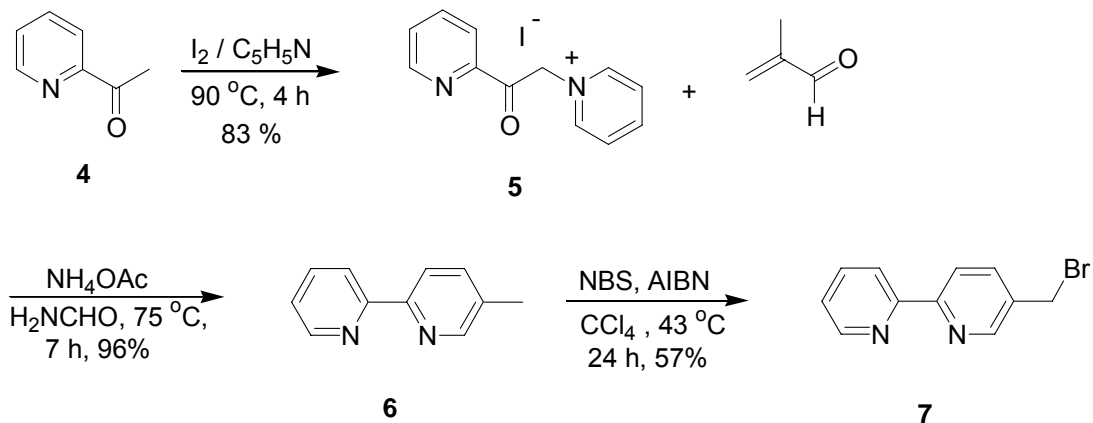


Figure 39 Synthesis of 5-bromomethyl-2,2'-bipyridine **6**.

giving 5-bromomethyl-2,2'-bipyridine **7**. Alkylation of alcohol **3Z** with bipyridine **7** using NaH afforded the bipyridine-coupled Förster precipiton **8Z** in 73 % yield (Figure 40).

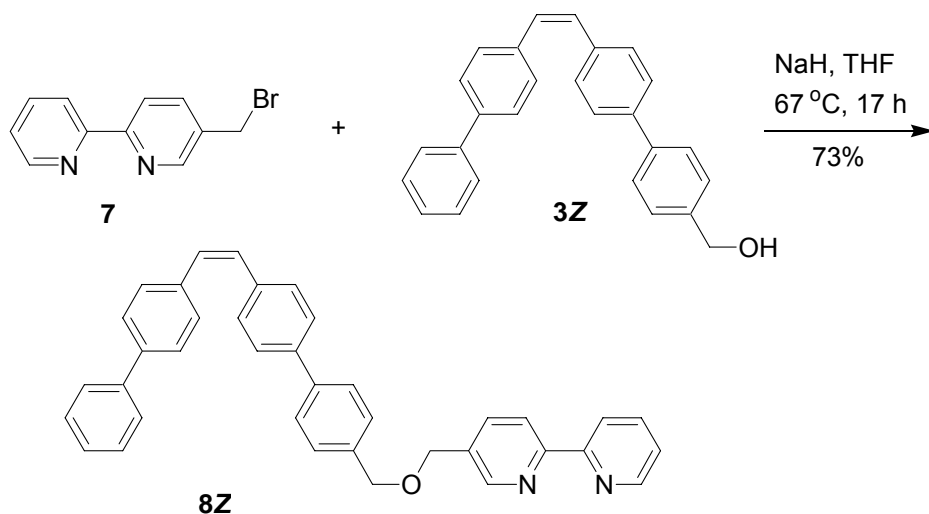


Figure 40 Alkylation of **7** with **3Z** to generate Förster precipiton **8Z**.

The ruthenium complex **9Z** was obtained in 49 % yield by treating *cis*-dichlorobis(2,2'-bipyridine)ruthenium(II)dihydrate with the ligand **8Z** and silver hexafluoroantimonate(V) in acetone,⁴³ followed by counterion exchange with ammonium hexafluorophosphate (Figure 41).

⁴³ Holder, E.; Schoetz, G.; Schurig, V.; Lindner, E. *Tetrahedron: Asymmetry* **2001**, *12*, 2289.

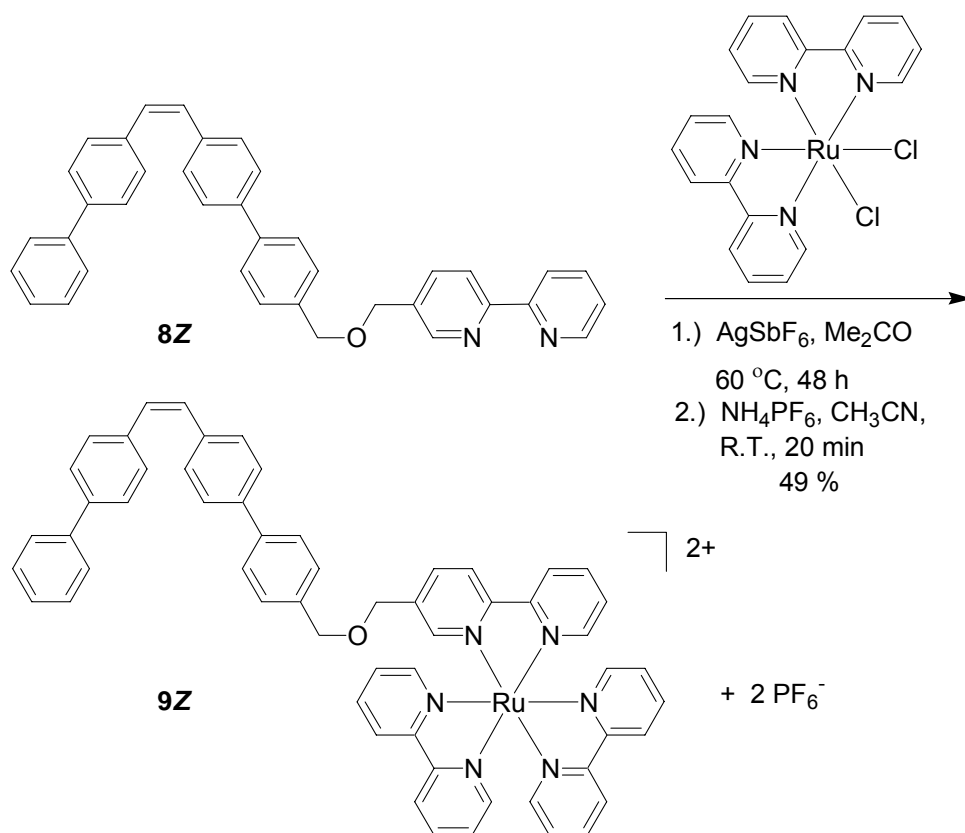


Figure 41 Synthesis of Ru-bound Förster precipiton **9Z**.

The corresponding *trans* isomer, **9E**, was prepared according to the synthetic sequence shown in Figure 42. Unmetallated Förster precipiton **8Z** was treated with diphenyl diselenide and heated in refluxing THF for 24 h to induce isomerization. The resulting product **8E** was treated with *cis*-dichlorobis(2,2'-bipyridine)ruthenium(II)dihydrate and silver hexafluoroantimonate(V) in acetone, followed by counterion exchange with ammonium hexafluorophosphate to obtain a mixture of E/Z isomers. A difficult separation employing repeated recrystallizations generated **9E** in 5 % yield. It was discovered in later experiments that **9Z** ↔ **9E** isomerization is very light sensitive.

Incidental light exposure from the overhead laboratory lamps may have caused some **9E**
 → **9Z** isomerization during the synthesis of **9E**.

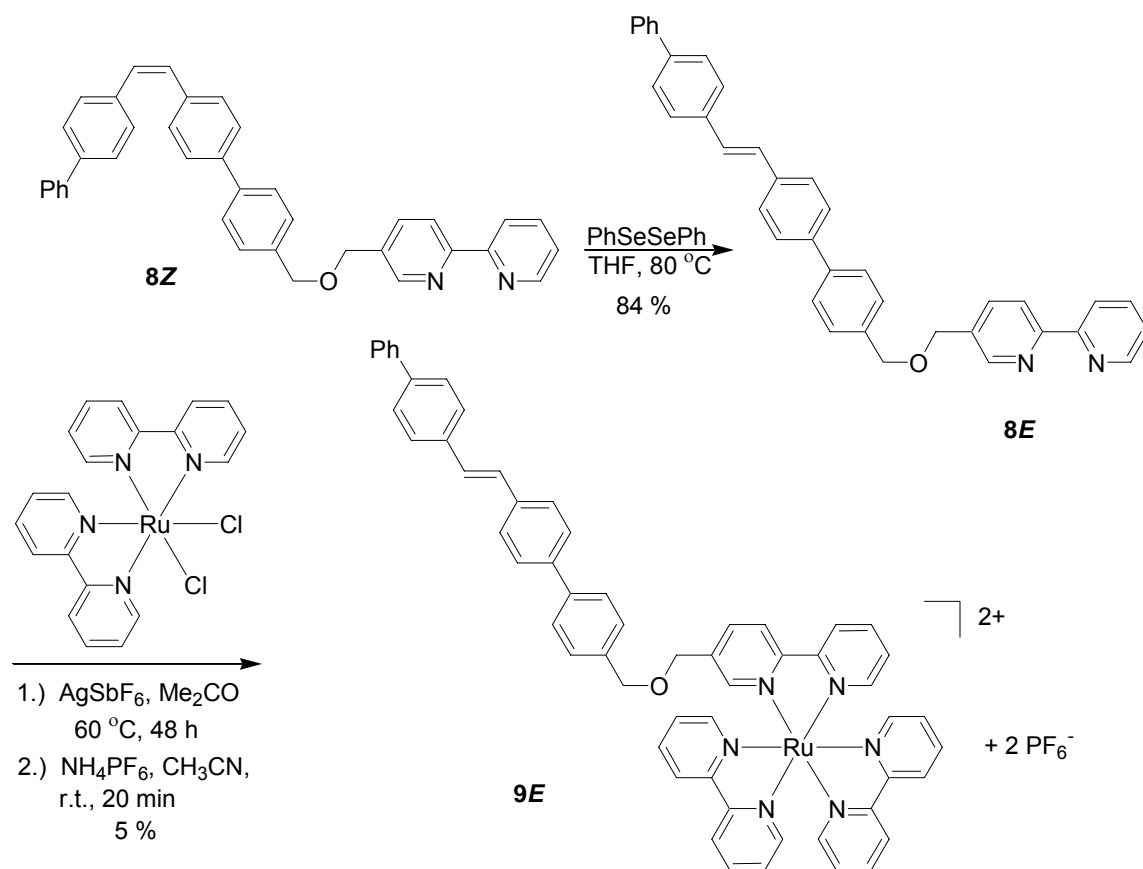


Figure 42 Synthesis of Ru-bound Förster precipiton **9E**.

3.3.2. Absorption and Emission Spectroscopy

For Förster energy transfer to occur, it is expected that the ether spacer in **9Z** provides both a spatial and electronic separation between the Ru and precipiton photoactive units.

The absorption spectrum of **9Z** should then be composed of the additive properties of the scarcely interacting Ru-based and precipiton based chromophores. Figure 43 displays the absorption spectra and Table 3 summarizes the absorption spectroscopic data for **9Z**, **8Z**, **3Z**, **9E**, $\text{Ru}(\text{bpy})_3^{2+}$, and 2,2'-bipyridine in acetonitrile.

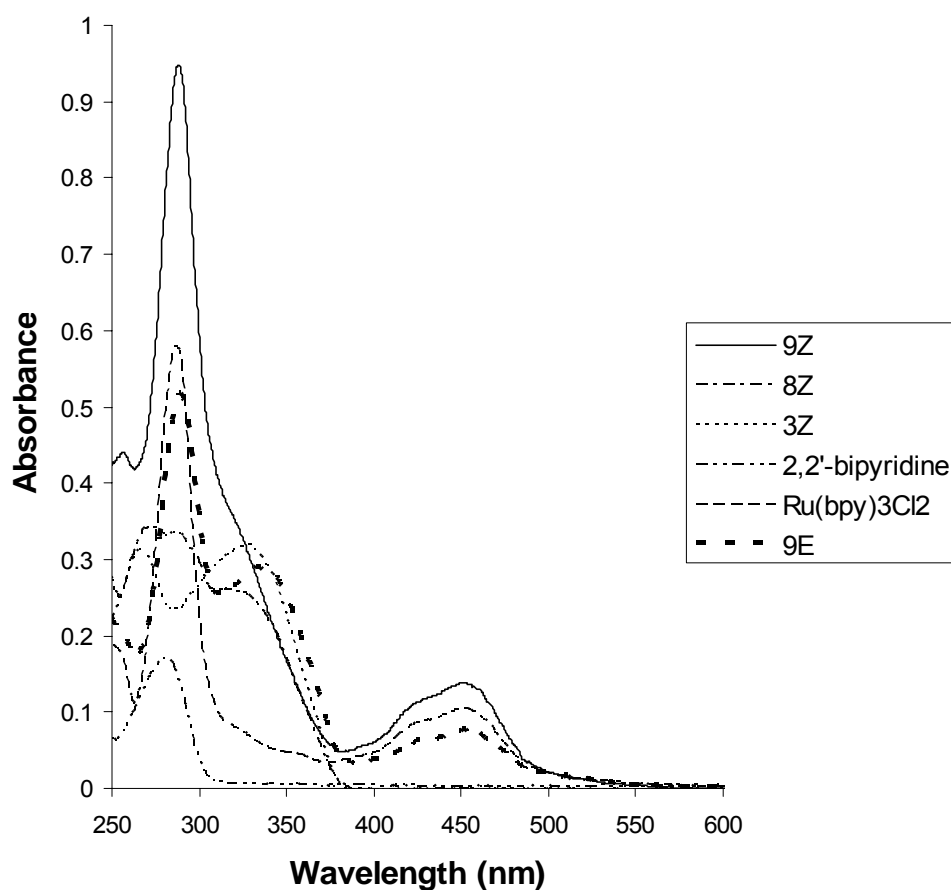


Figure 43 Absorption spectra of complex **9Z** and related components (10 μM , air equilibrated CH_3CN , $T = 298 \text{ K}$).

Table 3 Summary of the absorption spectroscopic data.

Compound	λ_{max}, nm (ϵ, M⁻¹ cm⁻¹)
3Z	268 (31 000), 331 (31 300)
8Z	274 (34 200), 290 (33 200), 330(24 800)
9Z	290 (91 800), 450 (13 700)
9E	290 (51 500), 339 (28 700), 456 (7 400)
Ru(bpy) ₃ ²⁺	288 (57 400), 450 (10 500)
2,2'-bipyridine	294 (16 900)

For complex **9Z**, the band maximum at 450 nm originates from the MLCT (Ru \rightarrow bpy) transition, as seen at the same wavelength for Ru(bpy)₃²⁺. The features in the 270 – 300 nm spectroscopic region are of bpy centered $\pi \rightarrow \pi^*$ transitions, as also observed for free 2,2'-bipyridine ligand and Ru(bpy)₃²⁺ in the same location (260 – 300 nm). The absorption characteristics in the region 260 – 370 nm are identified as being $\pi \rightarrow \pi^*$ transitions of precipiton origin. **3Z** and uncomplexed Förster precipiton **8Z** also exhibit $\pi \rightarrow \pi^*$ transitions in this same vicinity.

Table 4 Summary of the emission spectroscopic data. a $\lambda_{\text{exc}} = 450$ nm. b $\lambda_{\text{exc}} = 285$ nm.

Compound	λ_{em}, nm
3Z	315 ^b
9Z	612 ^a
9E	612 ^a
Ru(bpy) ₃ ²⁺	613 ^a

The room-temperature emission data of **9Z** and **9E** are shown in Table 4.⁴⁴ For comparative purposes, emission spectra for **3Z** and Ru(bpy)₃²⁺ are also listed. Figure 44 displays the room-temperature (uncorrected) excitation spectra of **9Z** and **9E** as observed at $\lambda_{\text{em}} = 610$ nm in air-equilibrated acetonitrile, in addition to the emission spectra of **9Z** and **9E** obtained using $\lambda_{\text{exc}} = 450$ nm. The excitation spectra are characterized by features typical of the Ru(bpy)₃²⁺ chromophore (Ru \rightarrow bpy MLCT at 450 nm and bpy $\pi \rightarrow \pi^*$ transitions at 290 nm) and of the 1,2-bis(biphenyl)ethene precipiton unit (260 – 370 nm range), consistent with their absorption profiles. The emission spectra of **9Z** and **9E**, when irradiated at $\lambda_{\text{exc}} = 450$ nm, exhibit overlapping profiles, with the band maxima

⁴⁴ A collaborative effort with Professor Sephane Petoud and Demetra Chengelis.

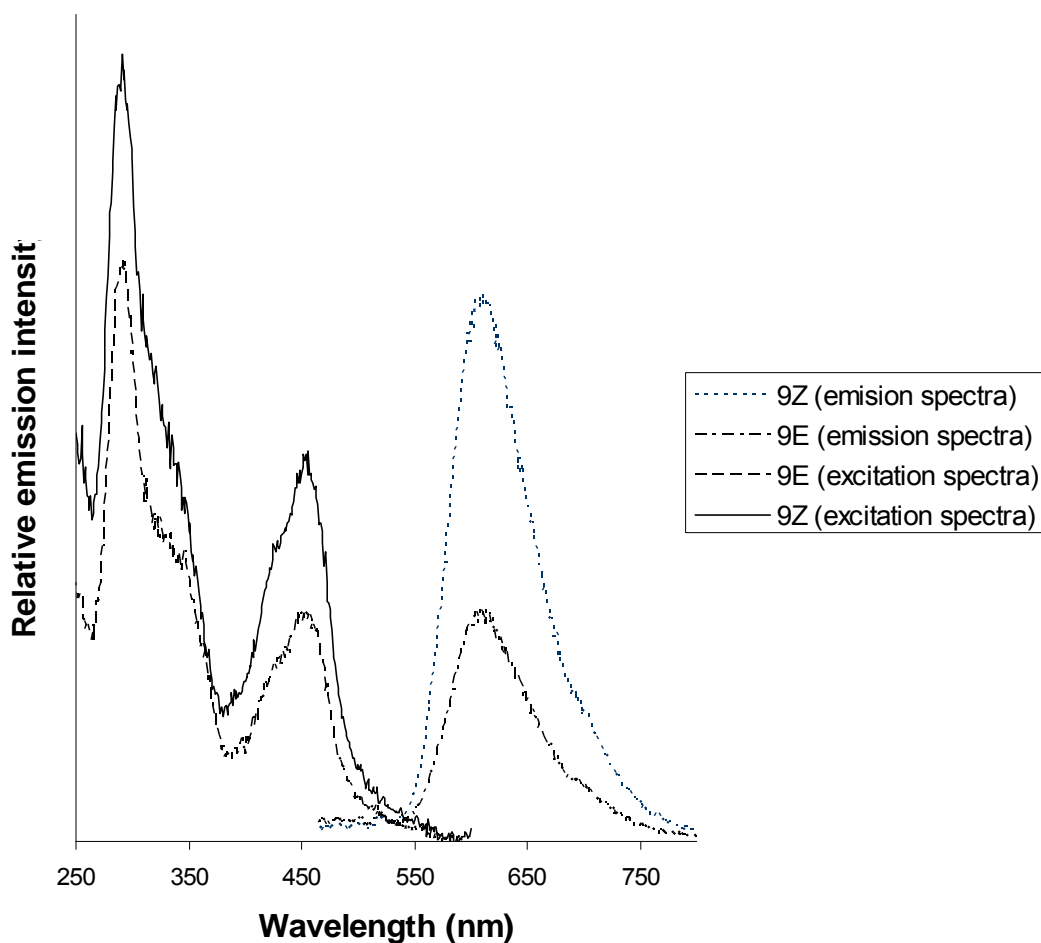


Figure 44 Excitation spectra ($\lambda_{em} = 610$ nm) and emission spectra ($\lambda_{exc} = 450$ nm) of complexes **9Z** and **9E** (10 μ M, air-equilibrated CH_3CN , T = 298 K).

peaking at 612 nm. These emission spectra are very similar to that of $\text{Ru}(\text{bpy})_3^{2+}$ ($\lambda_{em} = 613$ nm) (Figure 45). It is important to note that the emissions of **9Z** and **9E** are less intense than $\text{Ru}(\text{bpy})_3^{2+}$. It seems likely that in the $^3\text{MLCT}$ excited states of **9Z** and **9E**,

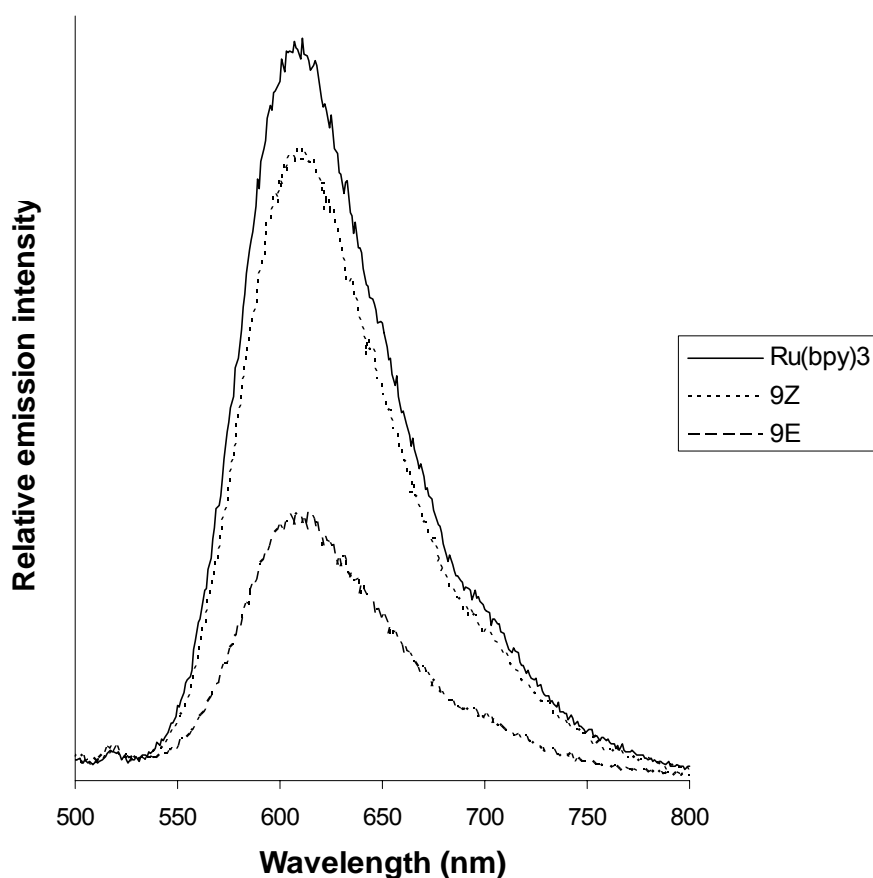


Figure 45 Emission spectra ($\lambda_{\text{exc}} = 450 \text{ nm}$) of complexes **9Z**, **9E**, and $\text{Ru}(\text{bpy})_3^{2+}$ ($10 \mu\text{M}$, air-equilibrated CH_3CN , $T = 298 \text{ K}$).

some of the excited state energy is intramolecularly transferred to the precipiton unit, providing an additional non-radiative deactivation pathway for the Ru unit. It is also noteworthy that the emission intensity of **9Z** is 2.5 times more intense than **9E**. It is known for stilbene that the triplet-state energy for the *cis* isomer (63 kcal/mol) is higher than that for the *trans* isomer (49 kcal/mol),⁴⁵ as a result of steric constraints in the *cis* isomer (which reduces π electron delocalization). Thus, it is likely to be more favorable

⁴⁵ Saltiel, J.; Marchland, G.; Kaminska, E.; Smothers, W.; Meuller, W.; Charlton, J. *J. Am. Chem. Soc.* **1984**, *106*, 3144.

for the *trans* isomer to accept triplet energy from the Ru unit ($E_T = 49$ kcal/mol) than the *cis* isomer, resulting in a lower emission spectrum for **9E**.⁴⁶

From the absorption properties of **9Z** and its components, one can see that the use of $\lambda_{\text{exc}} \geq 400$ nm irradiation would result in selective excitation of the $\text{Ru}(\text{bpy})_3^{2+}$ chromophore unit of the Förster precipiton **9Z** (use of $\lambda_{\text{exc}} \leq 370$ nm irradiation would lead to excited states of both $\text{Ru}(\text{bpy})_3^{2+}$ and precipiton components) (Figure 46). Selective, direct excitation of the $\text{Ru}(\text{bpy})_3^{2+}$ chromophore forms the $^1\text{MLCT}$ state, followed by intersystem crossing to the $^3\text{MLCT}$ state. The $^3\text{MLCT}$ state then undergoes triplet-triplet energy transfer to the precipiton chromophore. This system takes on a receiver-antenna relationship where the $\text{Ru}(\text{bpy})_3^{2+}$ acts as an antenna by: 1) absorbing visible light 2) converting light into triplet energy; and 3) transferring that energy to the receiving precipiton (Figure 47).

⁴⁶ Yam, V.; Chor-Yue, V.; Wu, L. *Dalton Trans.* **1998**, 1461.

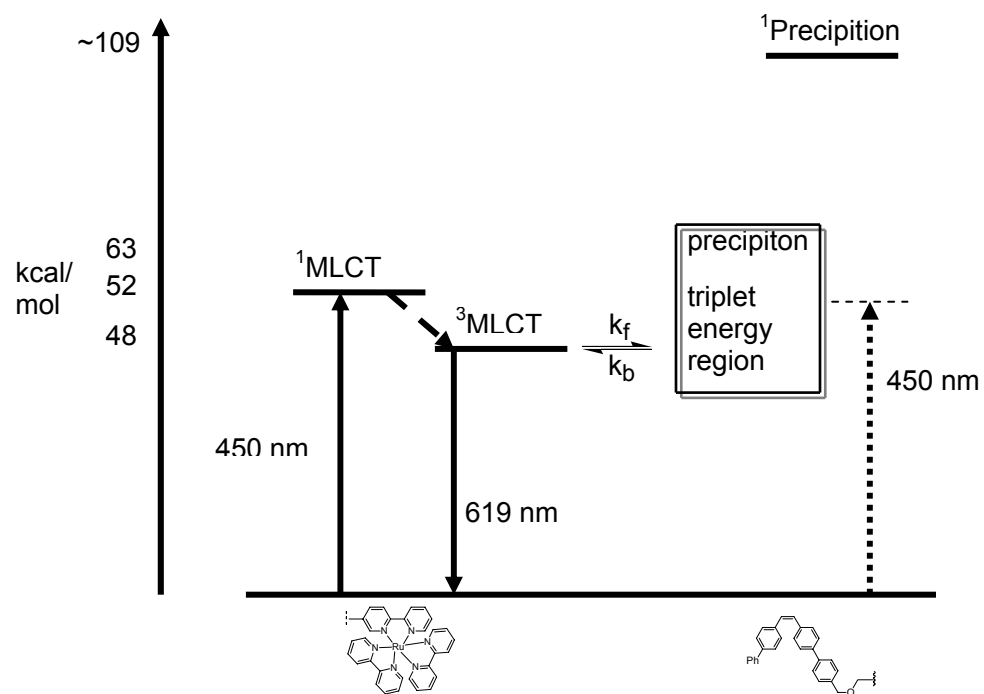


Figure 46 Energy level diagram describing the photophysical processes of 9Z.

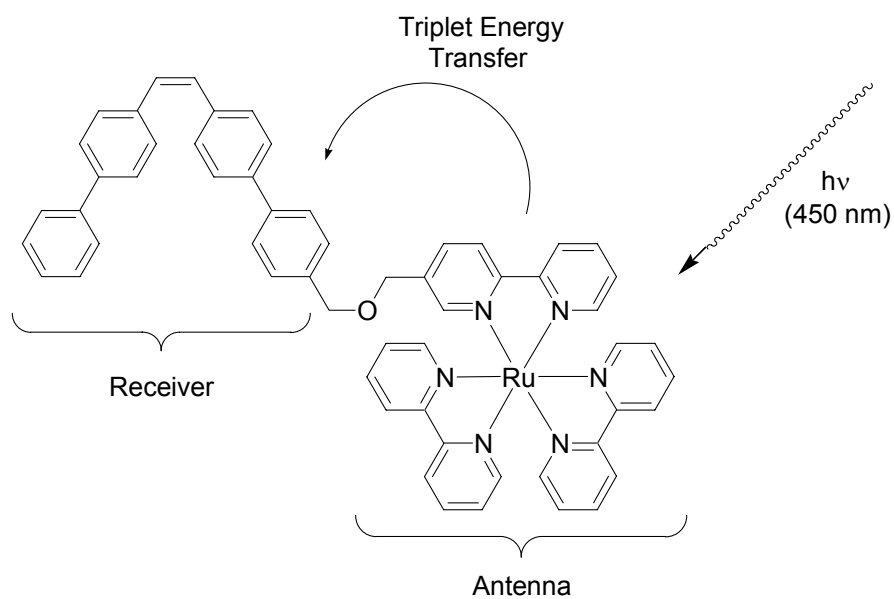


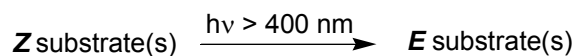
Figure 47 Receiver-antenna relationship of complex 9Z.

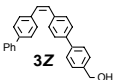
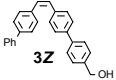
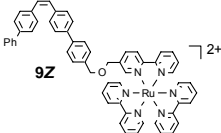
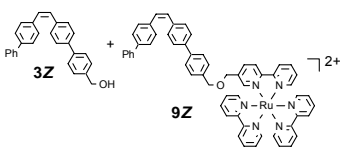
3.3.3. Photoisomerization Reactivity

3.3.3.1. Key Reaction Rate Comparisons

We hypothesized that if complex **9Z** is capable of an efficient intramolecular triplet energy transfer pathway, then its isomerization rate would be enhanced relative to an intermolecular sensitization in the same precipiton system. With complex **9Z** in hand, we envisioned comparing 4 key photoisomerization rates that would help determine the effect of an attached sensitizer (Table 5).

Table 5 Key experiments for comparison of relative photoisomerization rates.



Reaction	Z Substrate(s)	Sensitizer
1		-----
2		$\text{Ru}(\text{bpy})_3^{2+}$
3		-----
4		-----

In reaction 1, **3Z** is irradiated without the presence of $\text{Ru}(\text{bpy})_3^{2+}$ sensitizer. We expect the isomerization rate to be slow, as shown in Figure 32, and the results will be used as a background/control. A comparison of sensitized **3Z** and **9Z** isomerization rates (reactions 2 and 3) will answer the essential question of the effect of sensitizer attachment. A comparison of **9Z** and **9Z + 3Z** isomerization rates (reactions 3 and 4) will determine the likelihood of selective isomerization. When **9Z** and **3Z** are combined, intramolecular sensitization and isomerization of **9Z** may or may not occur without concurrent intermolecular sensitization of **3Z**. For the purposes of sequestration, we are

interested in selectively isomerizing and precipitating only those precipitons that are intramolecularly sensitized. Finally, comparison of reactions 2 and 4 inquires into the effectiveness of $\text{Ru}(\text{bpy})_3^{2+}$ as an intermolecular sensitizer when modified by covalent attachment to a precipiton. Reaction 3 was performed first.

3.3.3.2. ^1H NMR Monitored Isomerization Studies

A concentration of 1 mM was the lower limit at which the photoisomerization process of complex **9Z** could be monitored by 300 MHz ^1H NMR spectroscopy. *Cis* and *trans* isomers of **9Z** are distinguishable by ^1H NMR due to chemical shift differences of the alkene and methylene protons. The chemical shifts of alkene protons H^{G} and $\text{H}^{\text{G}'}$ are downfield in **9E** (7.38 ppm) relative to that of **9Z** (6.74 ppm) (Figure 48). The methylene protons H^{E} and $\text{H}^{\text{E}'}$ of **9Z**, which neighbor the chiral $\text{Ru}(\text{bpy})_3^{2+}$ unit, produce an AB quartet and are distinguishable from an AB quartet in **9E**.

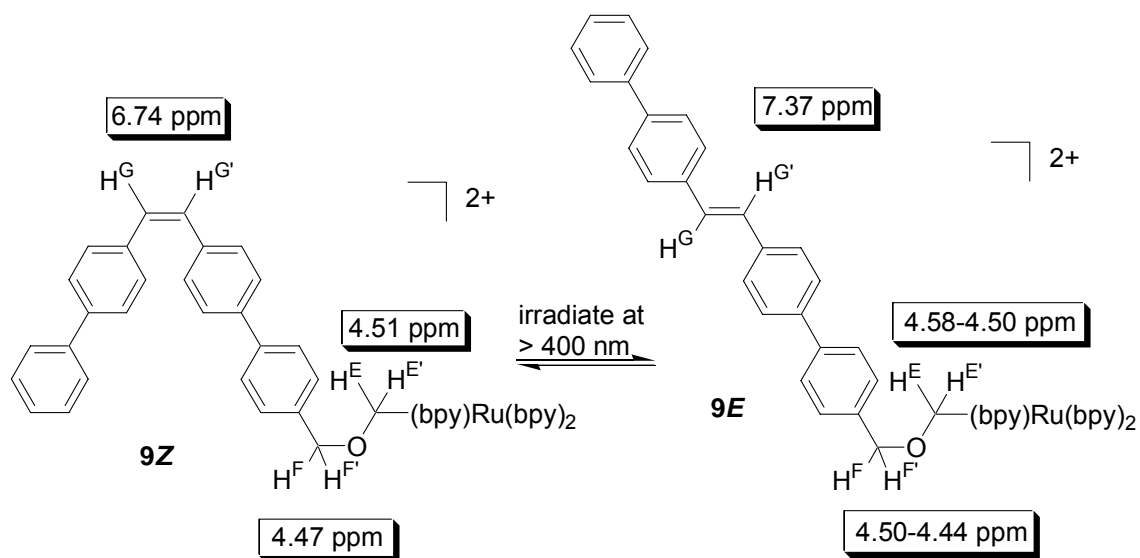


Figure 48 ^1H NMR spectroscopic changes of **9Z** and **9E** in CD_3CN at 298 K during irradiation at $\lambda_{\text{exc}} = 400\text{nm}$.

A 1 mM solution of **9Z** in CD_3CN was syringed into an NMR tube and degassed. The reaction mixture was irradiated at $\lambda_{\text{exc}} \geq 400\text{ nm}$ and the ^1H NMR spectroscopic changes of **9Z** were observed by the “disturbed” Method A. The percent yield of *trans* isomer formed from complex **9Z** relative to irradiation time is shown in Figure 49. Upon irradiation at $\geq 400\text{ nm}$, the amount of *trans*-isomer increased rapidly, with a concomitant decrease in the amount of *cis*-isomer until a photostationary state was reached within 2 min. A photostationary state of 58 % *cis*-isomer and 42 % *trans*-isomer was achieved upon irradiation of the pure *cis*-isomer.

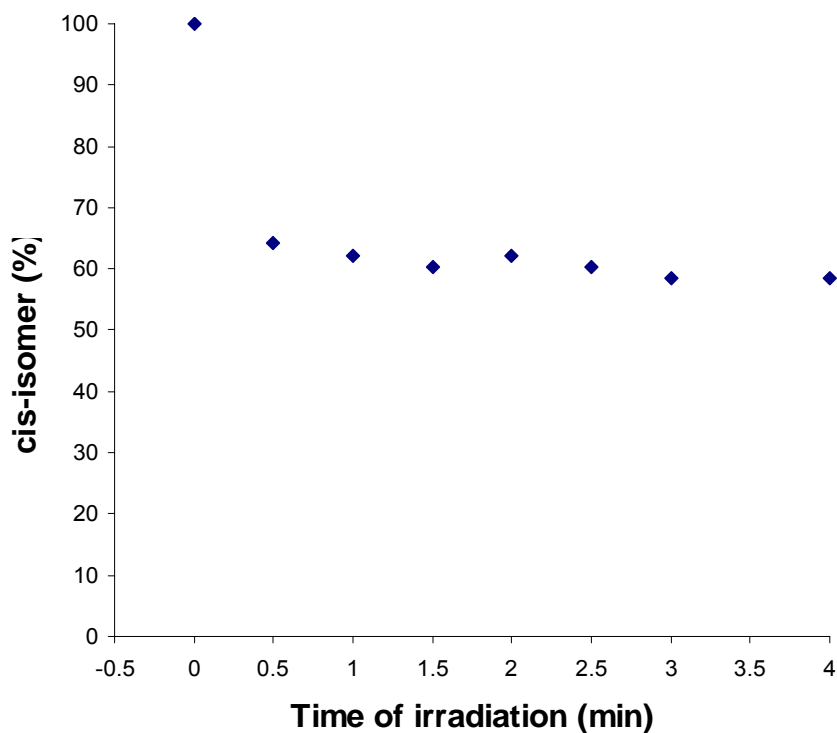


Figure 49 Plot of the percentage decrease of **9Z** against time of irradiation at ≥ 400 nm (1mM, degassed CD_3CN , $T = 298$ K).

3.3.3.3. Electronic Absorption Monitored Isomerization Studies

To reduce the probability of intermolecular quenching processes between precipitons, photoisomerization studies of **9Z/E** were also performed at a lower concentration (10 μM). At 10 μM , the average distance between molecules is approximately 500-1000 Å if all molecules are arranged on a 3D grid. A 10 μM solution of **9Z** in CH_3CN was

prepared, syringed into a cuvette and degassed. The reaction mixture was irradiated at $\lambda_{\text{exc}} \geq 400$ nm and the absorption spectroscopic changes of **9Z** were observed by the “disturbed” Method A. The intense absorption band centered at $\lambda = 320\text{-}385$ nm rapidly increased in intensity and then stopped within 2 min (Figure 50).

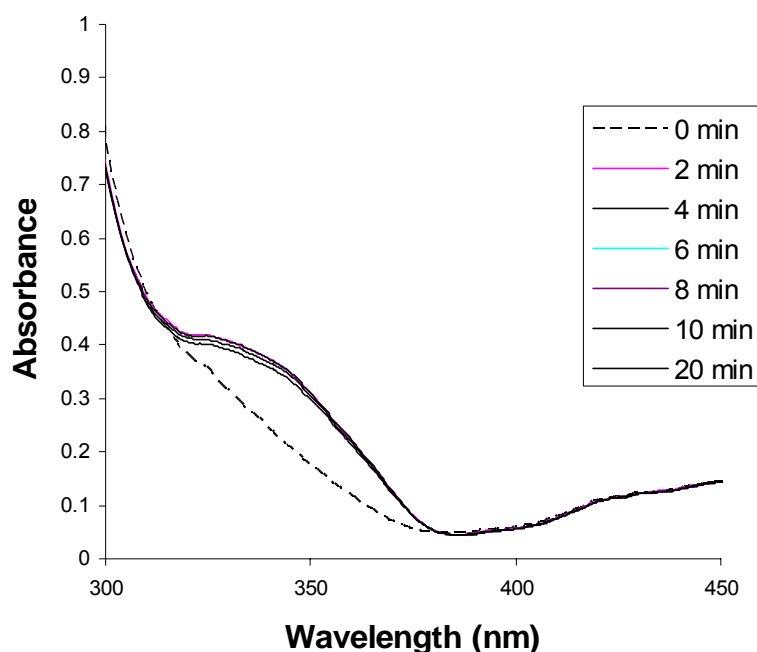


Figure 50 Photoisomerization of **9Z** upon irradiation at ≥ 400 nm ($10 \mu\text{M}$, degassed CH_3CN , $T = 298$ K).

Considering that the ^1H NMR data for the photoisomerization of **9Z** occurred on the same time scale, we are confident that the absorption spectroscopic changes are attributed to the *cis* \rightarrow *trans* isomerization of the $-\text{CH}=\text{CH}-$ functionality. Since **9Z** reaches a photostationary state upon irradiation, irradiation of **9E** should also lead to the same photostationary state mixture. A $10 \mu\text{M}$ solution of **9E** was prepared and irradiated in the

same manner as **9Z**. The intense absorption band centered at $\lambda = 300\text{-}385$ nm rapidly decreases in intensity as *cis* formed and then stopped within 2 min (Figure 51). Further irradiation of either complex **9Z/E** after 2 min lead to no further increase or decrease in absorption intensity. The ratio of isomers at the photostationary state under these conditions is currently being determined and will be compared to the photostationary state ratio observed in the 1mM ^1H NMR experiment (Section 3.3.3.2).

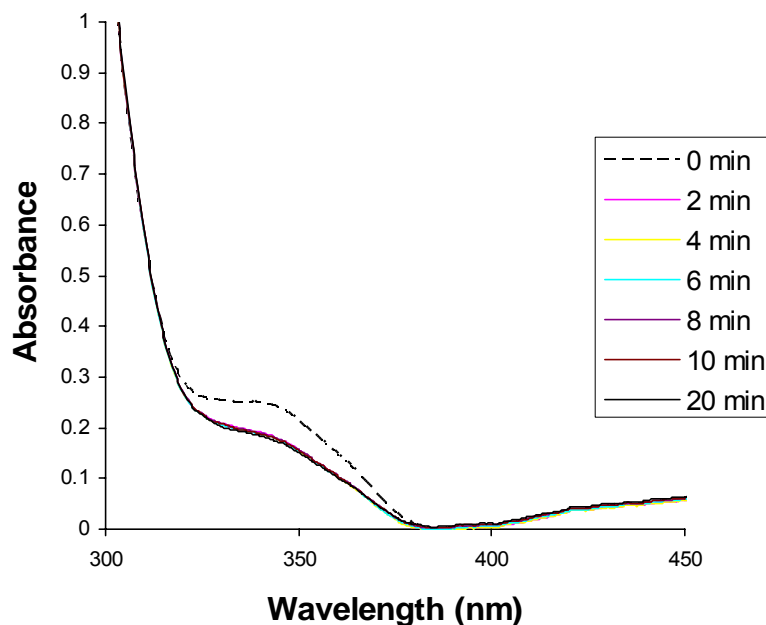


Figure 51 Photoisomerization of **9E** upon irradiation at ≥ 400 nm (10 μM , degassed CH_3CN , T = 298 K)

The attainment of a photostationary state in ≤ 2 min for *cis* \leftrightarrow *trans* isomerization is the fastest we have observed in any of our precipiton systems. In the absorption studies above, no intermediate isomerization growth/decay points were obtained before 2 min because a PSS was reached before the first spectroscopic measurement was recorded. These observations are consistent with the presence of an efficient photosensitization

pathway such as an intramolecular energy transfer pathway from the $^3\text{MLCT}$ state of $\text{Ru}(\text{bpy})_3^{2+}$ unit to the 1,2-bis(biphenyl)ethene unit.

3.4. Investigation of Tetraethyldiethylenetriamine (TEDETA) Functionalized Precipitons

It was demonstrated by Brittain that TEDETA functionalized precipitons were successful at scavenging CuBr catalyst from ATRP reactions of methyl methacrylate (Section 1.4, Figure 11). However, it was not determined if the copper binding to the precipiton resulted in an intramolecular energy transfer process to cause isomerization, or if a different energy pathway was responsible. To answer this question, 1,2-bis(biphenyl)-ethene TEDETA precipiton **13Z** was synthesized and then isomerized under various reaction conditions. The synthesis of **13Z** is outlined in Figure 52.

1,2-Bis(biphenyl)ethene alcohol **3Z** was treated with phthalimide under Mitsunobu conditions to afford imide **10Z**, and then subsequently cleaved with hydrazine to provide amine **11Z**. Treatment of amine **11Z** with a 20 % solution of phosgene in toluene generated isocyanate **12Z**. **12Z** was treated with TEDETA to produce ligand **13Z** in 72 % yield.

Table 6 summarizes the conditions for photoisomerization of **13Z**. In each reaction, a 20 mM solution of **13Z**, internal standard, and 50 μM sensitizer (where appropriate) was prepared in air-equilibrated toluene- D_8 and syringed into an NMR tube. The reaction mixture was irradiated at the specified wavelength and the ^1H NMR spectroscopic changes of **13Z** were observed by the “disturbed” Method A.

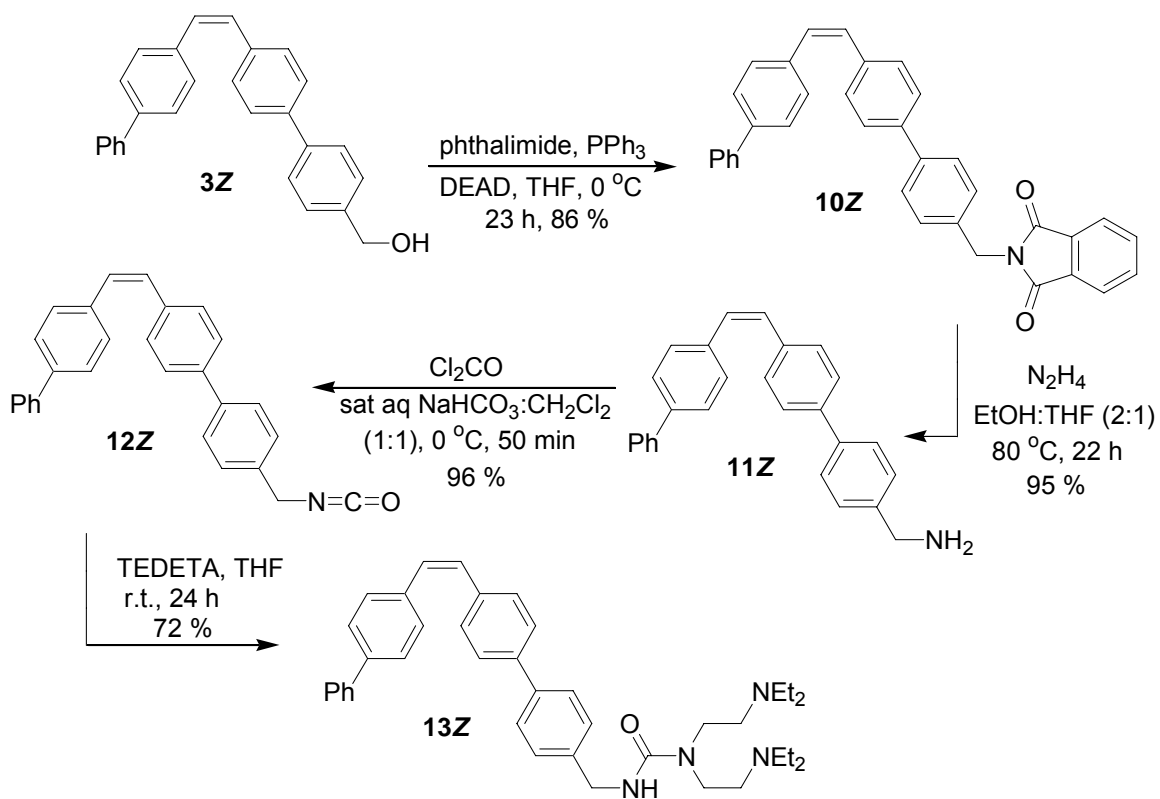
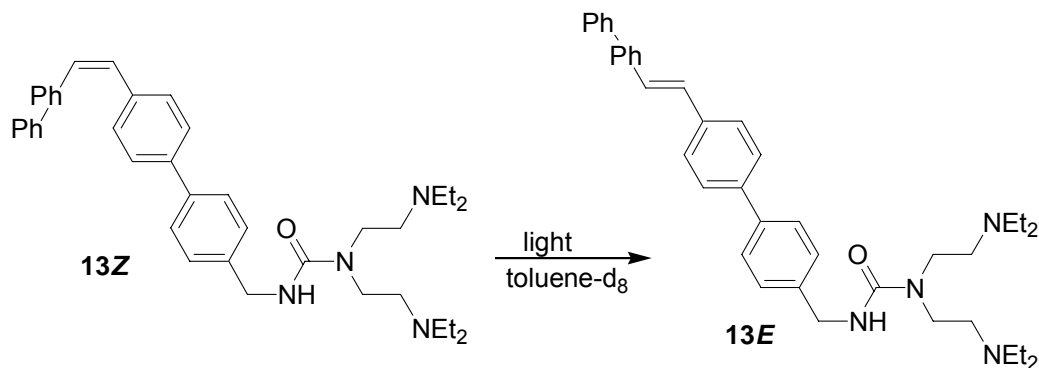


Figure 52 Synthesis of TEDETA functionalized precipiton **13Z**.

Table 6 Outcome of photochemical isomerization studies of 13Z.

Rxn	Light (nm)	Catalyst (eq)	Time (h)	Product
1	> 400	-----	8.5	15% E
2	> 400	CuBr (1.5)	6.5	17% E
3	> 400	erythrosin B (0.05)	5	96% E
4	> 400	CuBr (1.0), erythrosine B (0.05)	9	44%
5	350	-----	0.6	18% E, 70% cyclobutane
6	350	CuBr (1.0)	3	15% E, 80% cyclobutane

13Z was irradiated at $\lambda_{\text{exc}} \geq 400$ nm for 8.5 h with and without the presence of CuBr (reaction 1 and 2) to give 15% and 17% conversion. Irradiation of **13Z** at $\lambda_{\text{exc}} \geq 400$ nm with erythrosine B resulted in 96% conversion to **13E**, evidence that CuBr was not acting as an efficient sensitizer. Irradiation of **13Z** in the presence of both CuBr and erythrosine B gave only 44% conversion. Irradiation of **13Z** at higher energy 350 nm light and no CuBr gave an 18% conversion to **13E**. Using ^1H NMR, we observed a signal at 4.54 ppm that was attributed to a [2+2] cycloaddition product. Three compounds were present, **13Z**, **13E**, and *cis* cyclobutane products **15** and **16** (Figure 53) in a 12:18:70 ratio. Irradiation of **13Z** at 350 nm in the presence of CuBr led to a mixture of **13Z**, **13E**, and *cis* cyclobutane products **15** and **16** in a 5:15:80 ratio. Comparison of reactions 5 and 6

indicated no significant outcome difference with and without the presence of CuBr. We conclude that CuBr has no influence on the isomerization process of **13Z**.

In our experiments, 2 of the 4 possible cyclobutane isomers were obtained from irradiation of **13Z** at 350 nm (reaction 5). *Cis* head-head **15** and *cis* head-tail **16** cyclobutanes were isolated in 15% and 56% yields by flash chromatography, respectively (Figure 53). Differentiation between a *cis* and an *trans* cyclobutane isomers was based on the difference in chemical shift of the cyclobutane protons. It is reported that the *cis* cyclobutane protons of 1,2-diarylethylene dimers appear near δ 4.5 ppm and the *trans* cyclobutane protons appear around δ 3.7 ppm.⁴⁷ We observed a signal at δ 4.68 ppm. *Cis* **15** head-head and **16** head-tail isomers were very similar by ¹H and ¹³C NMR. The only significant difference between the isomers was their R_f value and it was used to

⁴⁷ (a) Ito, Y.; Kajita, T.; Kunimoto, K.; Matsuura, T. *J. Org. Chem.* **1998**, *54*, 587. (b) Rao, K. S. S. P.; Hubig, S. M.; Moorthy, J.N.; Kochi, J. K. *J. Org. Chem.* **1999**, *64*, 8098. (c) Leigh, W. J.; Lweis, T. J.; Lin, V.; Postigo, J. A. *Can. J. Chem.* **1995**, *74*, 263. (d) Jones, A. J.; Teitei, T. *Aust. J. Chem.* **1984**, *37*, 561. (e) Green, B.S.; Heller, L. *J. Org. Chem.* **1974**, *39*, 196.

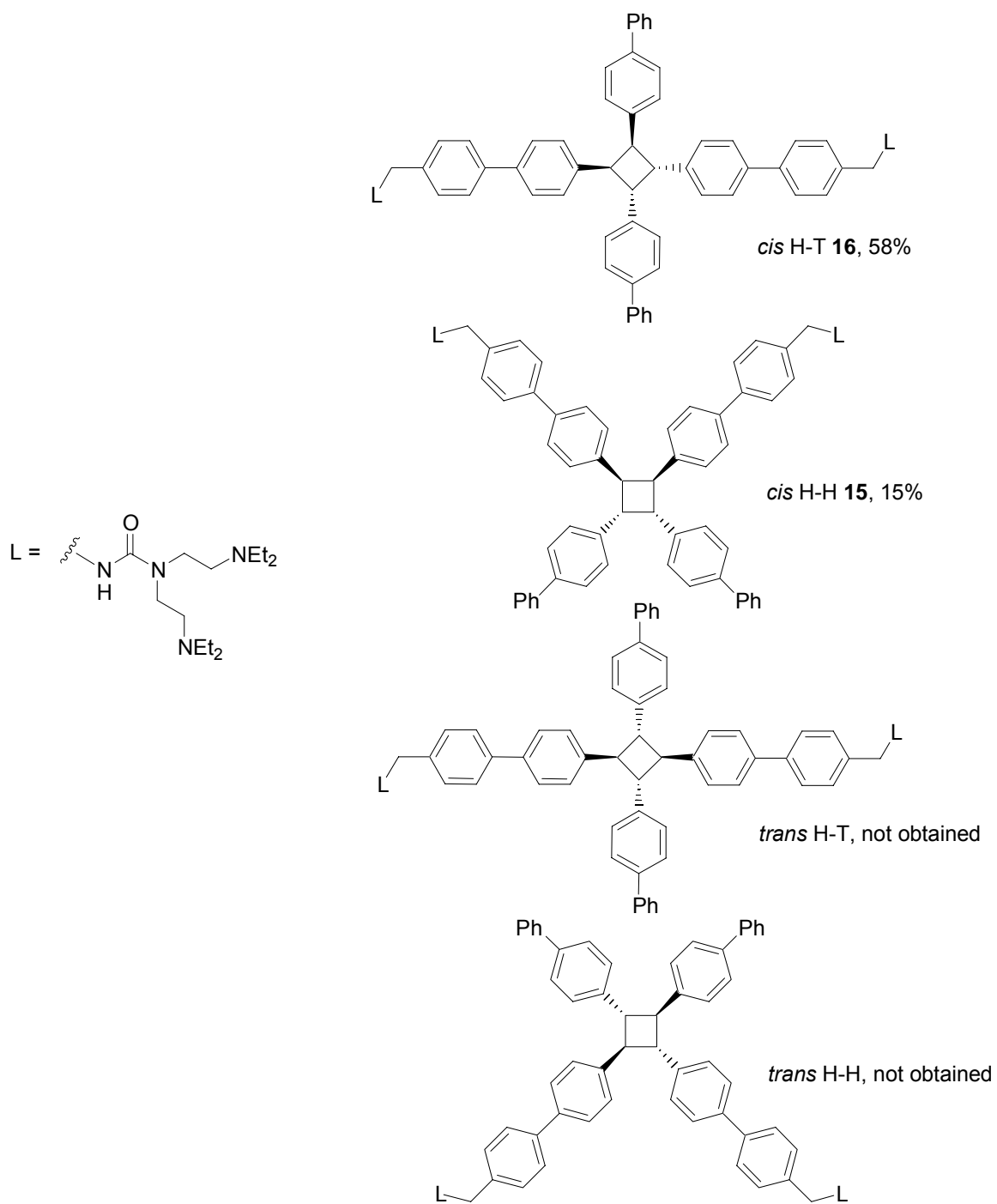


Figure 53 Cycloaddition products possible from 350 nm irradiation of 13Z.

assign their structures. The isomer with the lower R_f was assigned to be the head-head regioisomer **15** where the dipoles are aligned and the TEDETA ligands are positioned to interact more strongly with the SiO_2 surface as compared to the head-tail regioisomer **16**. *Trans* cyclobutane isomers were not obtained.

3.5. Dexter Class Precipiton

Our practical goal for developing intramolecularly sensitized precipitons is the sequestration of contaminants from solution. Toward this goal, our first experiments were performed to examine the behavior of an attached metal sensitizer to a precipiton. In a real world application of this decontamination strategy, the target contaminant would need to bind to the precipiton. We examined the possibility of capturing ruthenium using Dexter-type precipiton **22Z** (Figure 54).

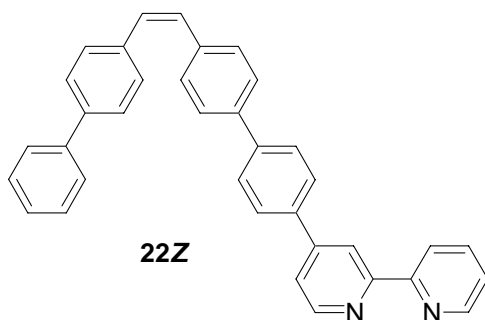


Figure 54 . Dexter-type precipiton **22Z**.

In order to observe a change in the isomerization rate of **22Z** due to sequestration, the isomerization rates of **22Z** and **3Z** were compared in 11 different conditions (Figure 55, 56). In each experiment, a 1 mM solution of precipiton, internal standard, and 50 μM sensitizer (where appropriate) was prepared in air-equilibrated 1/1 $\text{CD}_2\text{Cl}_2/\text{CD}_3\text{CN}$ and

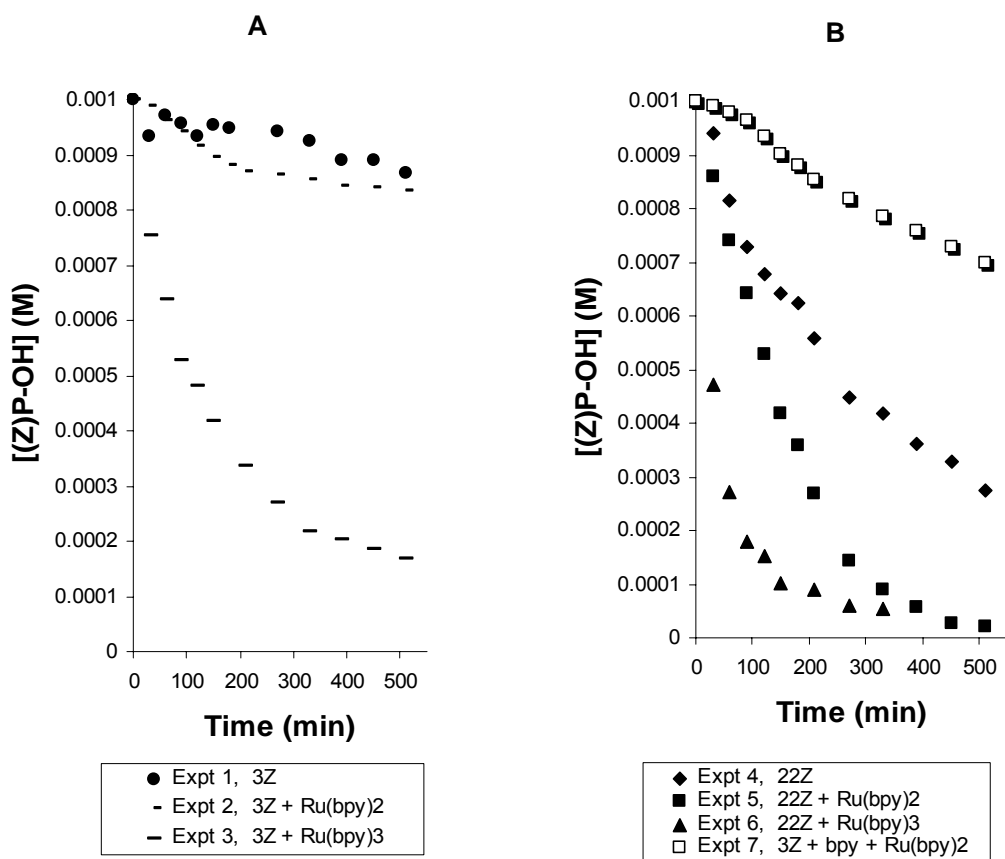


Figure 55 Plot of photoisomerization reactions 1-7 ($[3Z]$, $[22Z] = 1\text{mM}$; $[\text{Ru}(\text{bpy})_3^{4+}]$, $[\text{Ru}(\text{bpy})_2^{4+}] = 50\ \mu\text{M}$, solvent = 1/1 $\text{CD}_2\text{Cl}_2/\text{CD}_3\text{CN}$).

syringed into an NMR tube. The reaction mixture was irradiated at $\lambda_{\text{exc}} \geq 400\ \text{nm}$ and the ^1H NMR spectroscopic changes of the precipiton were observed by Method A. A plot of

the reaction progress for each experiment is given in Figure 55 and 56. Table 7 summarizes the isomerization rates for **22Z** and **3Z**.

The effectiveness of Ru(bpy)₂²⁺ and Ru(bpy)₃²⁺ sensitizers on the isomerization of **3Z** were compared, as shown in Figure 55A. **3Z** isomerized 75% in the presence of Ru(bpy)₃²⁺, but only isomerized 16% in the presence of Ru(bpy)₂²⁺ (similar to the background experiment 1). Isomerization of **3Z** in the presence of Ru(bpy)₂²⁺ and 2,2'-bipyridine (experiment 7) had the same initial rate ($k = 0.56 \times 10^{-8}$) as when 2,2'-bipyridine is not present (experiment 2), and is 23 times slower than when Ru(bpy)₃²⁺ is present (experiment 3). However, the isomerization rate in experiment 7 does increase over time (> 100 min), which suggests slow bipyridine binding to Ru(bpy)₂²⁺. Based on approximate half-life times, isomerization of **22Z** in the presence of Ru(bpy)₂²⁺ was 2 times faster than the **22Z** background reaction while isomerization with Ru(bpy)₃²⁺ was 10 times faster (Figure 55B).

Table 7 Summary of isomerization rates after 30 min of irradiation.

Expt	Slope ($\times 10^{-8}$)	k ($\times 10^{-5}$)(sec ⁻¹)	pseudo 1 st -order rxn rate ($\times 10^{-8}$) (sec ⁻¹ M)	% conversion (510 min)
1	3.6	3.6	3.6	13
2	0.56	5.6	0.56	16
3	12.9	12.9	12.9	83
4	3.3	3.4	3.3	72
5	7.7	7.8	7.7	98
6	29.4	29.4	29.4	100
7	0.56	5.6	0.56	30
8	6.9	6.9	6.69	92
9	2.0	2.0	2.01	73
10	28.1	28.1	28.1	90
11	15.0	15.0	15.0	82

When **3Z** and **22Z** are combined in the same NMR tube with $\text{Ru}(\text{bpy})_2^{2+}$ the initial isomerization rate of **22Z** remained nearly unchanged but the isomerization rate of **3Z** increased 3.5 times (Figure 56A). When **3Z** and **22Z** are combined in the same tube with $\text{Ru}(\text{bpy})_3^{2+}$ their respective isomerization rates were essentially unchanged from the rates when they were not combined (Figure 56B).

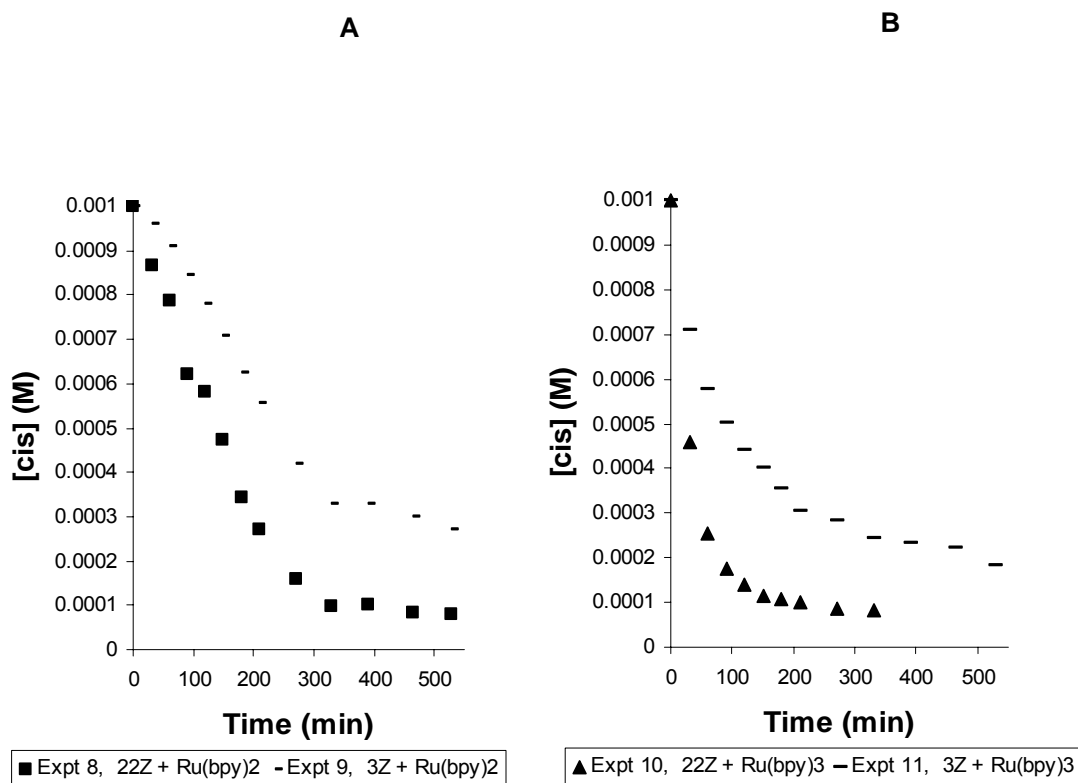


Figure 56 Plot of photoisomerization reactions 8-11. Reactions 8 and 9 are performed in one NMR tube and reactions 10 and 11 are performed in one NMR tube.

We have made the following conclusions from the above data. First, $\text{Ru}(\text{bpy})_3^{2+}$ is an overall better triplet energy sensitizer than $\text{Ru}(\text{bpy})_2^{2+}$, based on the % conversions of **3Z** and **22Z**. Second, direct irradiation of **3Z** and **22Z** at $\lambda_{\text{exc}} \geq 400$ nm showed that **22Z** is a

better chromophore for isomerization. Third, the initially slow isomerization rate of **3Z** in experiment 7 showed that 2,2'-bipyridine binding to $\text{Ru}(\text{bpy})_2^{2+}$ is slow if occurring at all. Although the initial isomerization rate of **3Z** in experiment 9 is 4 times faster than experiment 2, consistent with $2\text{2Z}:\text{Ru}(\text{bpy})_2^{2+}$ binding, the isomerization rate of **22Z** (experiment 8) did not show a characteristic increase. Complexities of the system prevented us from making any other conclusions. Those complexities were 1.) the heterogeneous nature of the reaction mixtures, 2.) the significant background isomerization rate due to absorbance of **22Z**, 3.) our lack of quantitative knowledge of ligand exchange rates. Discussion of these complexities and the synthesis of **22Z** are provided in Appendix 1. Although further experiments may have overcome some of these problems, it was the background isomerization issue that led us to discontinue studies of **22Z**.

4. SUMMARY

We have discovered that $\text{Ru}(\text{bpy})_3^{2+}$ is a very effective triplet energy sensitizer in our precipiton systems. Intermolecular sensitization of a 1,2-bis(biphenyl)ethene alcohol precipiton **3Z** using $\text{Ru}(\text{bpy})_3^{2+}$ was demonstrated to obey first-order kinetics. Discovery of microcrystal formation as part of the precipitation process of **3Z** has led to the development of “disturbed” and “undisturbed” methods for monitoring the reaction kinetics by ^1H NMR. Förster and Dexter class precipitons have been designed, synthesized, characterized and studied kinetically. We have successfully attached a $\text{Ru}(\text{bpy})_3^{2+}$ sensitizer to the Förster class precipiton as a strategy for demonstrating intramolecular energy transfer. Upon attachment and irradiation with ≥ 400 nm light, the Förster precipiton **9Z** reached a photostationary state within 2 min. This is the fastest photoisomerization rate we have observed with precipitons, and is strong evidence of an intramolecular energy transfer process.

5. FUTURE DIRECTIONS

Attachment of a metal sensitizer to a precipiton for the purpose of demonstrating intramolecular energy transfer is an important step in developing precipitons as light-driven scavengers. Of the four key reaction rate comparisons (Table 10), I have performed only one. My near future goals include completion of the remaining three reactions and drawing final conclusions on the effect of $\text{Ru}(\text{bpy})_3^{2+}$ sensitizer attachment on Förster precipiton **9Z**.

Several challenges must be addressed in order to meet the goal of employing our sequestration precipitons in chemical applications. Palladium, for example, is a very commonly used transition metal catalyst in organic synthesis. For the light-driven sequestration of palladium, suitable ligands that allow MLCT with palladium must be identified. Another challenge involves minimizing the rate of metal-precipiton ligand exchange. In the ideal case, precipiton binding to the metal target is fast but dissociation is slow relative to the time needed for isomerization and precipitation.

The ability to intramolecularly sensitize a precipiton opens the imagination to new types of sequestration precipitons. For example, we envision a precipiton containing a separate but linked organic sensitizer. In this case, the system is much simpler in the sense that unique MLCT-capable ligands are not required. These precipitons would also be useful because the sensitizer is essentially “built in” the precipiton unit, eliminating the need of adding a separate sensitizer to the reaction mixture and subsequently

removing it. In addition, these intramolecularly sensitized precipitons may be used at a much lower concentration than intermolecularly sensitized precipitons.

6. EXPERIMENTAL

6.1. General

^1H NMR and ^1H - ^1H COSY spectra were recorded on a Bruker Avance 300 at 300 MHz. ^{13}C NMR spectra were recorded on a Bruker Avance 300 at 75 MHz or a Bruker Avance 600 at 150 MHz. The chemical shifts are given in parts per million (ppm) on the delta scale (δ), and the coupling constant values (J) are in hertz. The solvent peak was used as the reference value. For ^1H NMR: $\text{CDCl}_3 = 7.27$ ppm; $\text{CD}_2\text{Cl}_2 = 5.32$; $\text{CD}_3\text{CN} = 1.94$. For ^{13}C NMR: $\text{CDCl}_3 = 77.23$ ppm; $\text{CD}_2\text{Cl}_2 = 54.00$; $\text{CD}_3\text{CN} = 1.39$. Abbreviations for NMR data: s = singlet; d = doublet; t = triplet; q = quartet; dd = doublet of doublets; dt = doublet of triples; dq = doublet of quartets; tt = triplet of triplets; m = multiplet; br = broad; app = apparent, ABq = AB quartet.

High resolution and low resolution mass spectra were recorded on a VG 7070 spectrometer. Infrared (IR) spectra were collected on an Avatar 380 Nicolet FT-IR spectrometer. Samples for IR were prepared either as a thin film on a NaCl plate by dissolving the sample in CH_2Cl_2 and then evaporating the CH_2Cl_2 or as a KBr pellet. Melting points were determined using a Thomas Hoover capillary melting point apparatus and are uncorrected. UV-Vis spectra were obtained in air-equilibrated or degassed solvent solution at 23 °C using an Ocean Optics S2000-TR fiber-optic

spectrometer with a Mikropack deuterium/halogen light source. Emission spectra were recorded in air-equilibrated solvent solution at 23 °C with a Cary Eclipse fluorescence spectrometer equipped with Varian software.

Thin layer chromatography (TLC) was performed using E. Merck silica gel 60F-254 (0.25 mm) analytical glass plates. Light absorption by compounds was observed using ultraviolet light (254 nm or 365 nm). Silica gel columns for flash chromatography, according to the method of Still, were prepared with E. Merck silica gel 60 (230-240 mesh ASTM).

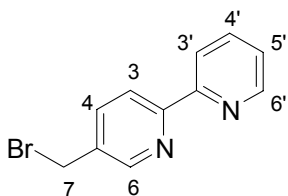
Dry solvents were distilled shortly before use from an appropriate drying agent under nitrogen atmosphere. Tetrahydrofuran (THF), diethyl ether (Et₂O), and toluene were distilled from sodium and benzophenone. Dry methanol was distilled from magnesium turnings and stored under nitrogen or was purchased as anhydrous and used as obtained. Ethyl acetate was dried over 4 Å molecular sieves for at least 24 h prior to use. N,N-Dimethylformamide (DMF) was dried over MgSO₄, distilled *in vacuo*, and stored over 4 Å molecular sieves. Pyridine was distilled from calcium hydride and stored over 4 Å molecular sieves. Hexane refers to the mixed hydrocarbon fraction (bp 68-70 °C), principally *n*-hexane, and was purified as follows: the commercial solvent was stirred over concentrated H₂SO₄ for at least 24 h, decanted, stirred over anhydrous NaHCO₃ for at least 6 h, decanted, and distilled. Benzene, methylene chloride (CH₂Cl₂) and triethylamine (TEA) were distilled from CaH₂. Anhydrous dimethylsulfoxide (DMSO) and acetonitrile (CH₃CN) were purchased from Acros and used as is. Other commercially available reagents and solvents were reagent grade and were used without further purification.

Reactions performed under a nitrogen atmosphere were arranged with a mercury bubbler so that the system could be alternately evacuated and filled with nitrogen and left under positive pressure. Syringes and reaction flasks were dried in an oven at 120 °C and cooled in a desiccator over calcium sulphate prior to use. Reactions at “room temperature” were conducted under ambient laboratory conditions $T = 20\text{-}27\text{ }^{\circ}\text{C}$, $p = 720\text{-}770\text{ mmHg}$. References to “removal of volatile components *in vacuo*” refer to rotary evaporation of the sample at $25\text{-}65\text{ }^{\circ}\text{C}$ *in vacuo* (18-25 mmHg), followed by removal of residual volatile materials under vacuum (0.05-0.5 mmHg) at room temperature.

6.2. Experimental Procedures

6.2.1. Synthesis and Characterization

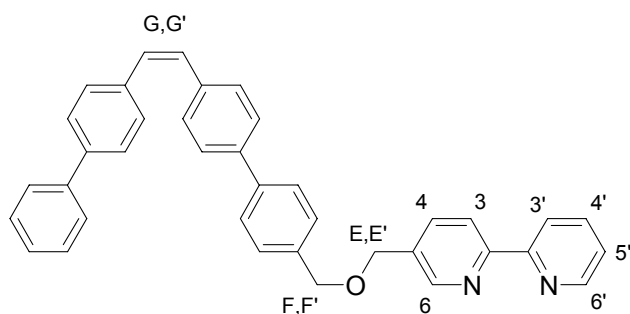
Assignments of the ^1H NMR signals of the bipyridine containing compounds were determined by examining and comparing their $^1\text{H}\text{-}^1\text{H}$ COSY spectra and coupling constants. Copies of the $^1\text{H}\text{-}^1\text{H}$ COSY spectra are provided at the end of the chapter.



5-Bromomethyl-2,2'-bipyridine (7). 5-Methyl-2,2'-bipyridine **6**

(1.99 g, 11.8 mmol), *N*-bromosuccinimide (2.09 g, 11.8 mmol), and azobis(isobutyronitrile) (483 mg, 2.94 mmol) were dissolved in CCl_4 (179 mL) under N_2 and the

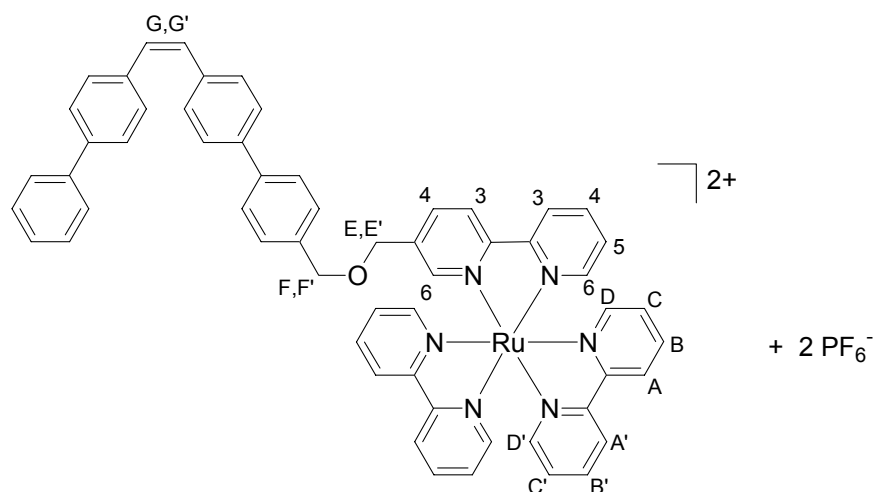
mixture was stirred at an internal temperature of 43 °C for 23 h. Reaction progress was monitored by ¹H NMR to observe the consumption of NBS and the formation of product. After 23 h, an additional 0.5 eq of NBS was added and the mixture was stirred at 43 °C for 2 additional h. The mixture was cooled to 23 °C, filtered, and the volatile components of the filtrate were removed *in vacuo* to afford a crude solid that was purified by flash chromatography (SiO₂, 5:1 Hex:EtOAc, column was pretreated with 19:1 Hex:NEt₃ then washed with 5:1 Hex:EtOAc) to afford bipyridine **7** as a white solid (1.35 g, 46%): R_f 0.15 (5:1 Hex:EtOAc, pretreated with 19:1 Hex:NEt₃); mp 74-76 °C; IR (KBr) 3050, 2998, 2967, 1596, 1556, 1461, 1434, 1392, 1252, 1203, 1127, 1088, 1039, 834, 797, 749, 730, 650; The ¹H and ¹³C NMR data matches the data described by Ballardini and coworkers: ¹H NMR (300 MHz, CDCl₃) δ 8.70 (app d, J = 2 Hz, 2 H, H⁶+H^{6'}), 8.43 (dd, J = 6, 2 Hz, 2 H, H³+H^{3'}), 7.89-7.81 (m, 2 H, H⁴+H^{4'}), 7.34 (ddd, J = 7, 5, 1 Hz, 1 H, H⁵), 4.55 (s, 2 H, H⁷); ¹³C NMR (75 MHz, CD₃CN) δ 156.3, 155.8, 149.6, 149.5, 137.8, 137.2, 133.9, 124.2, 121.5, 121.3, 29.9.



(Z)-5-[4'-(2-Biphenyl-4-yl-vinyl)-biphenyl-4-ylmethoxymethyl]-[2,2']bipyridine (8Z).

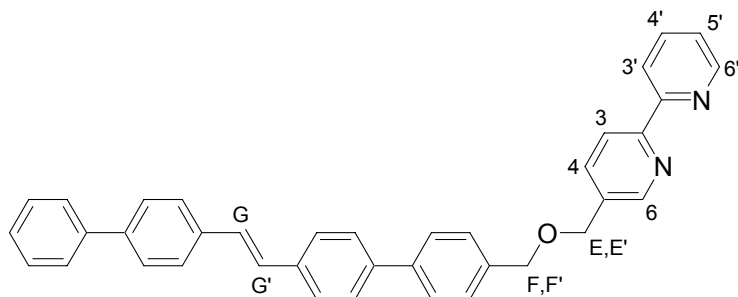
To a cooled solution (0 °C) of benzyl alcohol **3Z** (500 mg, 1.38 mmol) in THF (138 mL) was added dry NaH (66.2 mg, 2.76 mmol). The solution was warmed to 23 °C and stirred for 2 h. Bipyridine **7** (354 mg, 1.42 mmol) was then added, stirred for 2 h at

23 °C, then heated at reflux for 17.5 h. The solution was cooled to 23 °C and volatile components of the reaction mixture were removed *in vacuo*. The crude solid was combined with H₂O (300 mL) and the solution was extracted with CH₂Cl₂ (3 x 20 mL). The combined organic phases were washed with brine (360 mL), dried with MgSO₄, and filtered. Volatile components in the filtrate were removed *in vacuo* to afford a crude solid that was purified by flash chromatography (SiO₂, CH₂Cl₂ then 99:1 CH₂Cl₂:MeOH) to afford **8Z** as a pale green solid (537 mg, 73%): R_f 0.31 (CH₂Cl₂); mp 113-115 °C; IR (KBr) 3030, 3003, 2857, 1598, 1588, 1557, 1460, 1395, 1353, 1088, 881, 815; UV-Vis (CH₃CN, 10 μM) λ_{max} 274 nm, ε 34200 M⁻¹cm⁻¹, 290 nm, ε 33200 M⁻¹cm⁻¹, 330 nm, ε 24800 M⁻¹cm⁻¹; ¹H NMR (300 MHz, CD₃CN) δ 8.69-8.66 (m, 2 H, H⁶+H^{6'}), 8.43-8.41 (app d, J = 8 Hz, 2 H, H³+H^{3'}), 7.95-7.90 (m, 2 H, H⁴+H^{4'}), 7.72-7.63 (m, 5 H, phenyl), 7.56 (app d, J = 7 Hz, 4 H, phenyl), 7.46 (app d, J = 8.5 Hz, 4 H, phenyl), 7.42 (app s, 1 H, H⁵), 7.34 (app d, J = 8 Hz, 4 H, phenyl), 6.72 (s, 2 H, H^G+H^{G'}), 4.67 (s, 2 H, H^E+H^{E'}), 4.65 (s, 2 H, H^F+H^{F'}); ¹³C NMR (75 MHz, CD₃CN) δ 156.1, 156.8, 149.3, 148.8, 140.8, 140.4, 140.0, 139.6, 137.0, 136.6, 136.5, 136.4, 130.2, 130.1, 129.6, 129.5, 129.8, 128.4, 127.4, 127.1, 127.0, 126.9, 124.0, 121.2, 121.0, 72.3, 69.6; HRMS(EI) *m/z* calcd for C₃₈H₃₀N₂O 530.2358, found 530.2383.



(Z)-[5-(4'-(2-Biphenyl-4-yl-vinyl)-biphenyl-4-ylmethoxymethyl)-[2,2']bipyridine]-bis(2,2'-bipyridine)ruthenium(II)- bis(hexafluorophosphate) (9Z). A solution of *cis*-dichlorobis(2,2'-bipyridine)ruthenium(II)dihydrate (90.8 mg, 0.188 mmol) and silver hexafluoroantimonate(V) (132 mg, 0.376 mmol) in acetone (12.5 mL) under N₂ was heated at reflux for 48 h, followed by filtration of AgCl. Bipyridine 8Z (99.8 mg, 0.188 mmol) was added to the filtrate and the mixture was heated at reflux for 24 h. Volatile components of the reaction mixture were removed *in vacuo* to afford a crude red solid that was purified by flash chromatography (SiO₂, 19:1 CH₃CN:0.4 M KNO₃(aq)). The desired fractions were combined and volatile components were reduced in volume to 25 mL. The solution was combined with 0.25 M NH₄PF₆ (10 mL), and then stirred at 23 °C for 20 min, and then extracted with CHCl₃ (3 x 100 mL). The organic extract was washed with H₂O (2 x 200 mL). Volatile components of the organic layer were removed *in vacuo* to afford complex 9Z as a red solid (114 mg, 49%): R_f 0.16 (19:1 CH₃CN:0.4 M KNO₃(aq) on pretreated silica); mp 164-166 °C; IR (KBr) 3027, 2919, 2853, 1603, 1464, 1446, 1093, 838, 761, 730, 699; UV-Vis (CH₃CN, 10 μM) λ_{max} 290 nm, ε 91800 M⁻¹cm⁻¹, 340 nm, ε 22900 M⁻¹cm⁻¹, 450 nm, ε 13700 M⁻¹cm⁻¹; ¹H NMR (300 MHz,

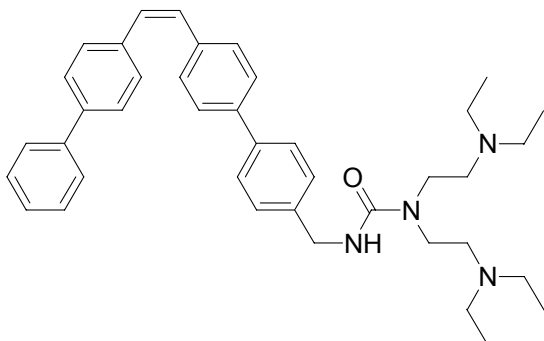
CD₃CN) δ 8.49-8.46 (m, 4 H, H^A+H^{A'}), 8.44-8.39 (m, 2 H, H³+H^{3'}), 8.06-8.01 (app t, J = 15, 8 Hz, 4 H, H^B+H^{B'}), 7.97 (dd, J = 5, 2 Hz, 1 H, H⁴ or H^{4'}), 7.92 (dd, J = 8, 1 Hz, 1 H, H⁴ or H^{4'}), 7.73-7.69 (m, 5 H, H^D+H^{D'} + phenyl), 7.65-7.60 (m, 6 H, H⁵+phenyl), 7.58-7.55 (m, 3 H, phenyl), 7.47-7.45 (m, 2 H, phenyl), 7.42-7.34 (m, 9 H, H^C+H^{C'}+phenyl), 7.33-7.27 (m, 1 H, phenyl), 7.23 (app d, J = 8, 2 Hz, 2 H, H⁶+H^{6'}), 6.74 (s, 2 H, H^G+H^{G'}), 4.51 (ABq, J = 14 Hz, 2 H, H^E+H^{E'}), 4.47 (s, 2 H, H^F+H^{F'}); ¹³C NMR (75 MHz, CD₃CN) δ 158.5, 158.4, 158.3, 157.4, 153.1, 153.0, 150.9, 141.7, 141.2, 141.0, 140.8, 140.6, 139.3, 139.2, 138.7, 138.1, 138.0, 137.7, 131.5, 131.4, 130.9, 130.8, 130.3, 129.8, 129.7, 129.6, 129.07, 129.04, 129.01, 128.97, 128.94, 128.90, 128.90, 128.2, 128.1, 125.7, 125.6, 125.5, 125.3, 73.6, 69.6; HRMS(ES) *m/z* calcd for C₅₈H₄₆F₆N₆OPRu [M – PF₆]⁺ 1089.2418, found 1089.2452, 944.14 [M – 2PF₆]⁺.



(E)-5-[4'-(2-Biphenyl-4-yl-vinyl)-biphenyl-4-ylmethoxymethyl]-[2,2']bipyridine (8E).

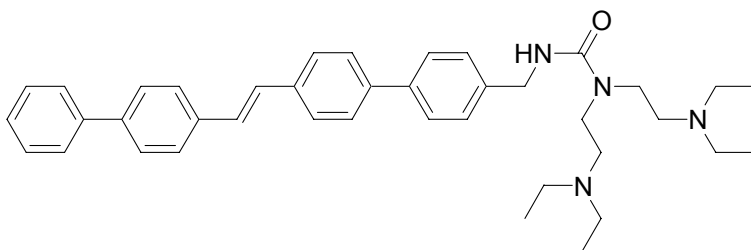
A solution of bipyridine **8Z** (153 mg, 0.289 mmol) and diphenyl diselenide (9.1 mg, 0.029 mmol) in THF (1.18 mL) was heated at reflux for 23 h. The solution was cooled to 23 °C and volatile components of the reaction mixture were removed *in vacuo*. The crude solid was triturated with Et₂O (3 x 5 mL), filtered, and the volatile components of the filtrate were removed *in vacuo* to afford ligand **8E** as a yellow solid (45.5 mg, 84%): mp 300-310 °C; IR (KBr) 3048, 3030, 2855, 1911, 1589, 1557, 1496, 1461, 1436, 1397, 1357, 1081, 970, 832, 807, 795, 763, 752, 742, 731, 691; ¹H NMR (300 MHz, CDCl₃) δ

residue that was recrystallized from CHCl₃/Et₂O and then CH₂Cl₂/EtOH to afford a red solid (3.6 mg, 5%): *R_f* 0.84 (19:1 CH₃CN:0.4 M KNO₃(aq) on pretreated silica); UV-Vis (CH₃CN, 10 μM) λ_{max} 290 nm, ε 51500 M⁻¹cm⁻¹, 339 nm, ε 28700 M⁻¹cm⁻¹, 456 nm, ε 7400 M⁻¹cm⁻¹; ¹H NMR (300 MHz, CD₃CN) 8.50-8.42 (m, 6 H, H^A+H^{A'}+H³+ H^{3'}), 8.07-7.99 (m, 4 H, H^B+H^{B'}), 7.99-7.93 (m, 2 H, H⁴+H^{4'}), 7.80-7.60 (m, 16 H, H^D+H^{D'}+H⁵+phenyl), 7.57-7.54 (m, 1 H, phenyl), 7.54-7.44 (m, 2 H, phenyl), 7.44-7.30 (m, 9H, H^C+H^{C'}+H^G+H^{G'}+phenyl), 7.26 (d, *J* = 8 Hz, 2 H, H⁶+H^{6'}), 4.58-4.50 (m, 2 H, H^E+H^{E'}), 4.50-4.44 (m, 2 H, H^F+H^{F'}); ¹³C NMR (151 MHz, CD₃CN) δ 157.97, 157.94, 157.90, 156.9, 152.72, 152.66, 152.63, 150.4, 141.26, 141.12, 140.82, 140.49, 140.31, 138.80, 138.79, 138.17, 137.85, 137.59, 137.17, 129.95, 129.28, 129.22, 129.04, 128.60, 128.56, 128.49, 128.42, 128.25, 128.22, 128.09, 128.04, 127.70, 125.25, 125.13, 124.85, 73.09, 69.12; HRMS(ES) *m/z* calcd for C₅₈H₄₆F₆N₆OPRu [M – PF₆]⁺ 1089.2418, found 1089.2368.



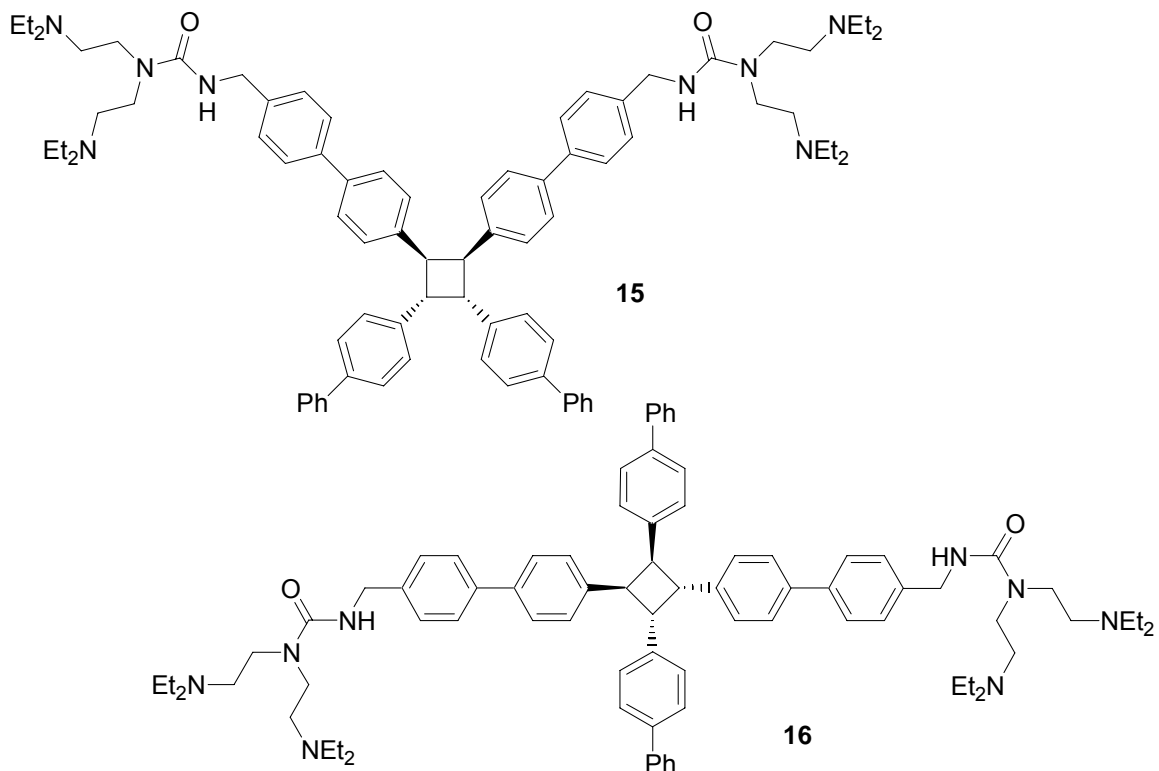
(Z)-3-(3-[4'-2-Biphenyl-4-yl-vinyl]-biphenyl-3-ylmethyl)-1,1-bis-(2-diethylamino-ethyl)urea (13Z). A solution of isocyanate **12Z** (635 mg, 1.64 mmol) and TEDETA (389 mg, 1.80 mmol) in THF (4.5 mL) under N₂ was stirred at 23 °C for 24 h. Volatile components of the reaction mixture were removed *in vacuo* to afford a yellow oil that was diluted with EtOAc (100 mL), washed with 25% aq NaHCO₃ (3 x 150 mL), dried

with MgSO₄, and filtered. Volatile components of the filtrate were removed *in vacuo* to afford a yellow oil which was purified by flash chromatography (SiO₂, 9:1 EtOAc:MeOH, then 10:1:1 EtOAc:MeOH:NEt₃) to afford ligand **13Z** as a yellow oil (711 mg, 72%): R_f 0.56 (10:1:1 EtOAc:MeOH:NEt₃); IR (neat) 3231, 3025, 2968, 2932, 2872, 2813, 1649, 1540, 1469, 1468, 1402, 1385, 1254, 1198, 1154, 1119, 1066, 1006, 884 cm⁻¹; ¹H NMR (300 MHz, CDCl₃) δ 8.45 (br t, J = 7 Hz, 1 H), 7.62-7.31 (m, 17 H), 6.65 (s, 2 H), 4.37 (d, J = 5 Hz, 2 H), 3.37 (t, J = 6 Hz, 4 H), 2.61 (t, J = 6 Hz, 4H), 2.51 (q, J = 7 Hz, 8 H), 0.96 (t, J = 7 Hz, 12 H); ¹³C NMR (75 MHz, CDCl₃) δ 160.6, 140.9, 140.0, 139.9, 139.8, 139.4, 136.6, 136.4, 130.2, 130.1, 129.5, 128.9, 128.5, 127.4, 127.1, 127.0, 126.9, 53.6, 48.1, 47.7, 44.5, 11.7; HRMS(ES) *m/z* calcd for C₄₀H₅₁N₄O [M + H] 603.4057, found 603.4082.



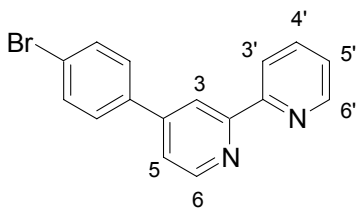
(E)-3-[4'-2-Biphenyl-4-yl-vinyl]-biphenyl-3-ylmethyl]-1,1-bis-(2-diethylaminoethyl)urea (**13E**). A solution of TEDETA ligand **13Z** (60.6 mg, 0.101 mmol) and diphenyl diselenide (31.9 mg, 0.101 mmol) in THF (0.42 mL) was heated at reflux for 23 h. The solution was cooled to 23 °C and volatile components of the reaction mixture were removed *in vacuo*. The crude solid was triturated with cold hexanes (3 x 3 mL) and filtered to afford TEDETA ligand **13E** as a tan solid (49.2 mg, 81%); mp 204 °C, IR (KBr) 3356, 3028, 2968, 1651, 1538, 1495, 1449, 1402, 1257, 1115, 968, 833, 804, 763, 729, 690; ¹H NMR (300 MHz, CDCl₃) δ 8.48 (br s, 1 H), 7.65-7.34 (m, 17 H), 7.20 (s, 2

H), 4.37 (d, J = 4 Hz, 2 H), 3.37 (t, J = 6 Hz, 4 H), 2.59 (t, J = 6 Hz, 4H), 2.51 (q, J = 7 Hz, 8 H), 0.96 (t, J = 7 Hz, 12 H); ^{13}C NMR, too insoluble to obtain. HRMS(ES) m/z calcd for $\text{C}_{40}\text{H}_{51}\text{N}_4\text{O}$ [M + H] 603.4063, found 603.4063.



Irradiation of 13Z at 350 nm. A solution of **13Z** (102 mg, 0.169 mmol) in toluene (9.47 mL) was irradiated at 350 nm for 14 h. Volatile components of the reaction mixture were removed *in vacuo* to afford a crude solid that was purified by flash chromatography (SiO_2 , 10:0.75 EtOAc: NEt_3 , then 100:10:1 CHCl_3 :MeOH: NH_4OH) to afford **15** (56.7 mg, 56%) and **16** (15.6 mg, 15%) as yellow oils. **Syn H-T cyclobutane 15:** R_f 0.13 (10:0.75 EtOAc: NEt_3); IR (neat) 3229, 3052, 2972, 2933, 2820, 2304, 1643, 1561, 1487, 1467, 1402, 1265, 1198, 1119, 1065, 1040, 1006, 909, 833 cm^{-1} ; ^1H NMR (300 MHz, CD_3CN) δ 8.50 (br t, J = 6 Hz, 2 H), 7.70-7.29 (m, 34 H), 4.68 (s, 4 H), 4.26 (d, J = 5 Hz, 4 H), 3.32 (t, J = 5 Hz, 8 H), 2.59 (t, J = 5 Hz, 8H), 2.52 (q, J = 7 Hz, 16 H), 0.92 (t, J = 7 Hz,

24 H); ^{13}C NMR (75 MHz, CDCl_3) δ 157.3, 141.0, 140.52, 140.0, 139.8, 139.0, 138.6, 128.9, 128.87, 128.81, 128.4, 127.2, 127.1, 126.9, 126.8, 126.6, 58.8, 47.8, 47.6, 47.5, 22.9, 22.8, 14.3, 11.1; HRMS(ES) m/z calcd for $\text{C}_{80}\text{H}_{101}\text{N}_8\text{O}_2$ [M + H] 1205.8048, found 1205.8087. **Syn H-H cyclobutane 16:** R_f 0.15 (100:10:1 CHCl_3 :MeOH: NH_4OH); IR (neat) 3054, 2986, 2928, 2854, 2305, 1711, 1648, 1421, 1265, 895, 738 cm^{-1} ; ^1H NMR (300 MHz, CD_3CN) δ 8.45 (br t, $J = 6$ Hz, 2 H), 7.66-7.30 (m, 34 H), 4.68 (s, 4 H), 4.26 (d, $J = 5$ Hz, 4 H), 3.31 (t, $J = 5$ Hz, 8 H), 2.57 (t, $J = 5$ Hz, 8H), 2.52 (q, $J = 7$ Hz, 16 H), 0.93 (t, $J = 7$ Hz, 24 H); ^{13}C NMR (75 MHz, CDCl_3) δ 160.6, 141.0, 140.15, 140.03, 140.0, 139.9, 139.6, 139.4, 138.9, 138.8, 128.9, 128.8, 128.7, 128.5, 128.4, 128.3, 127.7, 127.5, 127.4, 127.3, 127.2, 127.1, 127.08, 127.02, 126.9, 126.8, 53.53, 53.52, 53.51, 51.79, 51.78, 51.77, 47.91, 47.77, 44.53, 29.89, 11.62, 11.50; HRMS(ES) m/z calcd for $\text{C}_{80}\text{H}_{101}\text{N}_8\text{O}_2$ [M + H] 1205.8048, found 1205.8049.

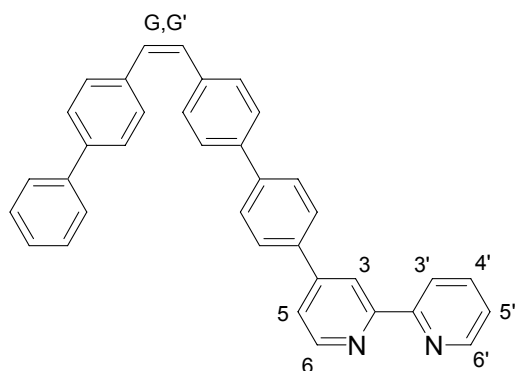


4-(4-Bromo-phenyl)-[2,2']bipyridine (21).⁴⁸ To a solution

of dihydropyran **20** (503 mg, 1.40 mmol) in acetonitrile (9.3 mL) was added $\text{H}_2\text{NOH}\cdot\text{HCl}$ (973 mg, 14.0 mmol). The solution was heated at reflux for 6 h then cooled to 23 °C. Volatile components of the reaction mixture were removed *in vacuo* to give a brownish-green solid. A solution of 10:1 brine: NH_4OH (20 mL) and CH_2Cl_2 (20 mL) were added to the solid and the mixture was stirred vigorously until all the solid dissolved. The organic layer was extracted with CH_2Cl_2 (4 x 20 mL), dried with Na_2SO_4 , and evaporated

⁴⁸ Cordaro, J.; McCusker, J.; Bergman, R. G. *Chem. Commun.* **2002**, 1496.

in vacuo to give a brown solid. The solid was extracted with warm ether (4 x 20 mL) and volatile components were removed *in vacuo* to give a yellow solid. The solid was recrystallized from hot methanol to yield white microcrystals (208 mg, 48%): mp 94-98 °C; IR (KBr) 3054, 1597, 1583, 1564, 1538, 1457, 1380, 1257, 1080, 1008, 990, 909, 817, 793, 739, 748, 661, 651; The ¹H and ¹³C NMR data matches the data described by Bergman and coworkers: ¹H NMR (300 MHz, CDCl₃) δ 8.74 (d, J = 5 Hz, 1 H, H⁶), 8.73-8.71 (m, 1 H, H^{6'}), 8.65 (d, J = 2 Hz, 1 H, H³), 8.46 (app d, J = 7 Hz, 1H, H^{3'}), 7.86 (dt, J = 7,7,2 Hz, 1 H, H⁴), 7.69-7.60 (m, 4 H, phenyl), 7.51 (dd, J = 5,2 Hz, 1 H, H⁵), 7.35 (ddd, J = 7,5,1 Hz, 1H, H^{5'}); ¹³C NMR (75 MHz, CDCl₃) δ 157.2, 156.3, 150.0, 149.5, 148.4, 137.5, 137.2, 132.5, 128.9, 124.2, 123.8, 121.6, 121.5, 119.0.



(Z)-4-[4'-(2-Biphenyl-4-yl-vinyl)-biphenyl-4-yl]-[2,2']bipyridine (22Z). A solution of 4-(4-bromo-phenyl)-[2,2']bipyridine **21** (100 mg, 0.321 mmol) and boronic ester **17Z** (135 mg, 0.353 mmol) in DME (2 mL) was deoxygenated by freeze-pump-thaw cycles (3 x) and kept under N₂. Sodium carbonate (102 mg, 0.963 mmol) was dissolved in a minimal amount of H₂O and degassed similarly. To the first flask was added tetrakis-(triphenylphosphine)palladium(0) (16 mg, 0.014 mmol) followed immediately by the sodium carbonate solution, transferred by cannula. The solution was stirred for 1 h at 23 °C, and then heated to 85 °C for 20 h. The solution was cooled to 23 °C and volatile

components of the reaction mixture were removed *in vacuo*. The crude solid was combined with H₂O (40 mL) and extracted with CH₂Cl₂ (3 x 20 mL). The combined organic layers were then washed with 10% NH₄⁺OH(aq) (3 x 30 mL), dried with K₂CO₃, and filtered. Volatile components of the filtrate were removed *in vacuo* to afford a crude solid that was purified by flash chromatography (SiO₂, CH₂Cl₂ then 99:1 CH₂Cl₂:MeOH, column pretreated with 19:1 CH₂Cl₂:NEt₃ then washed with CH₂Cl₂) to afford **22Z** as a pale yellow solid (112.7 mg, 72%): R_f 0.24 (99:1 CH₂Cl₂:MeOH, pretreated with 19:1 CH₂Cl₂:NEt₃); mp 116-118 °C; IR (KBr) 3053, 3028, 1583, 1598, 1565, 1497, 1485, 1457, 1387, 910, 821; UV-Vis (CH₂Cl₂, 8.3 μM) λ_{max} 345 nm, ε 4465 M⁻¹cm⁻¹, 293 nm, ε 3109 M⁻¹cm⁻¹, 569 nm, ε 792 M⁻¹cm⁻¹, 687 nm, ε 1560 M⁻¹cm⁻¹; ¹H NMR (300 MHz, CDCl₃) δ 8.80 (br d, J = 7 Hz, 1 H, H⁶), 8.77-8.75 (m, 2 H, H⁶+H³), 8.58 (br d, J = 7 Hz, 1 H, H³), 7.94-7.88 (m, 1 H, H⁴), 7.88 (app d, J = 8 Hz, 2 H, phenyl), 7.76 (app d, J = 8 Hz, 2 H, phenyl), 7.67 (br d, J = 7 Hz, 1 H, H⁵), 7.63-7.51 (m, 8 H, phenyl), 7.47-7.36 (m, 7 H, phenyl), 7.36-7.31 (m, 1 H, H⁵), 6.68 (s, 2 H, G+G'); ¹³C NMR (75 MHz, CD₃CN) δ 156.9, 156.4, 149.9, 149.4, 149.0, 141.6, 140.9, 140.1, 139.1, 137.2, 137.1, 137.0, 136.5, 130.4, 130.0, 127.7, 129.6, 128.9, 127.7, 127.6, 127.5, 127.1, 127.0, 124.0, 121.5, 119.0; HRMS(EI) *m/z* calcd for C₃₆H₂₆N₂ 486.2095, found 486.2090.

6.2.2. Photoisomerization Studies

All isomerizations were performed in air-equilibrated solvent that was used as received, unless otherwise specified as degassed. In a typical ¹H NMR-monitored

isomerization experiment, the chosen amounts of precipiton, triplet sensitizer, and isomenthol standard was dissolved in deuterated solvent and syringed into an NMR tube. The tube was capped and a ^1H NMR spectrum was recorded. If the reaction mixture was to be irradiated at $\lambda_{\text{exc}} \geq 400$ nm, the tube was then placed within a pyrex water-cooling jacket to stabilize the reaction temperature at ~ 23 °C. A 300 watt incandescent lamp (allowed to warm up for 30 min), positioned 5 cm from the sample, irradiated the reaction mixture. Light above 400 nm was selected by wrapping the jacket with a 400 nm cutoff filter. The reaction mixtures were irradiated for specific time intervals, removed from the light source and their spectra recorded by ^1H NMR. If “disturbed” conditions were employed (Method A), the reaction mixture was irradiated again and the corresponding spectra recorded until the isomerization was complete. If “undisturbed” conditions were applied (Method B), the reaction mixture would not be irradiated further (see Section 3.1). If the reaction mixture was to be irradiated at $\lambda_{\text{exc}} = 350$ nm, the tube was placed in a Rayonet photoreactor. The internal temperature of the photoreactor was 40 °C.

Reaction mixtures containing **9Z** or **9E** were first degassed by performing 3 x freeze-pump-thaw cycles in sealed NMR tubes or a quartz cuvette before irradiation. Due to the light sensitivity of complexes **9Z** and **9E**, it was necessary to perform all operations in a darkened laboratory. In cases where isomerizations of **9Z** and **9E** were monitored by UV-Vis spectroscopy, a sealed cuvette containing 2-3 mL of the degassed sample solution was irradiated for a short time period and then the absorption spectrum was measured. The procedure was repeated until no further absorption changes were observed.

APPENDIX A

6.3. Dexter Class Precipiton

6.3.1. Synthesis

Synthesis of Dexter precipiton **22Z** was achieved through a Suzuki cross-coupling reaction between 4-(4-bromo-phenyl)-[2,2']bipyridine **21** and pinacolatoboronic ester **17Z**. The bromide **2Z** was converted to the pinacolatoboronic ester **17Z** with bis(pinacolato)-diboron in the presence of palladium (Figure 57).

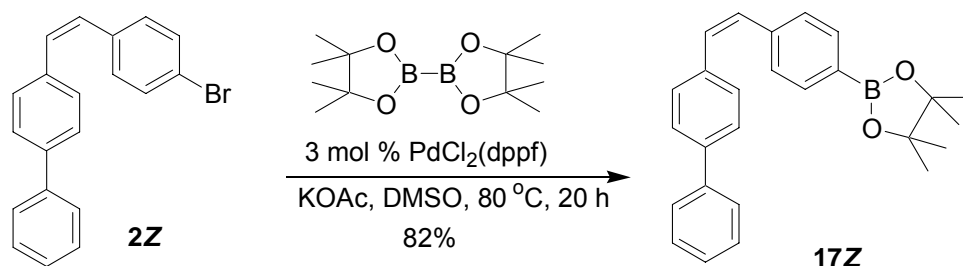


Figure 57 Synthesis of pinacolatoboronic ester **17Z**.

Separately, 4-(4-bromo-phenyl)-[2,2']bipyridine **21** was synthesized according to protocol outlined by Bergman and coworkers (Figure 58). 2-Acetylpyridine **4** underwent an aldol condensation with 4-bromo-benzaldehyde **18** in the presence of sodium hydroxide in methanol to generate hetero-diene **19**. A yttrium catalyzed hetero-Diels-Alder reaction between **19** and ethyl vinyl ether gave dihydropyran **20** in 79 % yield. Treatment of dihydropyran **20** with H₂NOH·HCl in refluxing acetonitrile generated 4-(4-bromo-phenyl)-[2,2']bipyridine **21**.

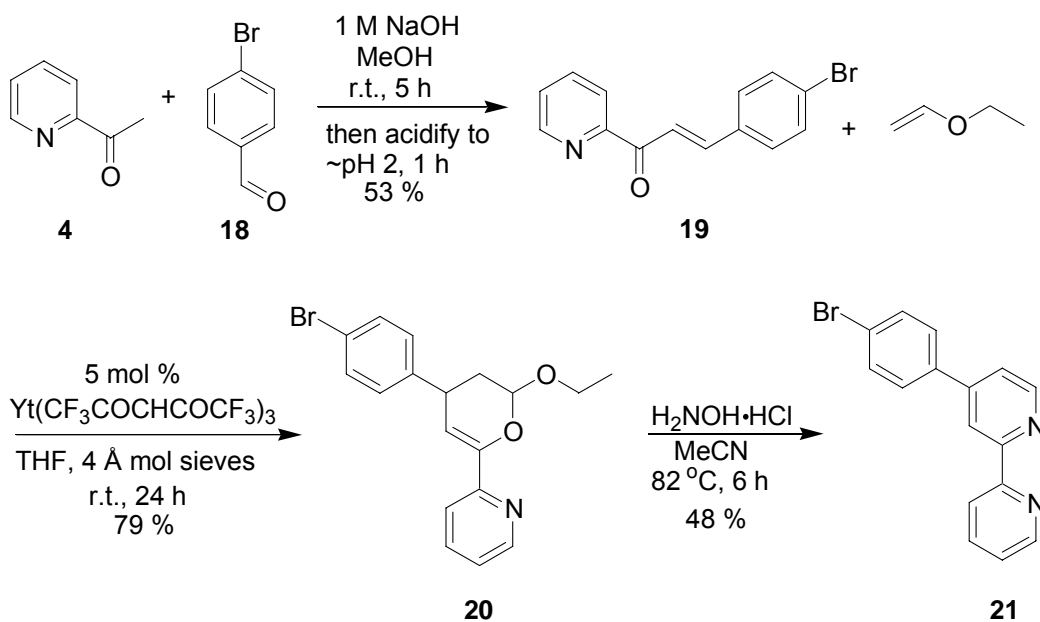


Figure 58 Synthesis of 4-(4-bromo-phenyl)-[2,2']bipyridine **21**.

The pinacolboronic ester **17Z** was coupled to bipyridine **21** in the presence of palladium to afford the Dexter class precipiton **22Z** in 72 % yield (Figure 59).⁴⁹

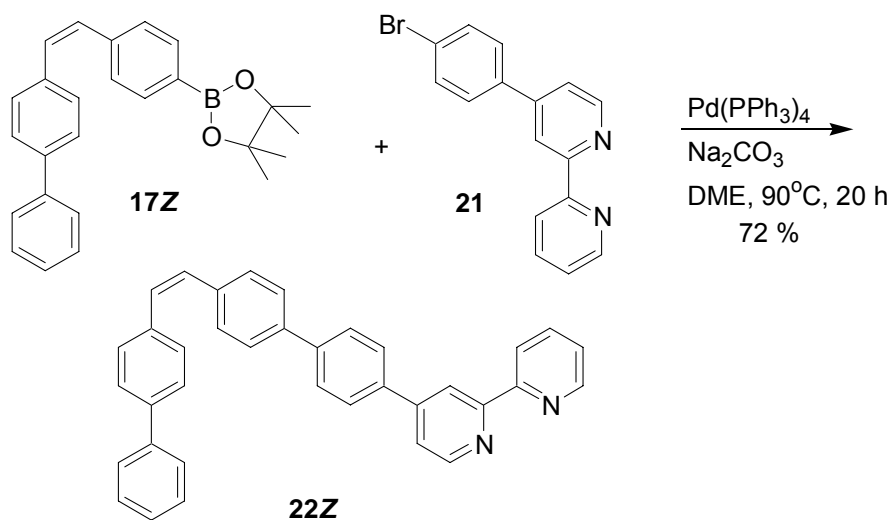


Figure 59 Synthesis of Dexter class precipiton **22Z**.

⁴⁹ Goodall, W.; Wild, K.; Arm, K.; Williams, G. *Perkin Trans. 2* **2002**, 1669.

6.3.2. Photochemical Challenges of Sequestration

An important assumption we made in our sequestration studies of **22Z** is that $\text{Ru}(\text{bpy})_2^{2+}$ binding to **22Z** is facile. Reaction 7 (Figure 55) showed no evidence of 2,2'-bipyridine binding to $\text{Ru}(\text{bpy})_2^{2+}$ in terms of an increased isomerization rate of **3Z** (compared to reaction 3). However, the increased isomerization rate of **3Z** in reaction 9 (Figure 56) suggested possible Ru:22Z binding. To resolve this question, determination of a binding constant was attempted. Dilution of a 1/1 mixture of 2,2'-bipyridine and $\text{Ru}(\text{bpy})_2^{2+}$ in 1/1 $\text{CH}_2\text{Cl}_2/\text{CH}_3\text{CN}$ adhered closely to Beer's law. This was strong evidence for low degrees of binding (Figure 60).

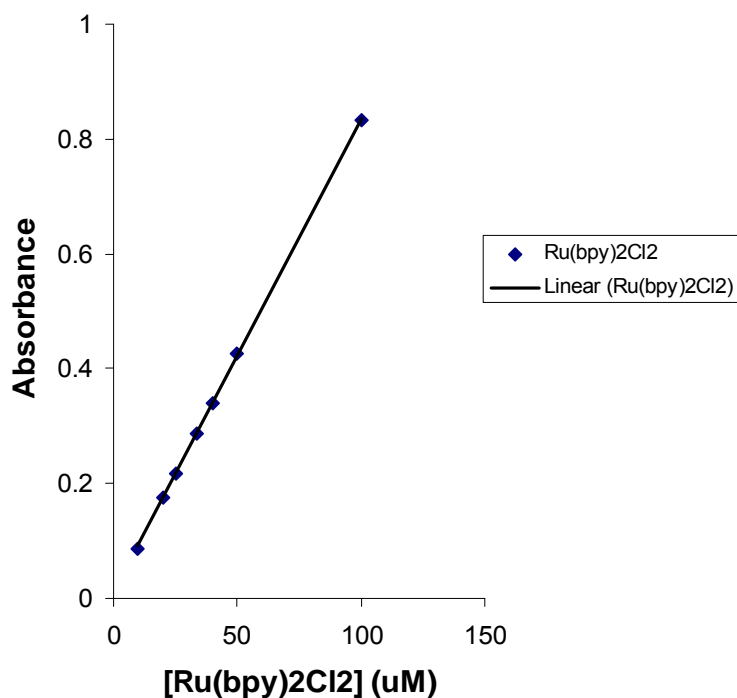


Figure 60 Absorbance spectra of the dilution of a 1/1 mixture of 2,2'-bipyridine and $\text{Ru}(\text{bpy})_2^{2+}$ (1/1 $\text{CH}_2\text{Cl}_2/\text{CH}_3\text{CN}$, $\lambda_{\text{abs}} = 376 \text{ nm}$, $R^2 = 0.999$).

The effect of Ru sensitizer on the isomerization rate of **22Z** is difficult to determine due to significant isomerization without the presence of Ru. The extended conjugation of **22Z** allows the absorption of visible light, causing isomerization. **3Z**, having less conjugation, does not isomerize significantly. The absorption spectra of **22Z** and **3Z** are shown in Figure 61.

The extended conjugation of **22Z** also makes it less soluble. **22Z** reaches saturation at approximately 0.002 mM in 1/1 CH₂Cl₂/CH₃CN. In every photoisomerization excluding reactions 1, 2, and 7 (Figure 55), precipitation occurred within 40 min of irradiation. Precipitation of **22E** complicates the comparison of reaction rates.

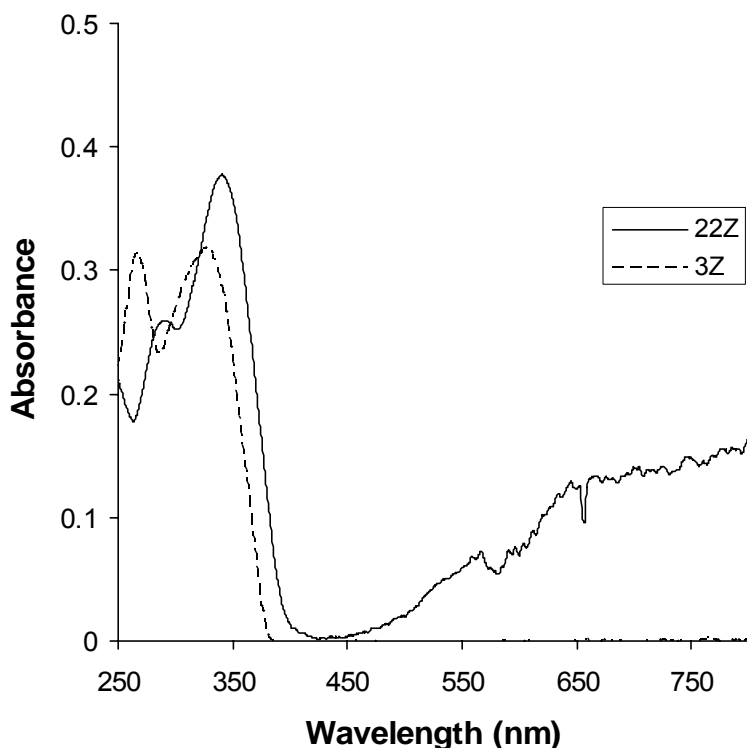


Figure 61 Room-temperature absorption spectra of **3Z** and **16Z** (10 μ M, air-equilibrated CH₃CN).

Isomerization of **22Z** in the presence of $\text{Ru}(\text{bpy})_2^{2+}$ and $\text{Ru}(\text{bpy})_3^{2+}$ (Figure 55, reactions 5, 6) results in precipitation and a color change of the solution from red and orange (at time = 0), respectively, to nearly colorless after approximately 120 min. This may be evidence of Ru removal by **22Z**. However, an alternative explanation that must be considered is photodissociation and photosubstitution of the Ru complexes. It is known that $^3\text{MLCT}$ state decay to the nearby ^3MC state of $\text{Ru}(\text{bpy})_3^{2+}$ can lead to a penta-coordinated square pyramidal intermediate (Figure 62).⁵⁰ In the presence of chloride ion, a hexacoordinated monodentate bipyridine intermediate forms, which can undergo loss of bpy to make $\text{Ru}(\text{bpy})_2\text{Cl}_2$. Photodissociation of the Ru sensitizer complicates the interpretation of **3Z** and **22Z** isomerization rates.

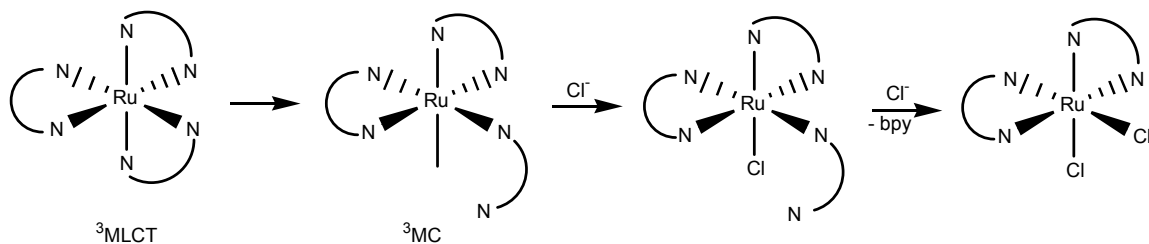


Figure 62 Modes of ring opening that can result in the formation of photosubstitution products.

⁵⁰ Yamagishi, A.; Naing, K.; Goto, Y.; Taniguchi, M.; Takahashi, M. *Dalton Trans.* **1994**, 2085.

6.4. ^1H - ^1H COSY SPECTRA

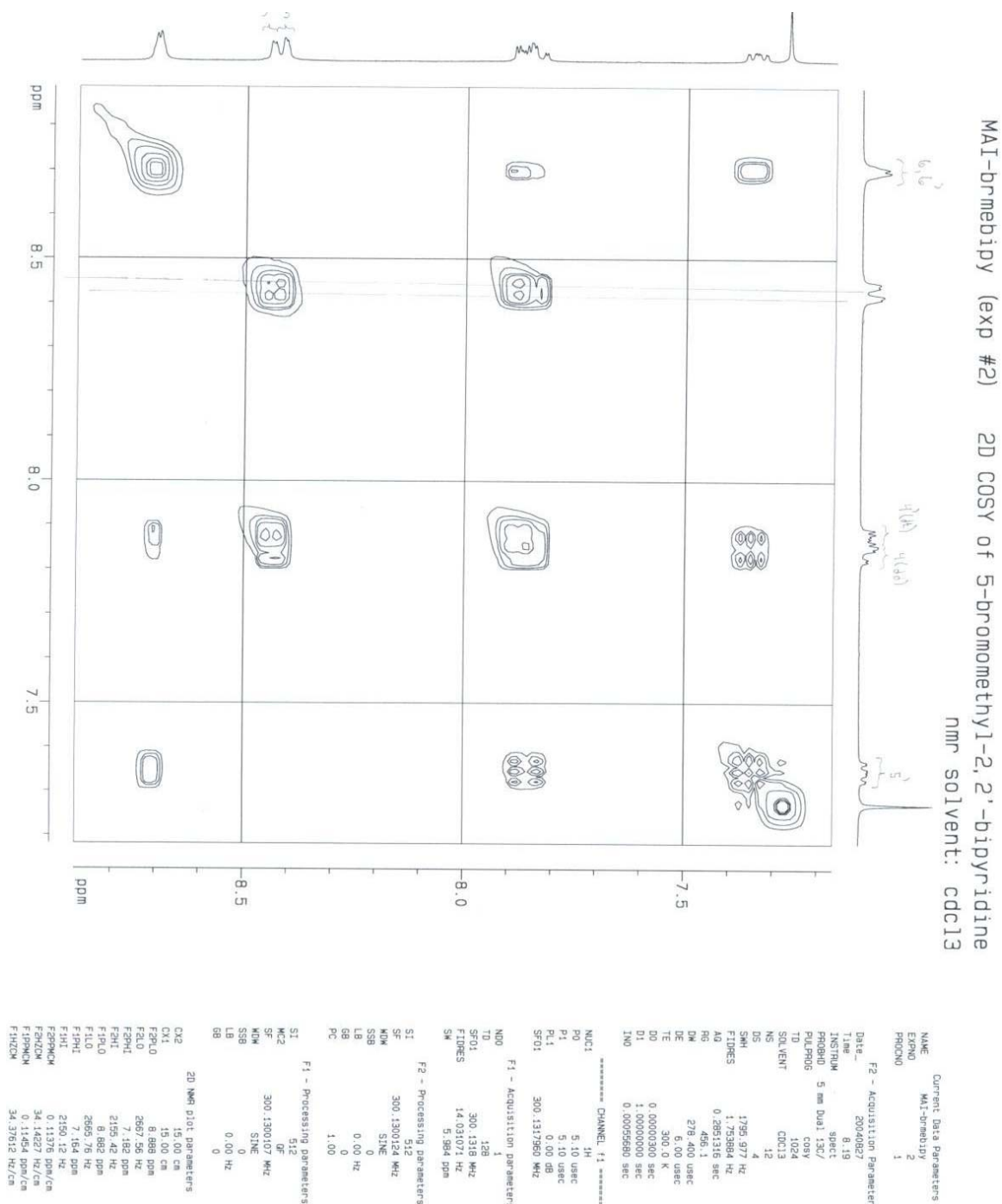


Figure 63 ^1H - ^1H COSY of compound 7.

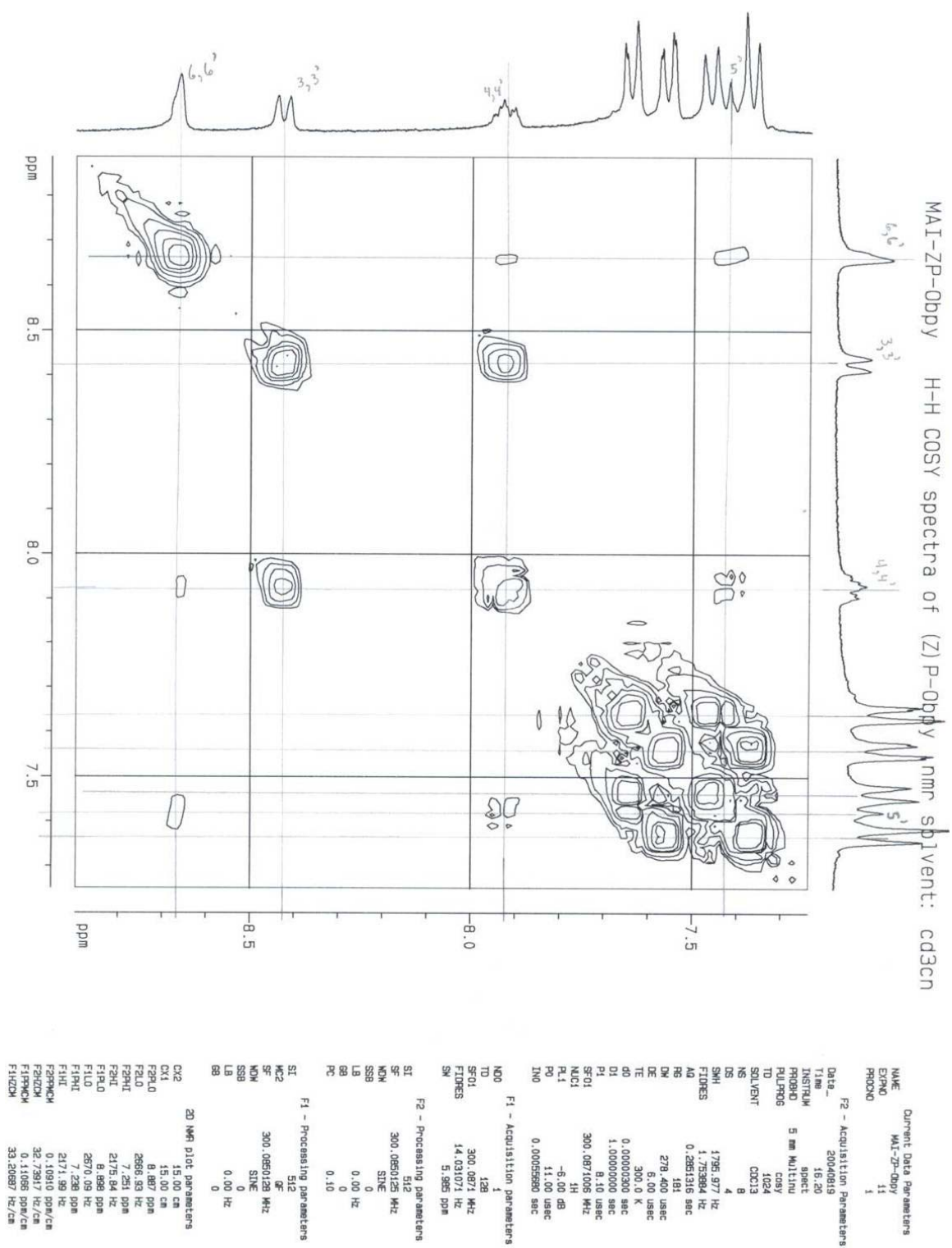
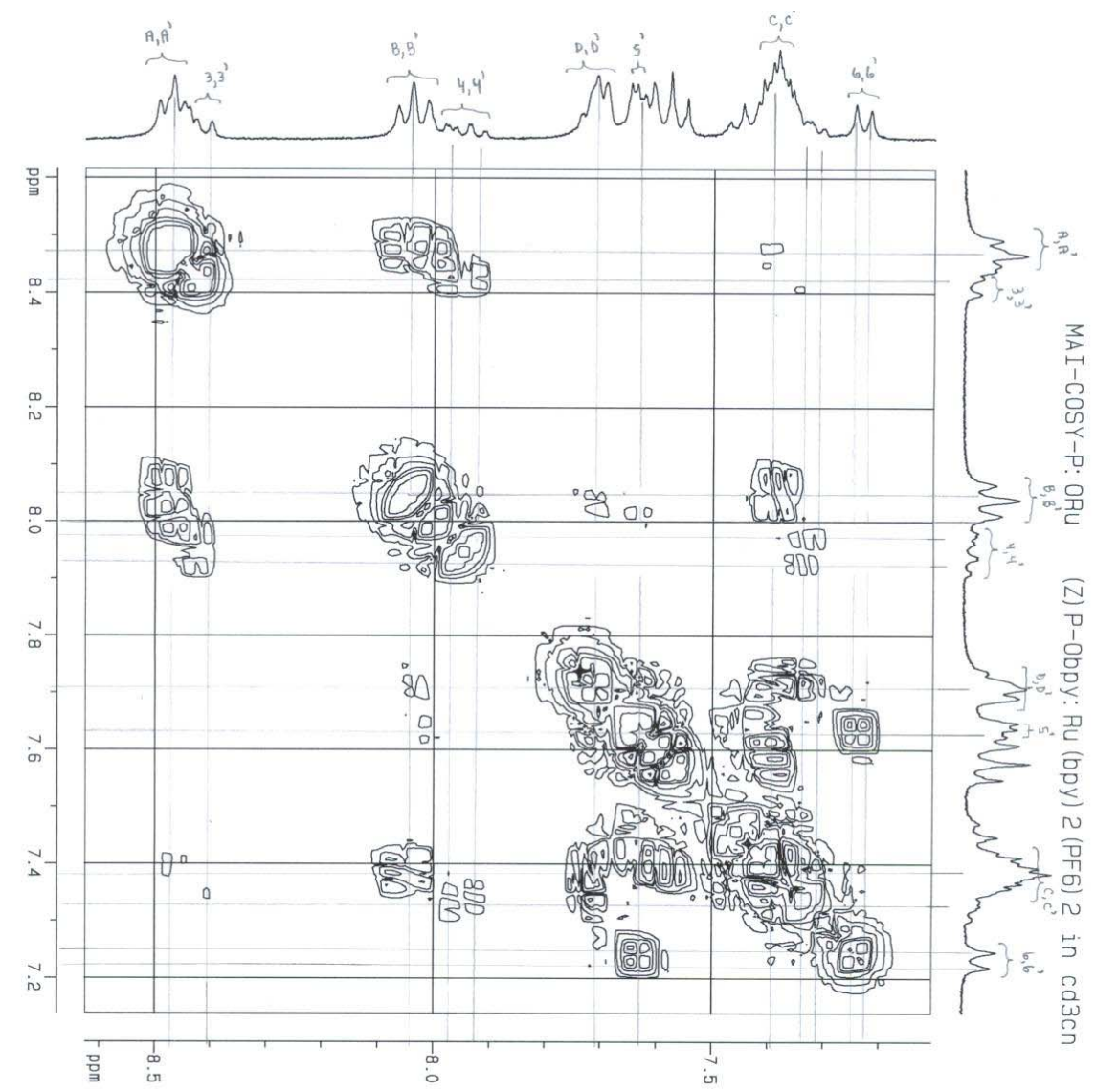


Figure 64 ^1H - ^1H COSY of compound 8Z.



Current Data Parameters
NAME MAI-COSY-P-ORU
EXPNO 110
PROCNO 1

F2 - Acquisition Parameters
Date_ 20040818
Time 15:42
INSTRUM spect
PROBHD 5 mm QNP 1H
PULPROG cosy
TD 1024
SOLVENT MeOH
NS 4
DS 4
SM 1489.801 Hz
FIDRES 1.469873 Hz
AQ 0.3416954 sec
RG 2048
DM 333.600 usec
DE 6.00 usec
TE 300.0 K
D0 0.00003300 sec
D1 1.00000000 sec
D2 0.00089720 sec

CHANNEL f1

NUC1 1H
P1 11.00 usec
PL 7.10 usec
RF1 -8.00 dB
SFO1 300.1315908 MHz

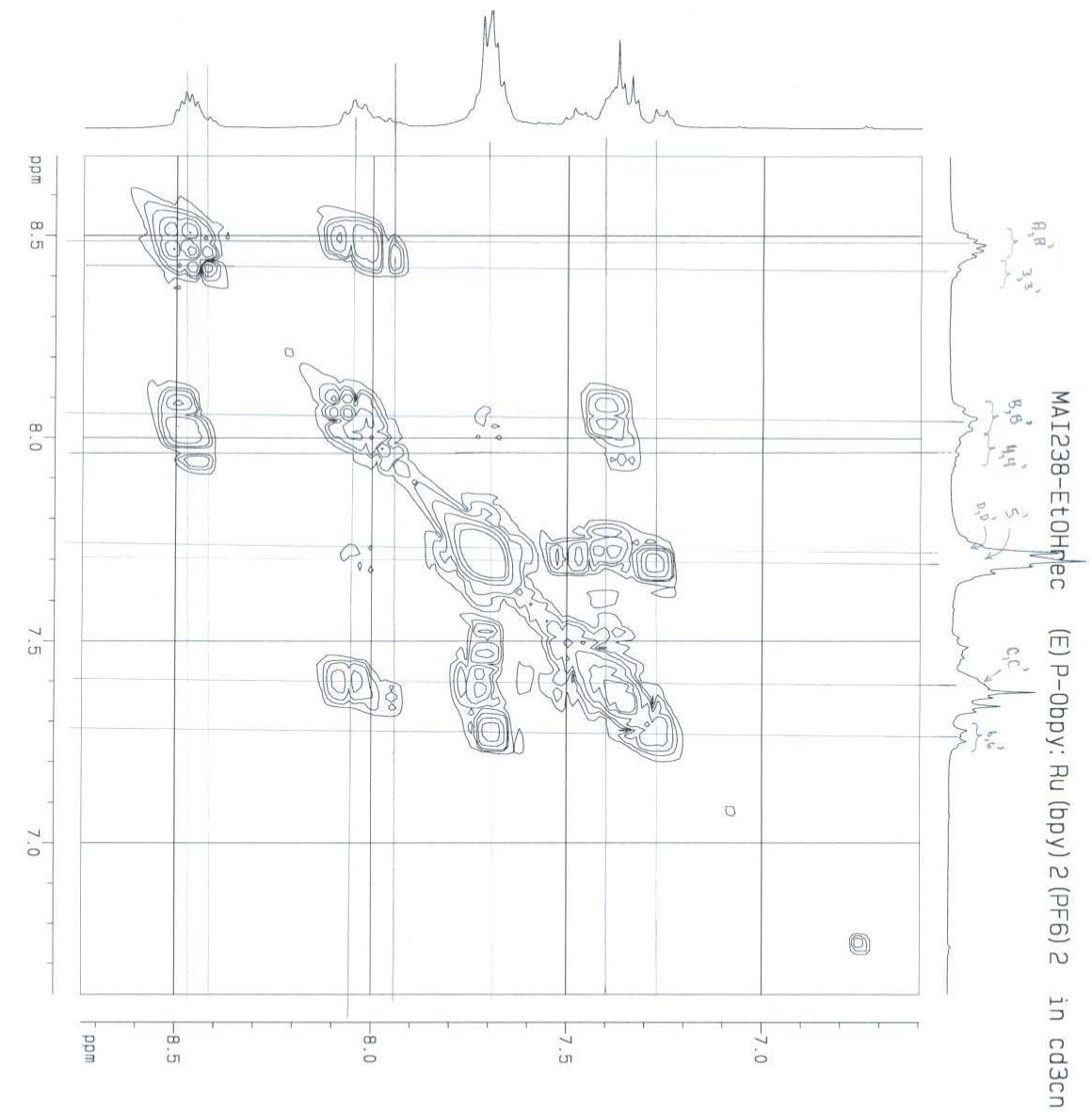
F1 - Acquisition Parameters
ND0 128
TD 300.132 MHz
SFO1 11.709382 Hz
FIDRES 4.994 ppm
SM

F2 - Processing parameters
SI 1024
SF 300.1300045 MHz
WDW SINE
SSB 0
LB 0.00 Hz
GB 0
PC 1.40

F1 - Processing parameters
SI 1024
SF 300.1300045 MHz
WDW SINE
SSB 0
LB 0.00 Hz
GB 0

2D NMR plot parameters
CX2 15.00 cm
CX1 15.00 cm
F2PUL0 8.616 ppm
F2LO 2665.92 Hz
F2PHI 7.138 ppm
F2H1 2142.43 Hz
F2PUL0 8.656 ppm
F2LO 2668.84 Hz
F2PHI 7.104 ppm
F1PH1 2132.18 Hz
F2PPHNCM 0.09851 ppm/cm
F2HZCM 29.56619 Hz/cm
F1PPHNCM 0.10144 ppm/cm
F1HZCM 30.44439 Hz/cm

Figure 65 ¹H-¹H COSY of compound 9Z.



Current Data Parameters
 NAME MA1238-EtOHrec
 EXPNO 2
 PROCNO 1

F2 - Acquisition Parameters
 Date_ 20/04/2012
 Time 8:38
 INSTRUM spect
 PROBRD 5 mm Dual 13C/
 PULPROG zgpg30
 TD 1024
 SOLVENT CDCl3
 NS 12
 DS 4
 SMH 2097.315 Hz
 FIDRES 2.048160 Hz
 AQ 0.2441716 sec
 RG 512
 DM 236.400 usec
 DE 6.00 usec
 TE 300.0 K
 D0 0.00000500 sec
 D1 1.00000500 sec
 IN0 0.00047580 sec

***** CHANNEL f1 *****
 NUC1 13C
 P1 5.10 usec
 PL1 5.10 usec
 RF1 0.00 dB
 SFO1 300.1320323 MHz

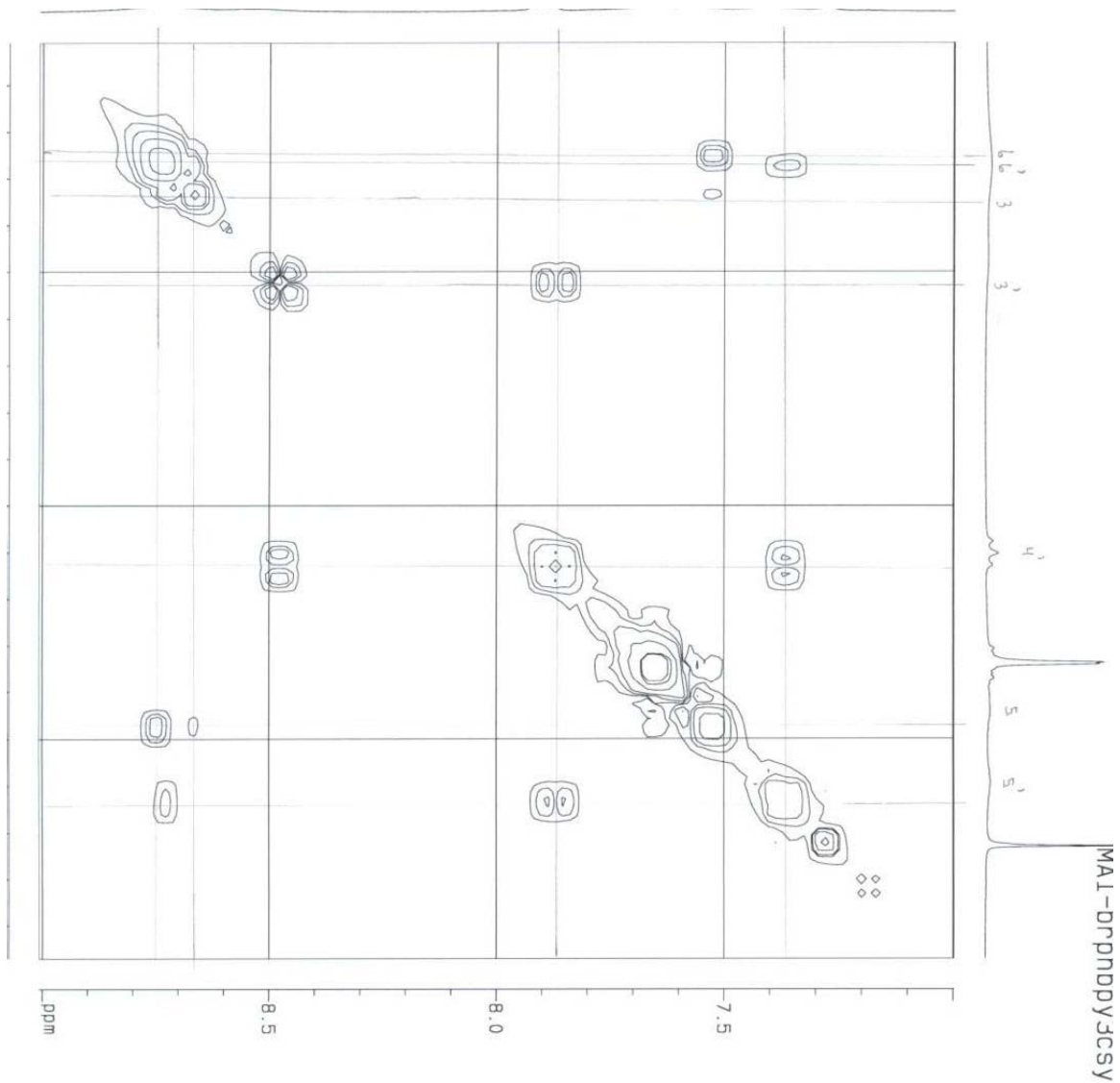
F1 - Acquisition Parameters
 N00 1
 TD 128
 SF01 300.1321 MHz
 FIDRES 16.358277 Hz
 SW 6.3988 ppm

F2 - Processing parameters
 SI 512
 SF 300.1300031 MHz
 MDW SINE
 USB 0.00 Hz
 GB 0
 PC 1.00

F1 - Processing parameters
 SI 512
 MK2 GF
 SF 300.1300028 MHz
 MDW SINE
 SSB 0
 LB 0.00 Hz
 GB 0

2D NMR Plot Parameters
 CX2 15.00 cm
 CX1 15.00 cm
 FENLO 8.897 ppm
 FELD 2610.33 Hz
 F2PH1 8.898 ppm
 F2PH2 1981.68 ppm
 F1PH0 8.739 ppm
 F1PH1 2622.95 Hz
 F1PH2 6.897 ppm
 F1HT 1979.89 Hz
 F2PRCKM 0.13850 ppm/cm
 F2HZCKM 41.50937 Hz/cm
 F1PRCKM 0.14285 ppm/cm
 F1HZCKM 42.87481 Hz/cm

Figure 66 ¹H-¹H COSY of compound 9E.



```

Current Data Param
NAME      MAL-DRPNDPPYJCSY
EXPNO     1
PROCNO    1

F2 - Acquisition Parameters
Date_     20040826
Time      8.33
INSTRUM   spect
PROBHD    5 mm Dual 130/
PULPROG   cosy
TD         1024
SOLVENT   CDCl3
NS         16
DS         4
SWH        2394.636 Hz
FIDRES     2.338512 Hz
AQ          0.2138512 s
RG          574.7
DM          208.800 us
DE          6.00 us
TE          300.0 K
D0          0.00000000 s
D1          1.00000000 s
D2          0.00041760 s
INO

***** CHANNEL f1 *****
NUC1       1H
P0          5.10 us
P1          5.10 us
PL1         0.00 dB
SFO1       300.1323946 MHz

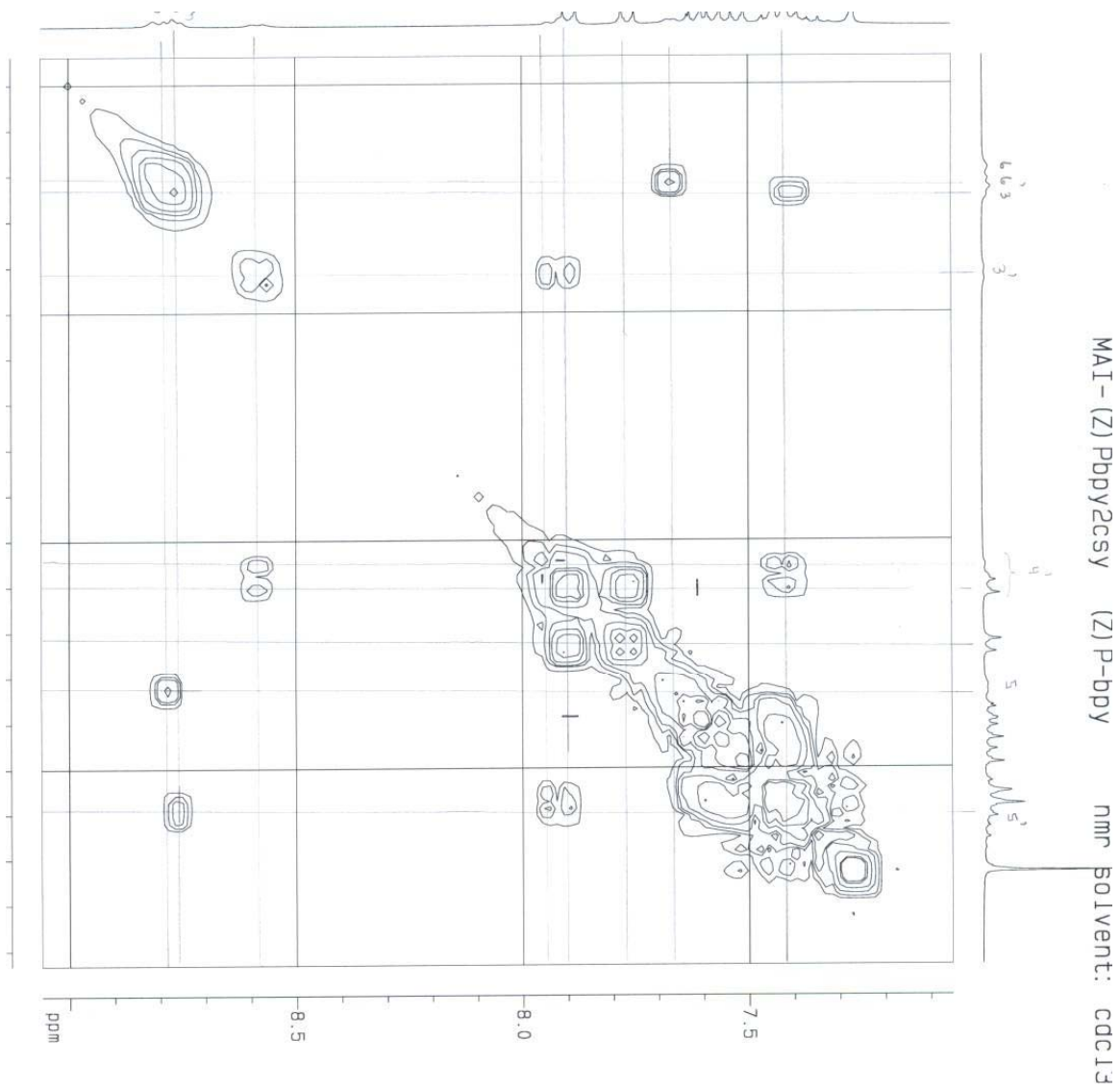
F1 - Acquisition Parameters
ND0         1
TD          128
SFO1       300.1324 MHz
FIDRES     18.708094 Hz
SM          7.979 DF

F2 - Processing parameters
SI          512
SF          300.1300094 MHz
WDW          SINE
SSB          0
LB           0.00 Hz
GB           0
PC           1.00

F1 - Processing parameters
SI          512
MC2         GF
SF          300.1300092 MHz
WDW          SINE
SSB          0
LB           0.00 Hz
GB           0

2D NMR Plot Parameters
CK2        15.00 cm
CK1        15.00 cm
F2PL0      8.392 DC
F2L0       2698.62 Hz
F2PHI      7.028 DC
F2HI       2109.31 Hz
F1PL0      9.008 DC
F1L0       2703.43 Hz
F1PHI      6.997 DC
F1HI       2100.10 Hz
F2PMCM     0.13090 DC
  
```

Figure 67 ^1H - ^1H COSY of compound 21.



```

Current Data Parameters
NAME      MAI-(Z)Pbbpy2csy
EXPNO    1
PROCNO   1
-----
F2 - Acquisition Parameters
Date_    20040825
Time     9.57
INSTRUM  spect
PROBHD   5 mm BBO1 13C/
PULPROG  zgpg30
TD       65536
SOLVENT  CDCl3
NS       12
DS       4
SWH      2394.636
FIDRES   0.239812
AQ       0.2138912
RG       208.800
DM       6.000
DE       3.000.0
TE       300.0
D0       0.00000300
D1       1.000000000
D10      0.00041750
INO
----- CHANNEL f1
NUC1     1H
PQ       5.10
P1       5.10
PL1      0.00
SFO1     300.1325946
-----
F1 - Acquisition Parameters
NUC0     13C
TD       132
SFO1     300.1324
FIDRES   19.46958E
SN       7.975
-----
F2 - Processing parameters
SI       312
SF       300.1300117
WDW      SINC
SSB      0
LB       0.00
GB       0
PC       1.00
-----
F1 - Processing parameters
SI       912
SF       300.1300117
WDW      SINC
SSB      0
LB       0.00
GB       0
PC       1
-----
2D NMR plot parameters
CX2      15.00
CX1      15.00
F2PRLO   9.066
F2PLHI   2719.7
F2PRLO   7.066
F2PLHI   2121.0
F1PRLO   9.066
F1PLHI   2719.7
F1PRLO   7.066
F1PLHI   2116.4
F2PRMIN   0.13329
  
```

Figure 68 ¹H-¹H COSY of compound 22Z.